THE JOURNAL OF THE ALABAMA ACADEMY OF SCIENCE

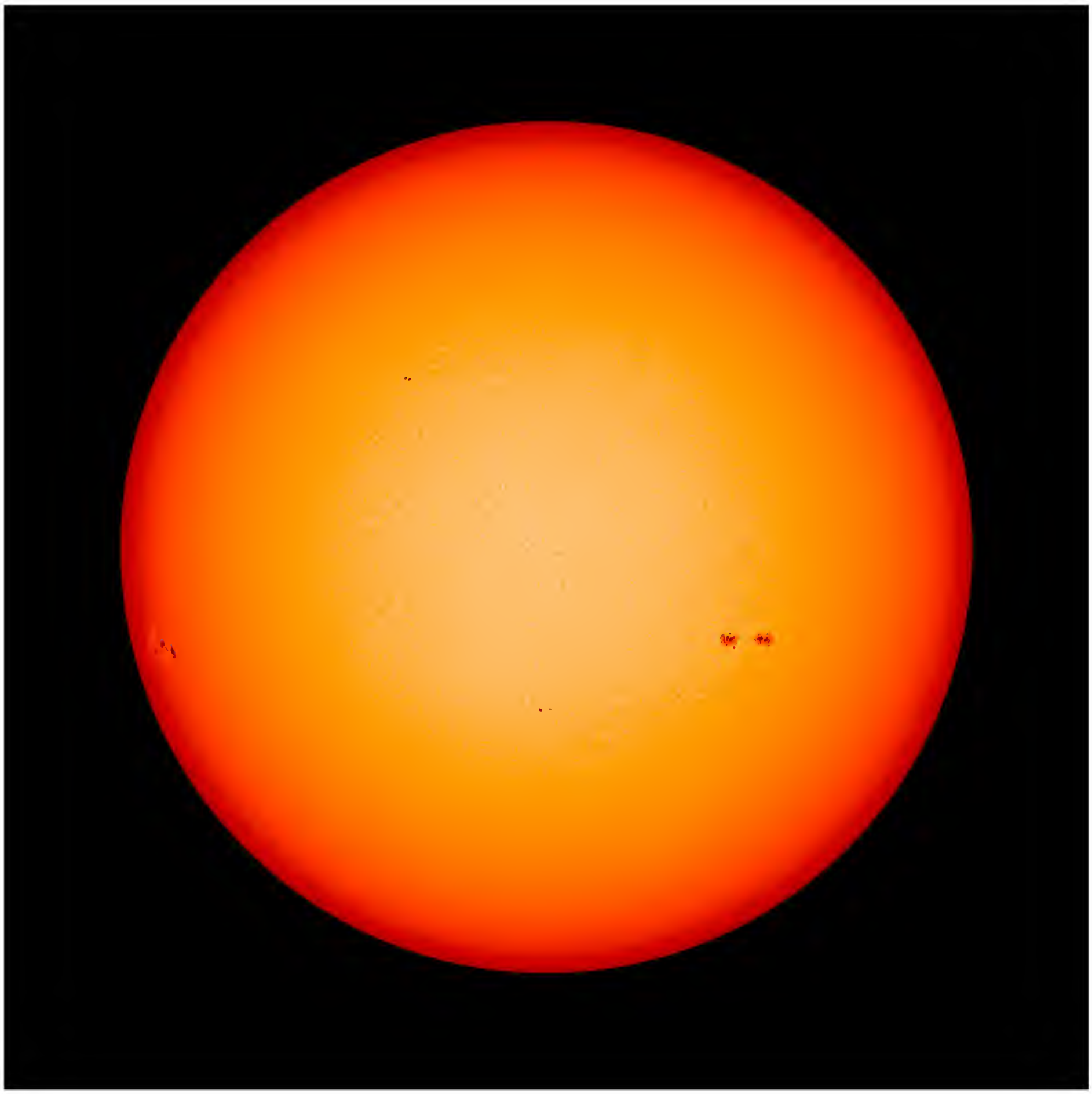

VOLUME 88 November 2017 No. 2

Cover Photograph: “Quiet Interlude in Solar Max”. Something unexpected is happening on the Sun. 2013 was supposed to be the year of "solar maximum," the peak of the 11-year sunspot cycle. Yet 2013 has arrived and solar activity is relatively low. Sunspot numbers are well below their values from 2011, and strong solar flares have been infrequent.
(Text and image courtesy NASA/SDO)

Photo is courtesy of: NASA/SDO published this image and text in the public domain on the nasa.gov website. More information about this image may be found online at the following link – https://www.nasa.gov/multimedia/imagegallery/image_feature_2464.html

Editorial Comment:
On behalf of the Alabama Academy of Science, I would like to express my gratitude and appreciation to the reviewers for their valuable contributions in reviewing the manuscripts of this issue.

Thanks!
Brian Toone
Editor: Alabama Academy of Science Journal

**THE JOURNAL OF THE
ALABAMA ACADEMY OF SCIENCE
AFFILIATED WITH THE
AMERICAN ASSOCIATION FOR THE
ADVANCEMENT OF SCIENCE**

VOLUME 88 NOVEMBER 2017 NO. 2

Publication and Subscription Policies:
Submit all manuscripts and pertinent correspondence to the Editor. Each manuscript will receive at least two simultaneous reviews. For style details, follow instructions to Authors available on the Alabama Academy of Science website – http://alabamaacademyofscience.org

Reprints requests must be addressed to Authors.

Subscriptions and Journal Exchanges: Address all Correspondence to the Chairman of the Editorial Board.

ISSN 002-4112

BENEFACTORS OF THE JOURNAL OF THE ALABAMA ACADEMY OF SCIENCE

The following have provided financial support to partially defray publication costs of the journal.

ALABAMA STATE UNIVERSITY
ATHENS STATE UNIVERSITY
AUBURN UNIVERSITY
AUBURN UNIVERSITY AT MONTGOMERY
BIRMINGHAM-SOUTHERN COLLEGE
JACKSONVILLE STATE UNIVERSITY
SAMFORD UNIVERSITY
TROY UNIVERSITY
TUSKEGEE UNIVERSITY
UNIVERSITY OF ALABAMA
UNIVERSITY OF ALABAMA AT BIRMINGHAM
UNIVERSITY OF MONTEVALLO
UNIVERSITY OF NORTH ALABAMA
UNIVERSITY OF SOUTH ALABAMA
UNIVERSITY OF WEST ALABAMA

TABLE OF CONTENTS

ARTICLES

Journal of Alabama Academy of Science, Vol.88, No. 2, November 2017

NUMBER OF SPOTLESS DAYS IN RELATION TO THE TIMING AND SIZE OF SUNSPOT CYCLE MINIMUM

Robert M. Wilson
NASA Marshall Space Flight Center, NSSTC, Huntsville, Alabama

robert.m.wilson@nasa.gov

ABSTRACT

Sunspot cycle (SC) 24, the present ongoing SC, is now in its 9th year, having had a minimum in annual sunspot number (SSN) in 2008, measuring 4.2, and a minimum in 'smoothed' SSN in December 2008, measuring 2.2. Its maximum annual SSN occurred in 2014, measuring 113.3, and its maximum smoothed SSN occurred in April 2014, measuring 116.4. Following smoothed SSN maximum (SSN max), the first spotless day (FSD) during the decline of SC24 was reported in July 2014, a mere 3 months following SC24's maximum SSN amplitude, an interval shorter than the 13 months found for SC12 and the 8 months for SC14. Through December 2016, some 27 spotless days (1 in 2014 and 26 in 2016) have been seen, with more to come as SC25's epoch of minimum approaches. Examined in this study are the following three factors: (1) the variation in number of spotless days (NSD) relative to the epochs of sunspot minimum (SSN min) and SSN max, (2) the association between the maximum NSD and the SSN min, and (3) cyclic variations of selected spotless day-associated parameters. It is suggested that SC25's epoch of SSN min likely will occur sometime in 2020 or later and that SC24's NSD behavior represents a return to that experienced during SC12 and SC14. Hence, another prolonged minimum, like that experienced for SC23/24, might well occur for SC24/25. For comparison, SC24's interval of spotless days from first to last spotless day bounding SSN min extended 84 months and totaled 816 spotless days, with 265 spotless days reported during the year of annual SSN min.

INTRODUCTION

Sunspots are the dark, cool regions of enhanced magnetic field strength found on the Sun that vary in number, size, and magnetic complexity over the course of the sunspot cycle (SC) (Wilson 2015). Indeed, it was on the basis of the annual number of spotless days (NSD) and number of newly appearing 'clusters of spots' that Samuel Heinrich Schwabe (1844) first showed that the Sun's activity varies from a sunspot minimum (SSN min) to a sunspot maximum (SSN max) and then to another minimum over a period of about a decade. Near SSN min, the NSD increases to a NSD maximum (NSD max), while near SSN max they rarely occur, being essentially nonexistent. On the other hand, near SSN min, the number of newly appearing clusters of spots (akin to the number of sunspot 'groups') is minimal, while near SSN max, they are maximal. Furthermore, Wilson (1995) showed that the occurrence of the first spotless day (FSD) during the declining portion of the SC can be used as a predictor for the timing and size of the following SSN min (cf. Harvey and White 1999, Wilson and Hathaway 2005, 2006).

SC24, the present ongoing SC, had its SSN min in 2008, measuring 4.2 in terms of the annual average (i.e., January–December). Its SSN max occurred in 2014, measuring 113.3 in terms of the annual average. Since 2014, the annual average of SSN has decreased, measuring 69.8 in 2015

and 39.9 in 2016. In terms of the 12-month moving average of SSN (also called the 13-month running mean or simply 'smoothed' SSN), SC24 had its minimum in December 2008 (this being the 'epoch' of SSN min, (Em)), measuring 2.2, and its maximum in April 2014 (this being the epoch of SSN max, (EM)), measuring 116.4. In June 2016 (the last available smoothed SSN at the time of writing this manuscript), the 12-month moving average of SSN had decreased to 41.5.

In terms of NSD, the FSD for SC24 occurred in November 2004 during the decline of SC23 (i.e., post EM cycle 23), and the last spotless day (LSD) occurred in January 2011 post Em for SC24 and prior to its EM, thus, spanning some 84 months and totaling 816 in number, these values being considerably longer and larger than those observed since SC15. In comparison to other modern era SCs (i.e., SC10–present), SC24's NSD is only the third largest, being smaller than SC12's 1,027 spotless days and SC15's 1,018 spotless days. In terms of the length from FSD to LSD, SC24 ranks as the fifth longest, shorter than SC12's 124 months, SC15's 120 months, SC14's 116 months, and SC10's 107 months. (Recall, FSD for cycle $n+1$ is defined as the first spotless day post EM for cycle n, and LSD for cycle $n+1$ is defined as the last spotless day prior to EM for cycle $n+1$.)

Following SC24's EM, the FSD for SC25, the next SC, made its appearance in July 2014, a mere 3 months following SC24's EM. Through December 2016, some 27 spotless days have been seen, with more to come as SC24 progresses towards SC25's Em, not expected to occur until about 2020 or later (Wilson 2015).

SC24 had a maximum amplitude that is the smallest since SC14 and had both an extended interval from FSD to LSD, as well as a large NSD. This has fostered the idea that the Sun might be entering another lull of activity, similar to the one called the 'Dalton minimum' that occurred with SC05 and SC06 (cf. Russell, Luhmann, and Jian 2010; Mordvinov and Kramynin 2010; Nielsen and Kjeldsen 2011; Zięba and Nieckarz 2012; Clette and Lefèvre 2012; Hady 2013; Zięba and Nieckarz 2014; McCracken and Beer 2014; and Mőrner 2015). In this article, the NSD is examined relative to the timing and size of cycle minimum and maximum, with a look toward predicting the occurrence of Em for SC25.

METHODS AND MATERIALS

SSN and NSD values were obtained using the newly revised SSN data taken from the "Sunspot Index and Long-term Solar Observations" webpage available online through the Solar Influences Data Analysis Center website <www.sidc.oma.be/index.php3>. Linear regression analysis, runs testing, and nonparametric analyses (i.e., Kendall's τ and Fisher's exact test for 2×2 contingency tables) are employed to evaluate the inferred relationships.

RESULTS AND DISCUSSION

Figure 1 displays the annual values of (a) SSN and (b) NSD for the interval 1849–2016, spanning the declining portions of SC09–SC24. Clearly, the occurrence of NSD max has always peaked with the occurrence of SSN min. The interval encompassing SC12–SC14 appears to represent a brief lull in solar activity (based on SSN), especially in comparison to the previous SC09–SC11 and subsequent SCs. In terms of SSN max, SC24 appears strikingly similar to that of SC12 and SC14.

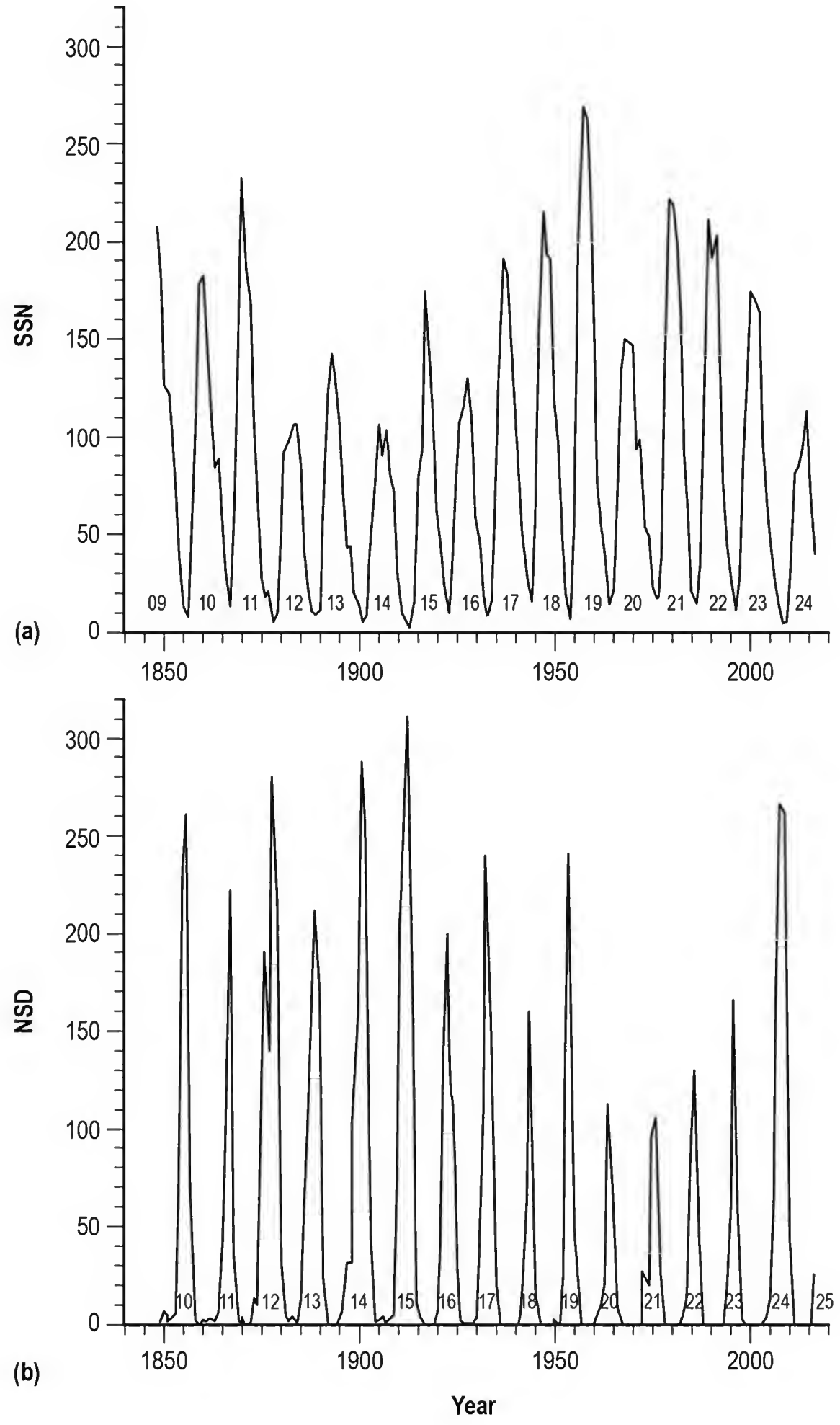

Figure 1. Annual variation of (a) sunspot number (SSN) and (b) number of spotless days (NSD) for the modern era of sunspot observations. The sunspot cycle (SC) number is identified for each cycle.

Regarding NSD, its rise to NSD maximum (NSD max) is shown to always precede the occurrence of SSN min, peaking at SSN min and then falling to zero prior to the occurrence of SSN max for all modern era SCs. Clearly, the size of SC24's NSD max, although quite large in comparison to recent SCs (SC20–SC23), is only the fourth largest NSD max (265 spotless days at SSN min), being below those of SC15 (311), SC14 (287), and SC12 (280). For convenience, Table 1 is included to provide the listing of the specific annual values of SSN and NSD plotted in Figure 1.

Table 1. Annual mean sunspot number (SSN) and annual number of spotless days (NSD), 1848–2016 (Continued).

Year	SSN	NSD	Comment
1848	208.3	#	SC09 SSN max
1849	182.5	1	
1850	126.3	7	
1851	122.0	0	
1852	102.7	4	
1853	74.1	6	
1854	39.0	70	
1855	12.7	234	
1856	8.2	261	SC10 SSN min, NSD max
1857	43.4	70	
1858	104.4	2	
1859	178.3	0	
1860	182.2	0	SC10 SSN max
1861	146.6	2	
1862	112.1	3	
1863	83.5	2	
1864	89.2	7	
1865	57.8	44	
1866	30.7	86	
1867	13.9	222	SC11 SSN min, NSD max
1868	62.8	37	
1869	123.6	2	
1870	232.0	0	SC11 SSN max
1871	185.3	0	
1872	169.2	0	
1873	110.1	14	
1874	74.5	12	
1875	28.3	131	
1876	18.9	190	
1877	20.7	140	
1878	5.7	280	SC12 SSN min, NSD max
1879	10.0	217	
1880	53.7	32	
1881	90.5	5	
1882	99.0	2	
1883	106.1	4	SC12 SSN max
1884	105.8	0	
1885	86.3	13	
1886	42.4	62	
1887	21.8	104	
1888	11.2	150	

Table 1. Annual mean sunspot number (SSN) and annual number of spotless days (NSD), 1848–2016 (Continued).

Year	SSN	NSD	Comment
1889	10.4	212	SC13 SSN min, NSD max
1890	11.8	171	
1891	59.5	24	
1892	121.7	0	
1893	142	0	SC13 SSN max
1894	130	0	
1895	106.6	1	
1896	69.4	7	
1897	43.8	32	
1898	44.4	32	
1899	20.2	104	
1900	15.7	158	
1901	4.6	287	SC14 SSN min, NSD max
1902	8.5	257	
1903	40.8	45	
1904	70.1	1	
1905	105.5	2	SC14 SSN max
1906	90.1	4	
1907	102.8	0	
1908	80.9	3	
1909	73.2	5	
1910	30.9	75	
1911	9.5	201	
1912	6.0	254	
1913	2.4	311	SC15 SSN min, NSD max
1914	16.1	153	
1915	79.0	12	
1916	95.0	4	
1917	173.6	0	SC15 SSN max
1918	134.6	0	
1919	105.7	0	
1920	62.7	7	
1921	43.5	46	
1922	23.7	134	
1923	9.7	200	SC16 SSN min, NSD max
1924	27.9	116	
1925	74.0	29	
1926	106.5	2	
1927	114.7	0	
1928	129.7	0	SC16 SSN max
1929	108.2	0	
1930	59.4	3	
1931	35.1	43	
1932	18.6	108	
1933	9.2	240	SC17 SSN min, NSD max
1934	14.6	154	
1935	60.2	20	
1936	132.8	0	
1937	190.6	0	SC17 SSN max
1938	182.6	0	
1939	148.0	0	

Table 1. Annual mean sunspot number (SSN) and annual number of spotless days (NSD), 1848–2016 (Continued).

Year	SSN	NSD	Comment
1940	113.0	0	
1941	79.2	5	
1942	50.8	24	
1943	27.1	65	
1944	16.1	159	SC18 SSN min, NSD max
1945	55.3	16	
1946	154.3	0	
1947	214.7	0	SC18 SSN max
1948	193.0	0	
1949	190.7	0	
1950	118.9	3	
1951	98.3	0	
1952	45.0	23	
1953	20.1	131	
1954	6.6	241	SC19 SSN min, NSD max
1955	54.2	48	
1956	200.7	0	
1957	269.3	0	SC19 SSN max
1958	261.7	0	
1959	225.1	0	
1960	159.0	0	
1961	76.4	6	
1962	53.4	10	
1963	39.9	21	
1964	15.0	112	SC20 SSN min, NSD max
1965	22.0	70	
1966	66.8	8	
1967	132.9	0	
1968	150.0	0	SC20 SSN max
1969	149.4	0	
1970	148.0	0	
1971	94.4	0	
1972	97.6	0	
1973	54.1	27	
1974	49.2	20	
1975	22.5	96	
1976	18.4	105	SC21 SSN min, NSD max
1977	39.3	25	
1978	131.0	0	
1979	220.1	0	SC21 SSN max
1980	218.9	0	
1981	198.9	0	
1982	162.4	0	
1983	91.0	4	
1984	60.5	13	
1985	20.6	83	
1986	14.8	129	SC22 SSN min, NSD max
1987	33.9	44	
1988	123.0	0	
1989	211.1	0	SC22 SSN max
1990	191.8	0	

Table 1. Annual mean sunspot number (SSN) and annual number of spotless days (NSD), 1848–2016 (Continued).

Year	SSN	NSD	Comment
1991	203.3	0	
1992	133.0	0	
1993	76.1	0	
1994	44.9	19	
1995	25.1	61	
1996	11.6	165	SC23 SSN min, NSD max
1997	28.9	61	
1998	88.3	3	
1999	136.3	0	
2000	173.9	0	SC23 SSN max
2001	170.4	0	
2002	163.6	0	
2003	99.3	0	
2004	65.3	3	
2005	45.8	13	
2006	24.7	65	
2007	12.6	163	
2008	4.2	265	SC24 SSN min, NSD max
2009	4.8	262	
2010	24.9	44	
2011	80.8	1	
2012	84.5	0	
2013	94.0	0	
2014	113.3	1	SC24 SSN max
2015	69.8	0	
2016	39.9	26	

means missing days during year; NSD uncertain

A comparison of SSN min against NSD max is shown in Figure 2. Based on linear regression analysis, the relationship between the two parameters is inferred to be $y = 24.536 - 0.068x$, where y is SSN min, and x is NSD max. The inferred regression has a coefficient of correlation $r = -0.925$ and a coefficient of determination $r^2 = 0.856$, meaning that the inferred regression can explain about 85.6% of the variance in SSN min, based on NSD max being the independent variable. The inferred standard error of estimate is $se = 1.844$ units of SSN, and the inferred relationship has a confidence level $cl > 99.9\%$. Instead, based on Kendall's τ (Gibbons 1993), a nonparametric technique, the association between SSN min and NSD max is computed to be about $\tau = -0.829$, having a Z-statistic equal to about 4.308, suggesting a very strong association to exist between the two parameters. Also given in Figure 2 is the result of Fisher's exact test for a 2×2 contingency table (Everitt 1977), determined by the medians of SSN min and NSD max (respectively, the horizontal and vertical lines shown in Figure 2). Hence, the probability P of obtaining the observed distribution, or one more suggestive of a departure from independence (i.e., chance), is computed to be $P = 0.00124$, a highly statistically significant result. Therefore, by assuming an approximate size of NSD max for a SC in advance, one can estimate the approximate size of its SSN min based on the inferred linear regression. As an example, presuming that SC25 will have NSD max = 265 (like that of SC24), one infers that

there is a 90% probability that SSN min for SC25 will be about 6.5 ± 3.3. A larger NSD max suggests a lower SSN min, while a smaller NSD max suggests a larger SSN min.

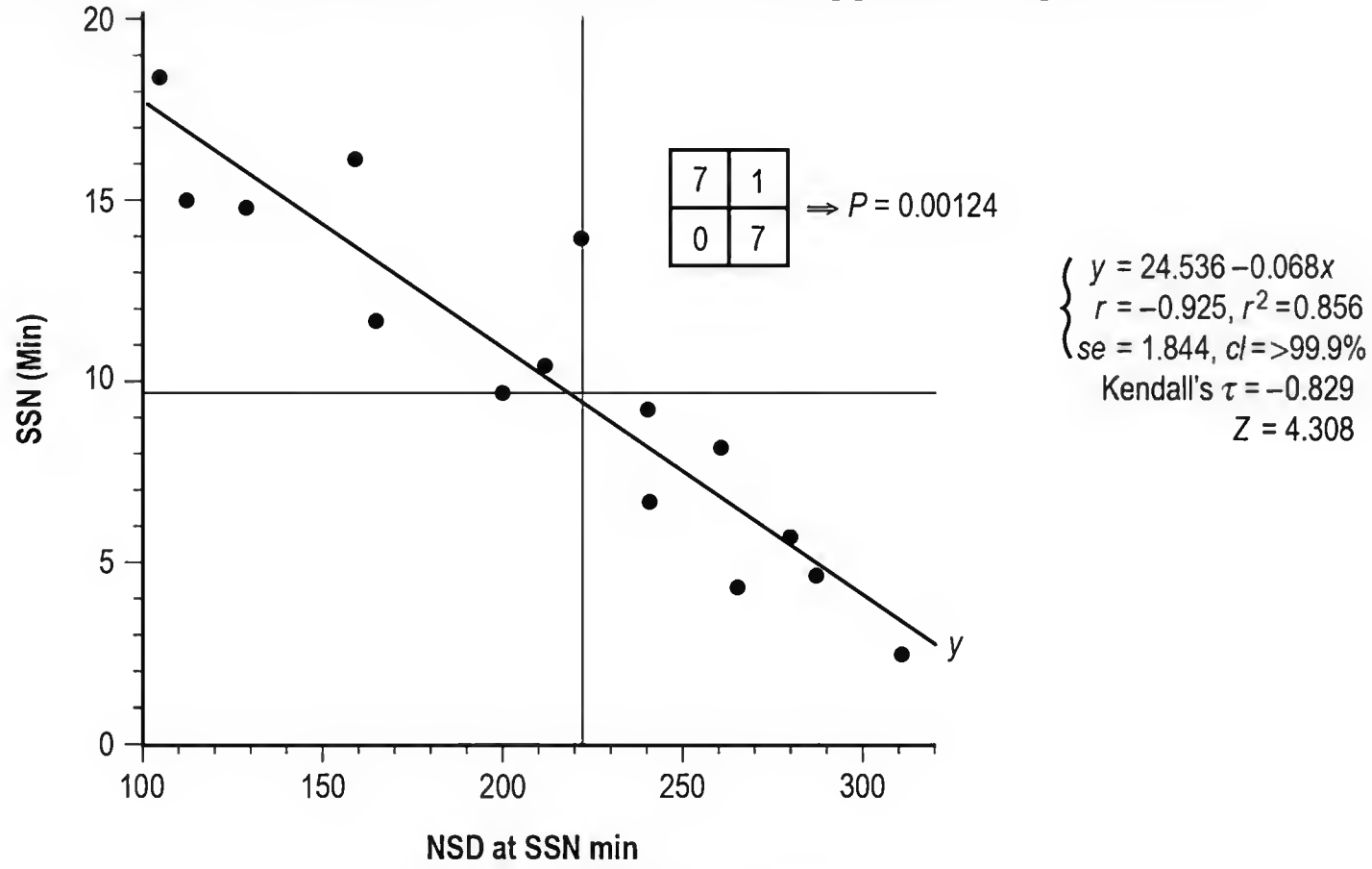

Figure 2. Scatterplot of sunspot number minimum (SSN min) versus the number of spotless days (NSD) at SSN min. The diagonal line is the inferred regression determined from linear regression analysis. The thin vertical and horizontal lines are the medians. The results of linear analysis and nonparametric analyses (both Kendall's τ and Fisher's exact test for 2 × 2 contingency tables) are given.

Figure 3(a) depicts NSD versus the elapsed time in years from SSN min (t) for t = –5 years to t = +3 years, in terms of the mean for SC10–SC24 (the thick line) and the greatest observed (GO) and least observed (LO) yearly values. On average, the mean NSD at t = 0 is 212.6 with GO = 311 (SC15) and LO = 105 (SC21). It should be noted that 10 of the 15 SCs have NSD ≥200 at t = 0, including SC10–SC17 and SC24; SC18–SC23 have NSD <200 at t = 0. For convenience, Table 2 is included to provide the yearly values, means, and standard deviation (*sd*) values for SC10–SC24 from t = –5 to t = +3. Figure 3(b) compares NSD for SC12 (dashed line), SC14 (thin line), and SC24 (thick line) for t = –5 to t = +3. All three SCs closely mimic each other from t = –1 to t = +3. Prior to t = –1, however, NSD for SC24 appears more closely to resemble that of SC14 rather than SC12. If SC14 can be used as a proxy for SC24, then this suggests that its cycle length will be about 12 years, inferring SSN min for SC25 in 2020. Figure 3(c) plots NSD versus elapsed time in years from SSN max (T) for T = 0 to T = +8 years, in terms of the mean for SC09–SC23 (the thick line) and the GO and LO yearly values. Also plotted are the three years for SC24 (filled circles) for T = 0 to T = +2 (i.e., 2014, 2015, and 2016; recall that NSD values post EM for cycle n are the NSD values for cycle n + 1, not cycle n). Noticeable is that at T = +2, the NSD for SC24 exceeds that of the GO value. The GO value for T = +3 years is 62 (SC12); so, if the year 2017 proves to be a year of rapid growth in NSD, then NSD might well exceed 62. For convenience, Table 3 is included to provide the yearly values, means, and *sd* values for SC09–SC23 at T = 0 to T = +8 and for SC24 at T = 0 to T = +2. (It should be noted that January 2017 had 10 spotless days.) Figure 3(d) compares NSD for SC12 (dashed line) and SC14 (thick line) for T = 0 to T = +8 and for SC24 (filled circles) for T = 0 to T

= +2. For $T = 0$ to $T = +2$, SC24 appears to more closely resemble that of SC12, suggesting that SSN min for SC25 might follow SC24's SSN max by about 6 years (i.e., 2020). (It should be noted that using SC14's NSD relative to SSN max as the template for SC24 suggests that SSN min for SC25 would be delayed until about 2022, inferring a cycle length of 14 years for SC24, a length never before seen in the modern era sunspot record.)

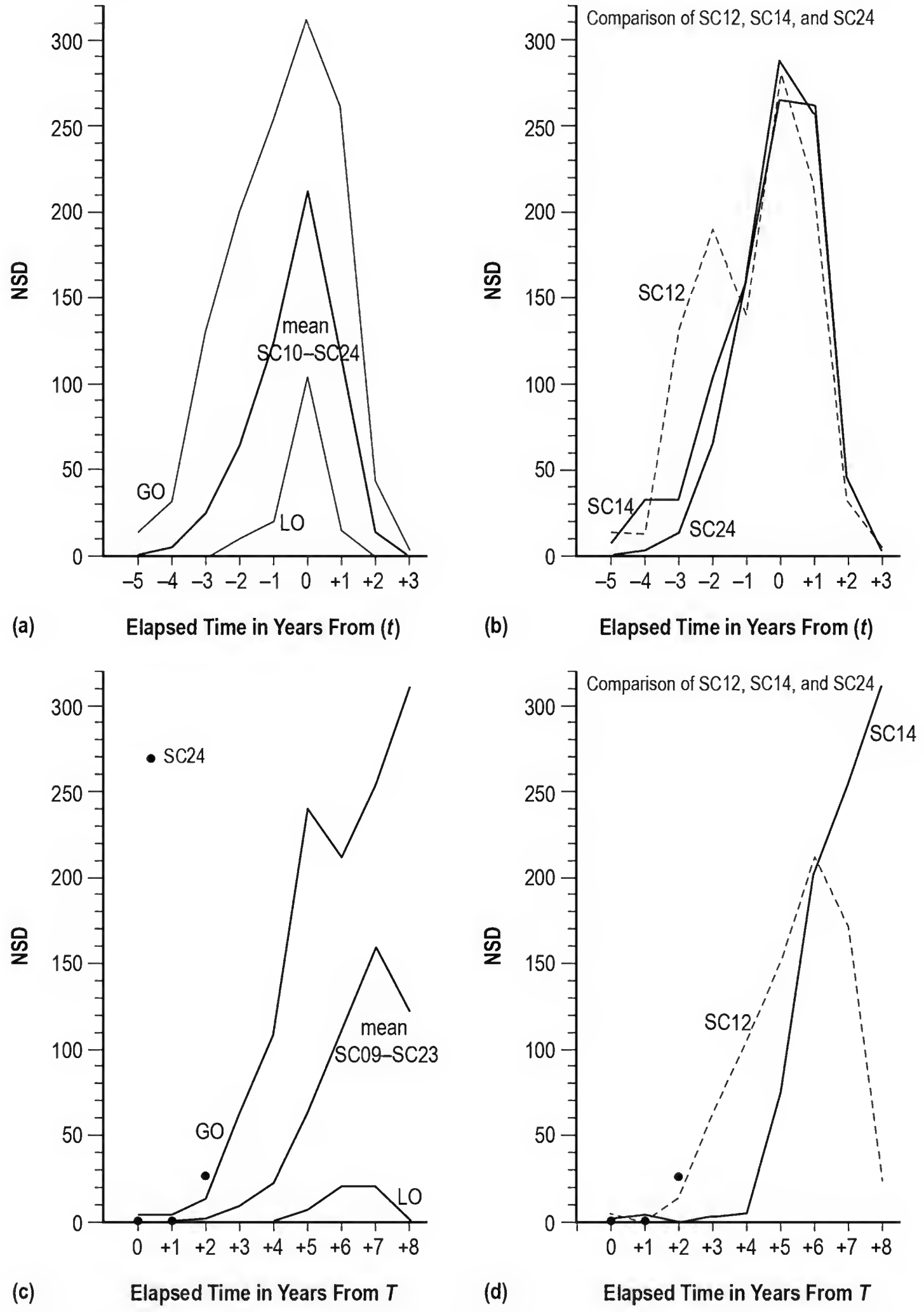

Figure 3. (a) The variation of the number of spotless days (NSD) in terms of the mean of sunspot cycles SC10–SC24, the lowest observed (LO) value and the greatest observed (GO) value for elapsed time (t) –5 years to +3 years relative to the elapsed time in years from

sunspot number minimum (SSN min) (*t*); (b) comparison of SC12, SC14 and SC24 number of spotless days (NSD) for *t* = –5 years to +3 years; (c) the variation of the NSD (Continued) in terms of the mean of SC10–SC24, the LO value and the GO value for elapsed time 0 to +8 years relative to the elapsed time in years from sunspot number maximum (SSN max) (*T*); and (d) comparison of SC12 and SC14 NSD for *T* = 0 to +8 years and SC24 NSD for *T* = 0 to +2 years.

Table 2. Number of spotless days (NSD) in vicinity of sunspot number minimum (SSN min) for elapsed time in years *t* = –5 to +3 years relative to SSN min occurrence (*t* = 0).

	NSD (*t*)								
Cycle	**–5**	**–4**	**–3**	**–2**	**–1**	**0**	**+1**	**+2**	**+3**
10	0	4	6	70	234	261	70	2	0
11	3	2	7	44	86	222	37	2	0
12	14	12	131	190	140	280	217	32	5
13	0	13	62	104	150	212	171	24	0
14	7	32	32	104	158	287	257	45	1
15	3	5	75	201	254	311	153	12	4
16	0	0	7	46	134	200	116	29	2
17	0	0	3	43	108	240	154	20	0
18	0	0	5	24	65	159	16	0	0
19	0	3	0	23	131	241	48	0	0
20	0	0	6	10	21	112	70	8	0
21	0	0	27	20	96	105	25	0	0
22	0	0	4	13	83	129	44	0	0
23	0	0	0	19	61	165	61	3	0
24	0	3	13	65	163	265	262	44	1
mean	1.8	4.9	25.2	65.1	125.6	212.6	113.4	14.7	0.9
sd	3.9	8.6	37.1	60.8	62.6	65.7	84.0	16.4	1.6

Table 3. Number of spotless days (NSD) from sunspot maximum (SSN max) for elapsed time in years *T* = 0 to +8 relative to SSN max occurrence (*T* = 0).

	NSD (*T*) for cycle *n* + 1								
Cycle	**0**	**+1**	**+2**	**+3**	**+4**	**+5**	**+6**	**+7**	**+8**
09	–	1	'	0	4	6	70	234	261
10	0	2	;	2	7	44	86	222	37
11	0	0	)	14	12	131	190	140	280
12	4	0	3	62	104	150	212	171	24
13	0	0		7	32	32	104	158	287
14	2	4	)	3	5	75	201	254	311
15	0	0	)	7	46	134	200	116	4
16	0	0	;	43	108	240	154	20	0
17	0	0	)	0	5	24	65	159	16
18	0	0	)	3	0	23	131	241	58
19	0	0	)	0	6	10	21	112	70
20	0	0	)	0	0	27	20	96	105
21	0	0	)	0	4	13	83	129	44
22	0	0	)	0	0	19	61	165	61
23	0	0	)	0	3	13	65	163	265
mean	0.4	0.5	.8	9.4	22.4	62.7	110.9	158.7	121.5
sd	1.2	1.1	.7	18.3	36.3	69.4	66.0	62.2	120.0
24	1	0	6	–	–	–	–	–	–

Figure 4 shows the variation of SSN using 12-month moving averages for the interval January 1989 through June 2016, spanning the declining portion of SC22 through the declining portion of SC24. The Em and EM are identified for each SC. Interesting is that all three SCs are double peaked, with maximum amplitude occurring with the first peak in SC22 but with the second peak in SC23 and SC24. Previously, Wilson (2015) showed that for SC24, the double peaking was related to hemispheric timing differences, with the first peak in SC24 being associated with the peak number of the northern hemispheric spots on the Sun and the second main peak being associated with the peak number of the southern hemispheric spots on the Sun. Across the top are the occurrences and values of NSD for SC23, SC24, and SC25, marking specific timing events and lengths. These events are FSD and LSD for each SC. From these events, one determines t_1, t_2, t_3, t_4, t_5, and t_6, where t_1 is the elapsed time in months from FSD (cycle n) to Em (cycle n), t_2 is the elapsed time in months from Em (cycle n) to LSD (cycle n), t_3 is the elapsed time in months from FSD (cycle n) to LSD (cycle n) or simply $t_1 + t_2$, t_4 is the elapsed time in months from LSD (cycle n) to FSD (cycle $n + 1$), t_5 is the elapsed time in months from FSD (cycle n) to FSD (cycle $n + 1$), and t_6 is the elapsed time from EM (cycle n) to FSD (cycle $n + 1$). For convenience, Table 4 is included to provide the Em, EM, FSD, and LSD dates for SC09–SC25 (when known), as well as the timing intervals $t_1 - t_6$ and the NSD for timing intervals $t_1 - t_3$.

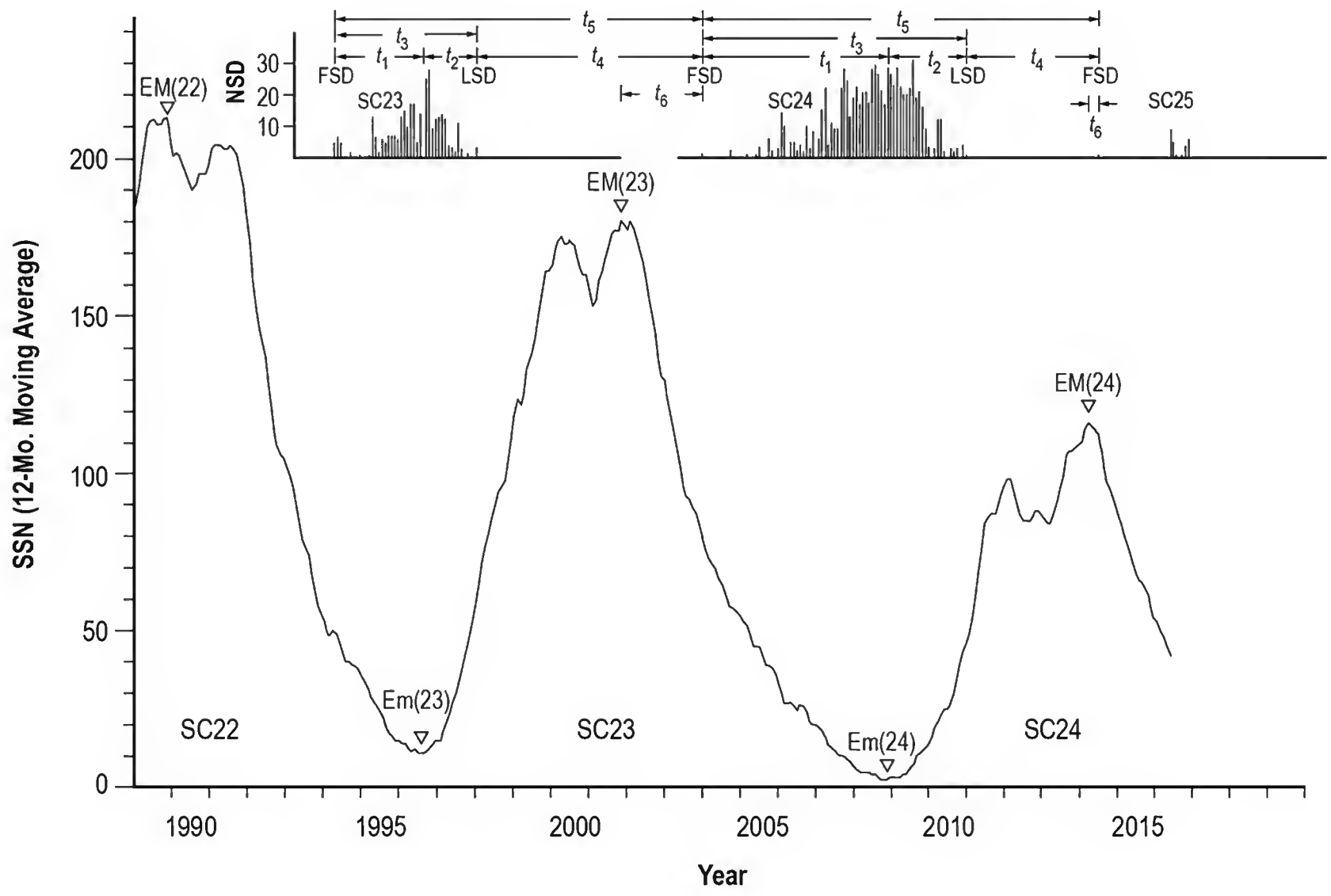

Figure 4. Bottom: The variation of 12-month moving average of monthly mean SSN for SC22–SC25. Epochs of minimum (Em) and epochs of maximum (EM) are identified. Top: The variation of monthly number of spotless days (NSD) for SC23–SC24. Also shown are t_1, t_2, t_3, t_4, t_5, and t_6, where t_1 is the elapsed time in months (t) from first spotless day (FSD) cycle n to epochs of minimum (Em) cycle n, t_2 is (t) from Em cycle n to last spotless day

(LSD) cycle *n*, t_3 is (*t*) from FSD (cycle *n*) to LSD (cycle *n*), t_4 (*t*) from LSD (cycle *n*) (Continued)
to FSD (cycle *n* + 1), t_5 is (*t*) from FSD (cycle *n*) to FSD (cycle *n* + 1), and t_6 is (*t*) from EM (cycle *n*) to FSD (cycle *n* + 1).

Table 4. First spotless day (FSD) and last spotless day (LSD) occurrences relative to the epochs of sunspot minimum (SSN min) (Em) and sunspot maximum (SSN max) (EM), number of months per timing interval, and NSD per timing interval.

Cycle	Em	EM	FSD	LSD	t_1	t_2	t_3	t_4	t_5	t_6	NSD (t_1)	NSD (t_2)	NSD (t_3)
09	1843-07	1848-02	–	–	–	–	–	–	–	15	–	–	–
10	1855-12	1860-02	1849-05?	1858-04	79	28	107	42	149	20	322	333	655
11	1867-03	1870-08	1861-10	1869-07	65	28	93	46	139	33	213	192	405
12	1878-12	1883-12	1873-05	1883-09	67	57	124	16	140	13	767	260	1027
13	1890-03	1894-01	1885-01	1891-12	62	21	83	47	130	22	599	137	736
14	1902-01	1906-02	1895-11	1905-07	74	42	116	15	131	8	641	289	930
15	1913-07	1917-08	1906-10	1916-10	81	39	120	42	150	32	721	297	1018
16	1923-08	1929-04	1920-04	1926-07	40	35	75	50	125	17	347	187	534
17	1933-09	1937-04	1930-09	1935-07	36	22	58	76	134	55	313	255	568
18	1944-02	1947-05	1941-11	1945-09	27	19	46	63	109	43	141	128	269
19	1954-04	1958-03	1950-12	1955-10	40	18	58	73	131	44	251	195	446
20	1964-10	1968-11	1961-11	1966-05	35	19	54	86	140	68	133	94	227
21	1976-03	1979-12	1973-07	1977-07	32	16	48	76	124	47	182	91	273
22	1986-09	1989-11	1983-11	1987-07	34	10	44	81	125	53	205	68	273
23	1996-08	2001-11	1994-04	1998-01	28	17	45	72	117	26	171	138	309
24	2008-12	2014-04	2004-01	2011-01	59	25	84	42	126	3	509	307	816
				mean	50.6	26.4	77.0	55.1	131.3	31.2	367.7	198.1	565.7
				sd	19.5	12.3	29.3	22.4	11.2	18.8	220.6	87.4	284.2
25	–	–	2014-07	–	29+	–	29+	–	29+	–	27+	–	27+

Note: t_1 = elapsed time in months from FSD (cycle *n*) to Em (cycle *n*).
t_2 = elapsed time in months from Em (cycle *n*) to LSD (cycle *n*).
t_3 = elapsed time in months from FSD (cycle *n*) to LSD (cycle *n*).
t_4 = elapsed time in months from LSD (cycle *n*) to FSD (cycle *n* + 1).
t_5 = elapsed time in months from FSD (cycle *n*) to FSD (cycle *n* + 1).
t_6 = elapsed time in months from EM (cycle *n*) to FSD (cycle *n* + 1).
NSD (t_1) = number of spotless days in t_1.
NSD (t_2) = number of spotless days in t_2.
NSD (t_3) = number of spotless days in t_3.

Figure 5 displays the cyclic variation of (a) t_1, (b) t_2, and (c) t_3. Concerning t_1, runs-testing (Langley 1971) suggests that the distribution of t_1 values is nonrandom at the 5% level of significance. Hence, one can divide the t_1 values into the following two groups: (1) those of longer t_1 values (i.e., long lead times between FSD and Em) and (2) those of shorter t_1 values (i.e., short lead times between FSD and Em). SC10–SC15 represent the longer lead time SCs (depicted by the open circles), and SC16–SC23 are the shorter lead time SCs (depicted by the filled circles). Longer lead time SCs average t_1 = 71.3 months, with sd = 7.8 months, while shorter lead time SCs average t_1 = 35.3 months, with sd = 4 months. The t_1 value for SC24 (depicted as an open square and equal to 59 months) appears to more closely resemble that of the longer lead time group. Certainly, its value falls within the 90% prediction interval of longer lead time SCs (71.3 ± 15.7 months) but not within the 90% prediction interval of shorter lead time SCs (35.3 ± 7.6 months). Therefore, it seems more likely that SC24 is best described as being a longer lead time SC rather than a shorter lead time SC. Furthermore, assuming that SC24 marks the beginning of a new string of longer lead time SCs (like SC10–SC15), one suspects that SC25's t_1 value might also be representative of the longer lead time SCs, suggesting that the Em for SC25 should not be expected until about April 2020 (i.e., July 2014 + 70 months). If true, then SC24's cycle length (i.e., Em cycle 24 to Em cycle 25) will be about 148 months, the same cycle length as was observed for SC23. (Previously, Zięba and Nieckarz (2014) have called SC10–SC15 'passive cycles' and SC16–SC23 'active cycles.')

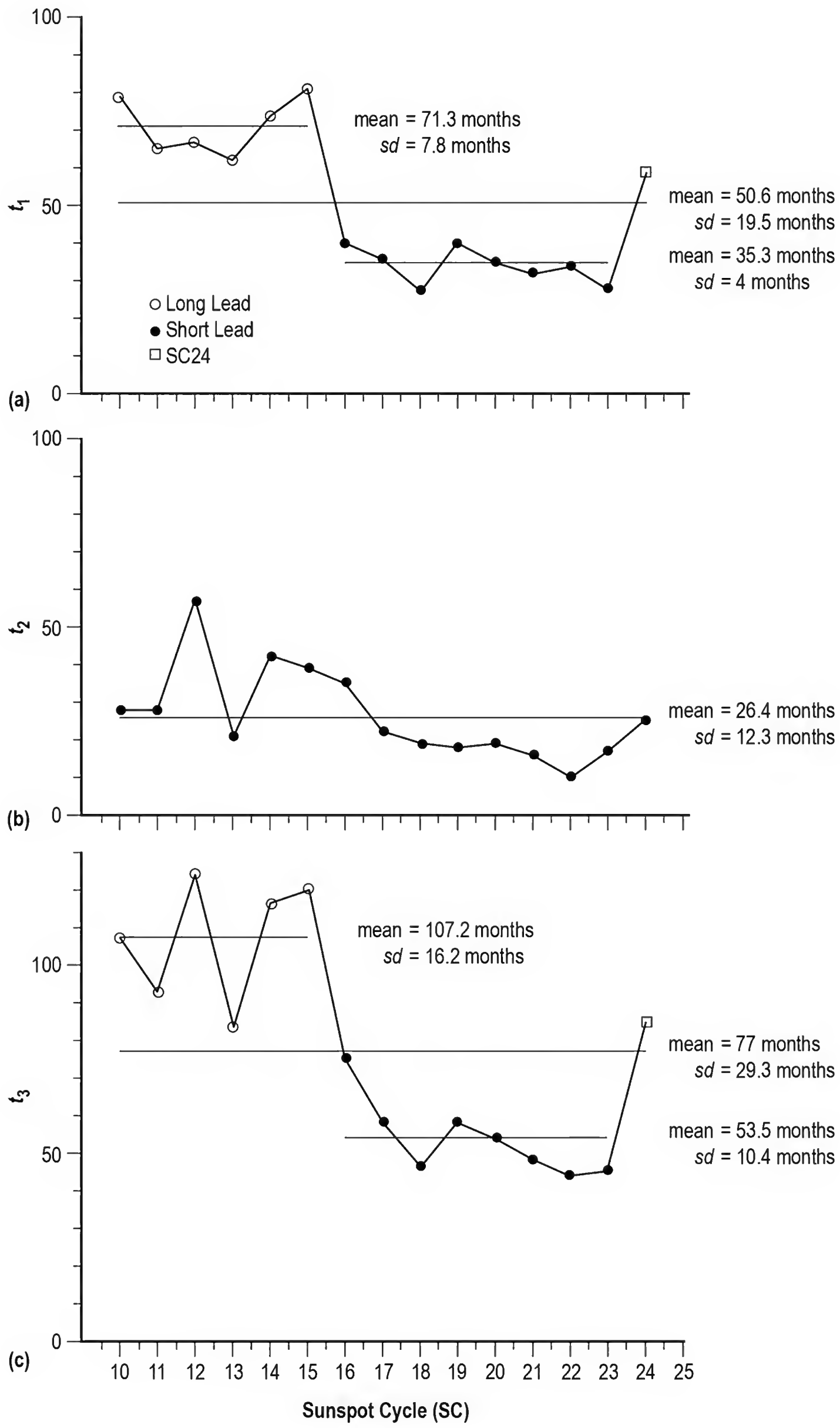

Figure 5. The cyclic variation of (a) t_1 (elapsed time in months from first spotless day (FSD) cycle *n* to epochs of minimum (Em) (cycle *n*)); (b) elapsed time in months (Continued)

from Em to the last spotless day (LSD); (t_2) and (c) elapsed time in months from FSD (cycle *n*) to FSD (cycle *n* + 1) (t_3). The overall means and standard deviations (*sd*) are given for each. Additionally, because runs-testing suggests that the distributions of t_1 and t_3 are nonrandom at the 5% level of significance, means and *sd* are also shown for the long lead (SC10–SC15) and short lead cycles (SC16–SC23). SC24's t_1 and t_3 values appear to resemble the t_1 and t_3 values for the long lead SCs.

Concerning t_2 (the elapsed time in months from Em for cycle *n* to LSD for cycle *n*), on average, its length is 26.4 months, with *sd* = 12.3 months. Presuming SC25's t_2 to be equal to 26.4 months, one surmises that SC25's LSD would not occur until about June 2022 (i.e., April 2020 + 26 months). (The 90% prediction interval for t_2 is 26.3 ± 21.7 months.)

Concerning t_3, like t_1, runs-testing suggests that its distribution is nonrandom at the 5% level of significance. Hence, t_3 can be divided into two groups as before with t_1. Presuming that SC24's t_3 is representative of the longer duration group (like SC10–SC15) and that it represents the start of another string of longer duration t_3 SCs, one suspects SC25's t_3 to be about 104 months in length, or that LSD for SC25 should not be expected until about July 2014 + 104 months, or about March 2023. If true, then this seems to suggest that SC25's t_2 will be longer than the 26-month average length (instead being about 45 months).

Figure 6 displays the cyclic variation of (a) t_4, (b) t_5, and (c) t_6. Concerning t_4, like t_1 and t_3, runs-testing suggests that its distribution is nonrandom at the 5% level of significance. The t_4 value for SC24 (depicted as an open square and equal to 42 months) appears to more closely resemble that of the t_4 values of SC10–SC15. Presuming that SC24 indeed marks the beginning of a new string of shorter t_4 cycles (like SC10–SC15), one expects SC25's t_4 value also to be representative of the shorter SCs, suggesting that the FSD for SC26 should not be expected until about 36 months following LSD for SC25 (or about March 2026 based on the LSD for SC25 being March 2023 from above).

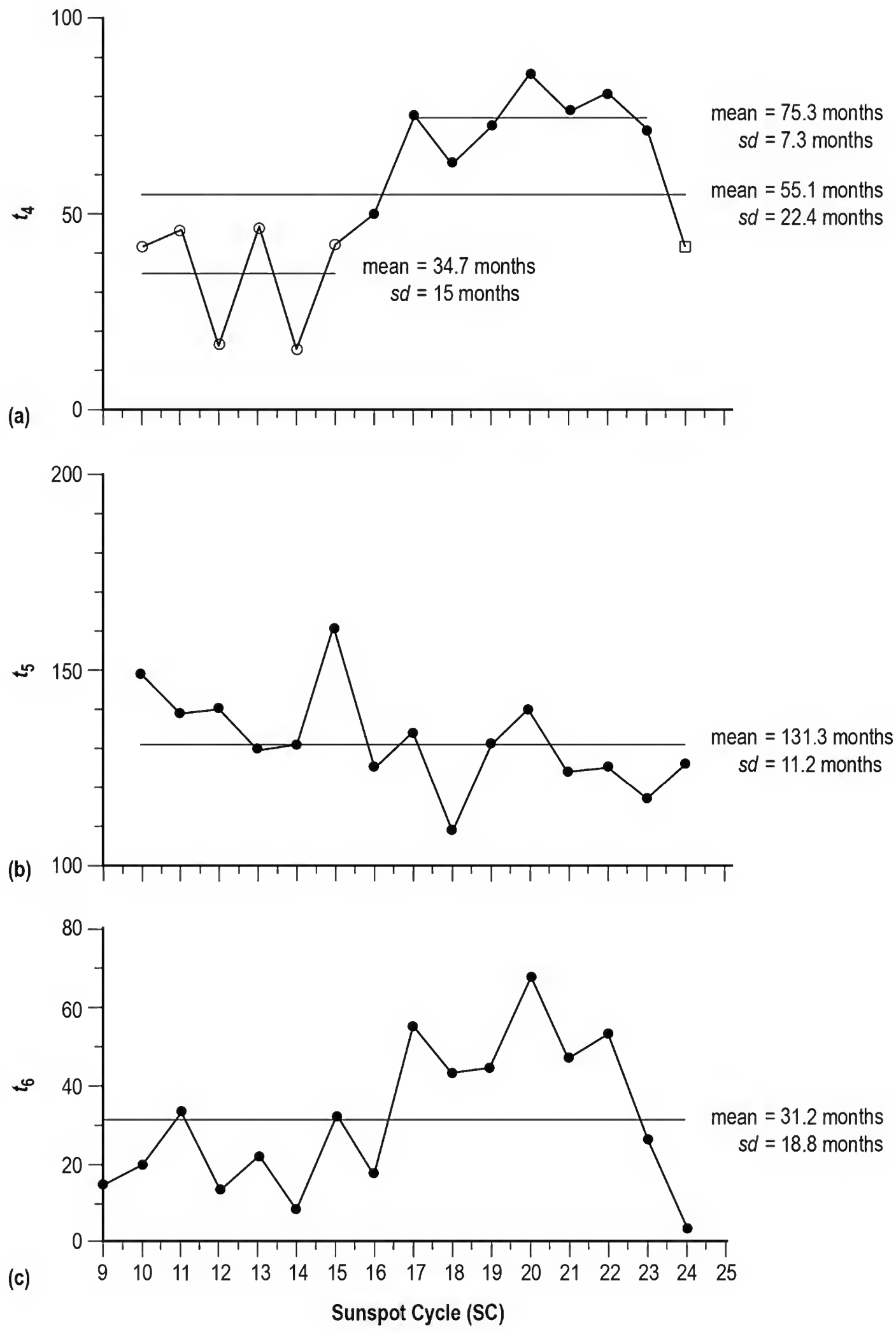

Figure 6. The cyclic variation of (a) t_4, (b) t_5, and (c) t_6. The overall means and standard deviations (*sd*) are given for each. Additionally, because runs-testing suggests that the distribution of t_4 is nonrandom at the 5% level of significance, the mean and *sd* for SC10–SC15 and SC17–SC23 are also shown. SC24's t_4 value appears to resemble the t_4 value for SC10–SC15.

Concerning t_5, its mean is 131.3 months, with sd = 11.2 months. Since FSD for SC25 is known to be July 2014, one doesn't expect FSD for SC26 to occur until about June 2025. (From above, FSD for SC26 is estimated to occur about March 2026, which, if true, suggests that SC25's t_5 would equal about 140 months. The 90% prediction interval for t_5 is 131.3 ± 19.7 months.)

Concerning t_6 (the elapsed time in months from EM cycle n to FSD cycle n + 1), on average, it measures about 31.2 months, with sd = 18.8 months. For SC24 it measured only 3 months, the shortest t_6 value in the modern era of sunspot observations. Noticeable is that 10 of the 15 SCs have had $t_6 \leq 33$ months, spanning 3–33 months and averaging about 18.9 months (sd = 9.8 months). Only SC17–SC22 had $t_6 > 33$ months, spanning 43–68 months and averaging about 51.7 months (sd = 9.3 months). Presuming SC25 will have t_6 = 19 months, one expects EM for SC25 to occur about August 2024, based on the presumed occurrence of SC26's FSD in March 2026 (from the discussion above for t_4), or to occur about November 2023, based on the presumed occurrence of SC26's FSD in June 2025 (from the discussion above for t_5).

Figure 7 shows the cyclic variation of (a) NSD (t_1), (b) NSD (t_2), and (c) NSD (t_3). Concerning NSD (t_1), on average, it measures about 367.7 days, with sd = 220.6 days. NSD (t_1) values are found to be well above the long-term mean for SC12–SC15 and SC24. For these SCs, they have an average NSD (t_1) = 647.4, with sd = 101.6, whereas for SC10–SC11 and SC16–SC23 the average NSD (t_1) = 227.8, with sd = 77.1. (It should be noted that, through January 2017, SC25 has NSD (t_1) = 37. Obviously, NSD (t_1) for SC25 will continue to increase as time goes on, exceeding about 400 if SC25 is similar to SC12–SC15 and SC24, or being less than about 370 if SC25 is more like SC10–SC11 and SC16–SC23, where these limits represent the 95% prediction interval extremes (lower and upper, respectively) for the two groupings.)

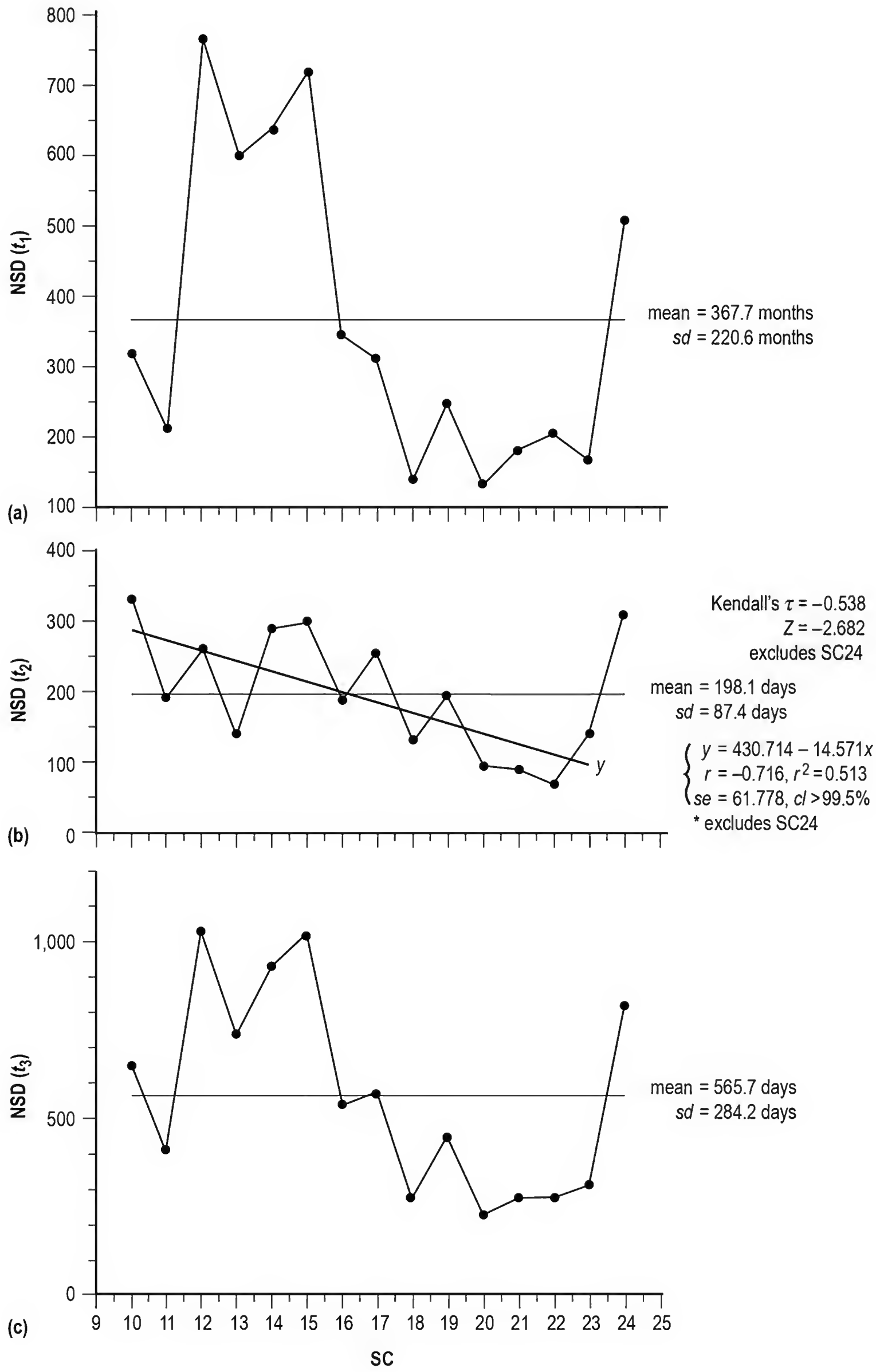

Figure 7. The cyclic variation of (a) the number of spotless days (NSD) during t_1 (NSD (t_1)), (b) the NSD during (t_2) (NSD (t_2)), and (c) the NSD during t_3 (NSD (t_3)). (Continued)

The overall means and standard deviation *sd* are given for each. Additionally, a statistically significant downward trend is noted for NSD (t_2) for SC10–SC23.

Concerning NSD (t_2), on average, it measures 198.1 days, with *sd* = 87.4 days. Interesting, however, is the apparent downward trend in NSD (t_2) values between SC10 and SC23. Based on linear regression analysis, the inferred relationship is described as $y = 430.714 - 14.571x$, where y is NSD (t_2), and x is SC number. The inferred regression has $r = -0.716$, $r^2 = 0.513$, *se* = 61.778, and *cl* >99.5%. Based on Kendall's $\tau = -0.588$ and $Z = -2.682$, one infers that the association between NSD (t_2) and SC is statistically important at the 2% level of significance. It is apparent, however, that SC24's NSD (t_2) value fails to adhere with the inferred trend (i.e., it is a statistical outlier), being about 3.7 *se* greater than what the inferred regression predicts (307 observed versus 81 from the inferred regression).

Concerning NSD (t_3), on average it measures 565.7 days, with *sd* = 284.2 days, having a cyclic behavior that mimics that of NSD (t_1). For SC12–SC15 and SC24, NSD (t_3) averages about 905.4 days, with *sd* = 127.2 days, while for SC10–SC11 and SC16–SC23, it averages about 395.9 days, with *sd* = 149.4 days.

Figure 8 depicts the scatter plot of NSD (t_3) versus NSD (t_1). Clearly, a very strong linear correlation exists between the two parameters, one described as $y = 105.711 + 1.251x$, where y is NSD (t_3) and x is NSD (t_1). The inferred linear regression has $r = 0.971$, $r^2 = 0.944$, *se* = 70.491, and *cl* » 99.9%. Based on Kendall's $\tau_b = 0.900$ and $Z = 4.674$ (one uses Kendall's τ_b because there was one tie), the association is inferred to be highly statistically important (*cl* > 99.9%). Based on Fisher's exact test for the 2×2 contingency table, one finds the probability P of obtaining the observed distribution, or one more suggestive of a departure from independence, to be $P = 0.00016$. Hence, given the NSD (t_1), one can estimate the total NSD that are expected to occur in the vicinity bounding Em for a SC (i.e., between FSD and LSD).

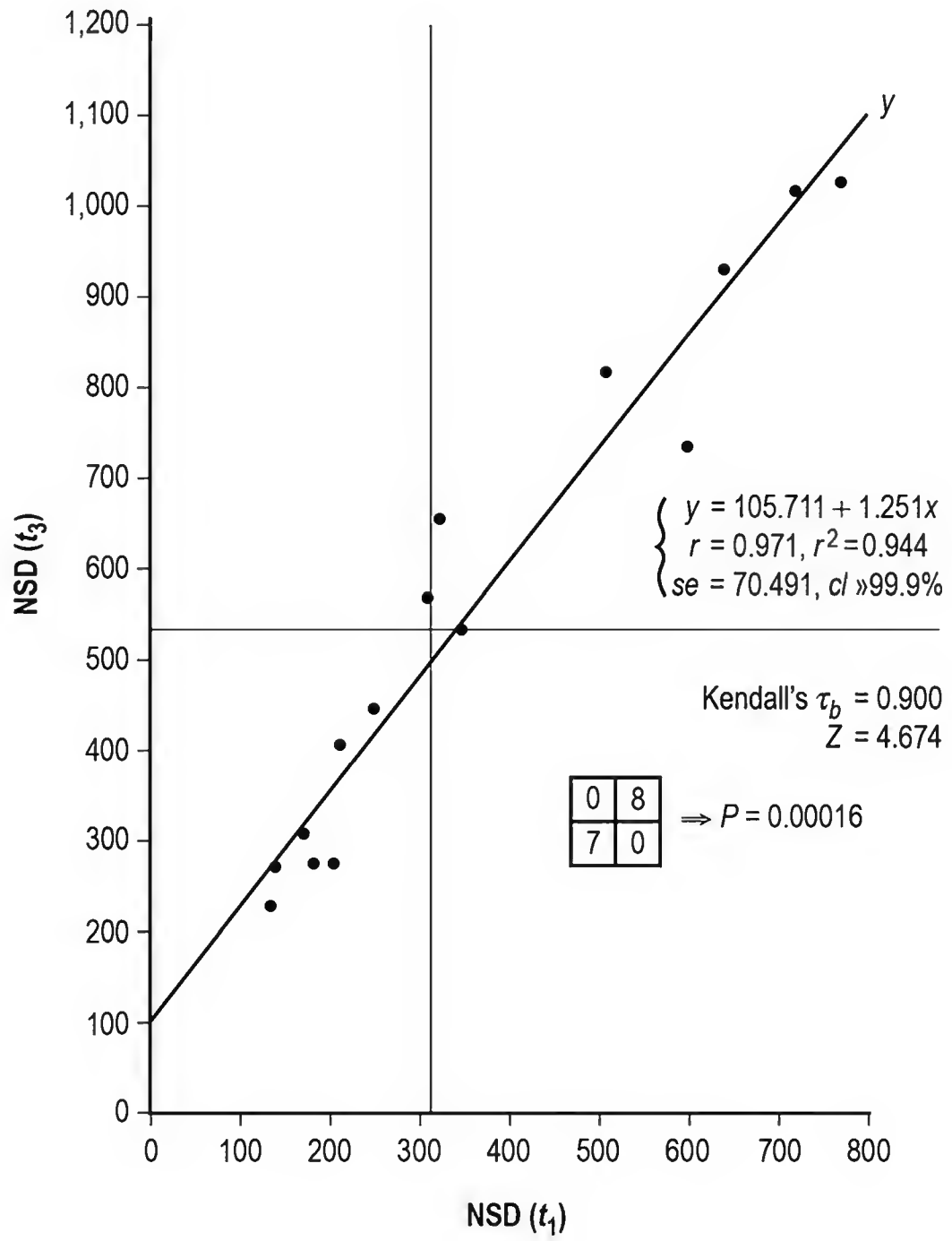

Figure 8. Scatterplot of number of spotless days (NSD) during t_3 (NSD (t_3)) versus the NSD during t_1 (NSD (t_1)). The results of linear regression analysis and nonparametric analyses are given.

Figure 9 plots (a) the mean and greatest observed (GO) monthly NSD value (based on SC10–SC24) relative to Em for elapsed time in months from $t = -36$ to $t = +24$ and (b) the number of SCs having monthly NSD >10 days (thin line) and monthly NSD >20 days (thick line) for the same interval $t = -36$ to $t = +24$. Clearly, at $t = -36$, only 2 of the 15 SCs (SC12 and SC13) had a monthly count of NSD >10 and none had NSD >20. It is not until $t = -14$ before the majority of SCs (8 of 15) had NSD >10 and not until $t = -4$ before monthly NSD >20 was observed for the majority of SCs. As yet (i.e., through January 2017), there has not been an occurrence of monthly NSD >10 for SC25. So, it seems likely that SC25's Em remains more than 36 months away, indicating Em for SC25 probably after January 2020. For convenience, Table 5 is included to provide monthly counts of NSD for SC10–SC24, the mean and *sd*, LO and GO monthly NSD values, and the number of SCs having monthly NSD >10 and >20.

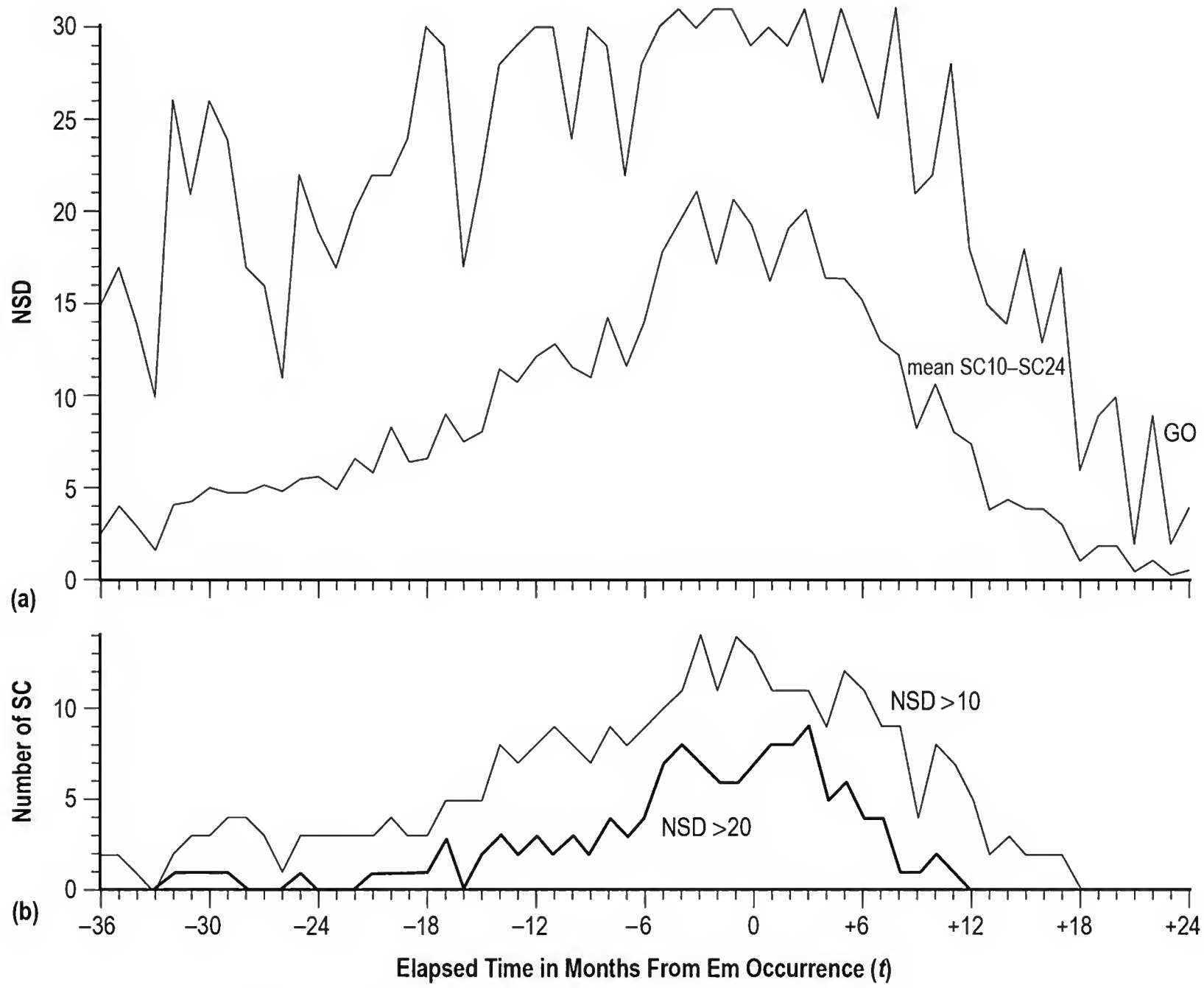

Figure 9. (a) The monthly variation of the number of spotless days (NSD) for elapsed time in months (*t*) relative to the epoch of sunspot minimum (Em) for *t* = –36 to +24 months, based on the mean of SC10–SC24 and the greatest observed (GO) values; (b) the number of sunspot cycles (SCs) having NSD >10 days per month (thin line) and >20 days per month (thick line).

Table 5. Monthly number of spotless days (NSD) for elapsed time from months (*t*) = –36 to *t* = +24 months relative to the epoch of sunspot minimum (SSN min) (Em) for sunspot cycles SC10–SC24 (Continued).

	SC																				
t	10	11	12	13	14	15	16	17	18	19	20	21	22	23	24	mean	sd	Least Observed	Greatest Observed	*n*>10	*n*>20
–36	0	0	15	15	2	5	1	1	0	0	0	0	0	0	0	2.6	5.2	0	15	2	0
–35	0	3	17	11	10	10	4	0	0	0	3	0	0	0	3	4.1	5.4	0	17	2	0
–34	0	0	9	5	4	4	0	1	0	0	3	0	4	0	14	2.9	4.1	0	14	1	0
–33	2	0	8	0	1	1	0	1	0	0	1	0	0	0	10	1.6	3.1	0	10	0	0
–32	1	0	26	4	7	19	0	4	0	0	0	0	0	0	0	4.1	7.9	0	26	2	1

Table 5. Monthly number of spotless days (NSD) for elapsed time from months (*t*) = –36 to *t* = +24 months relative to the epoch of sunspot minimum (SSN min) (Em) for sunspot cycles SC10–SC24 (Continued).

	SC																				
t	10	11	12	13	14	15	16	17	18	19	20	21	22	23	24	mean	sd	Least Observed	Greatest Observed	*n*>10	*n*>20
–31	0	2	21	11	2	16	0	1	0	0	0	0	0	0	4	4.2	6.6	0	21	3	1
–30	1	1	26	12	9	19	0	0	0	0	0	0	0	0	5	5.0	8.1	0	26	3	1
–29	1	0	11	11	24	13	3	0	0	0	0	0	0	0	2	4.7	7.1	0	24	4	1
–28	0	0	17	13	11	14	1	0	0	0	0	6	0	5	4	4.7	6.1	0	17	4	0
–27	1	1	14	4	16	5	6	11	3	0	1	7	0	6	2	5.1	5.0	0	16	3	0
–26	0	0	7	7	10	11	1	3	2	6	3	7	0	5	10	4.8	3.8	0	11	1	0
–25	0	0	15	12	8	22	0	10	1	9	0	2	0	0	3	5.5	6.9	0	22	3	1
–24	0	2	19	12	10	19	5	0	0	0	0	1	8	0	8	5.6	6.8	0	19	3	0
–23	6	2	7	11	13	17	4	5	1	0	1	0	4	2	0	4.9	5.2	0	17	3	0
–22	8	2	8	17	14	20	7	7	0	0	4	5	1	0	6	6.6	6.2	0	20	3	0
–21	7	2	15	10	3	22	9	2	2	0	0	0	0	0	15	5.8	7.0	0	22	3	1
–20	4	2	11	16	8	15	10	7	6	0	1	0	11	1	22	8.3	7.1	0	22	4	1
–19	8	1	2	20	9	24	10	11	5	2	2	0	0	0	4	6.5	7.3	0	24	3	1
–18	1	7	4	6	14	30	4	8	2	2	6	1	5	0	11	6.7	7.5	0	30	3	1
–17	5	10	16	21	21	29	3	12	1	2	0	0	7	1	9	9.1	9.0	0	29	5	3
–16	4	4	17	7	13	17	13	5	3	2	0	0	0	13	9	7.6	5.9	0	17	5	0
–15	6	12	4	11	8	21	14	1	3	7	0	4	1	7	22	8.1	6.8	0	22	5	2
–14	16	0	23	28	16	16	14	10	0	17	1	2	0	2	28	11.5	10.2	0	28	8	3
–13	0	1	10	15	29	16	13	14	4	11	3	9	7	6	24	10.8	8.1	0	29	7	2
–12	5	0	23	15	30	22	17	16	2	8	2	9	16	5	13	12.2	8.8	0	30	8	3
–11	17	2	22	17	20	30	12	6	1	8	1	18	14	7	19	12.9	8.6	1	30	9	2
–10	9	6	20	24	23	8	14	12	0	0	5	13	11	7	22	11.6	7.8	0	24	8	3
–9	6	3	15	17	30	21	9	6	0	14	1	9	11	7	17	11.1	8.1	0	30	7	2
–8	21	9	29	11	18	27	11	12	9	9	8	0	24	6	20	14.3	8.4	0	29	9	4
–7	19	5	22	8	15	17	21	12	7	1	2	0	4	13	21	11.7	7.4	0	22	8	3
–6	21	13	18	13	28	22	23	9	3	9	7	7	6	15	17	14.1	7.3	3	28	9	4
–5	30	5	30	20	27	19	21	22	13	25	4	9	5	10	28	17.9	9.5	4	30	10	7
–4	25	15	31	27	28	29	13	21	10	22	10	6	9	17	29	19.5	8.5	6	31	11	8
–3	30	27	18	17	21	27	19	14	10	30	20	14	26	17	26	21.1	6.3	10	30	14	7
–2	9	31	28	16	16	31	14	24	6	26	11	16	5	5	21	17.3	9.2	5	31	11	6
–1	21	26	18	25	31	30	20	30	20	14	18	18	8	14	17	20.7	6.6	8	31	14	6

Table 5. Monthly number of spotless days (NSD) for elapsed time from months (*t*) = –36 to *t* = +24 months relative to the epoch of sunspot minimum (SSN min) (Em) for sunspot cycles SC10–SC24 (Continued).

	SC																				
t	10	11	12	13	14	15	16	17	18	19	20	21	22	23	24	mean	sd	Least Observed	Greatest Observed	*n*>10	*n*>20
0	26	12	29	17	20	25	29	15	27	24	15	5	18	0	28	19.3	8.9	0	29	13	7
1	30	20	26	20	28	30	4	23	12	28	10	2	2	25	26	16.4	11.9	2	30	11	8
2	19	24	26	16	17	27	3	28	29	29	6	6	5	28	23	19.1	9.7	3	29	11	8
3	30	26	31	23	30	21	9	30	26	14	2	7	17	9	28	20.2	9.8	2	31	11	9
4	17	18	17	10	20	27	24	21	10	10	4	24	7	12	27	16.5	7.4	7	27	9	5
5	31	20	24	14	25	23	29	8	13	24	4	0	19	13	20	16.5	9.6	0	31	12	6
6	22	16	20	2	28	24	22	18	5	12	13	3	2	13	20	15.3	7.8	2	28	11	4
7	20	13	12	9	22	21	25	10	5	15	8	3	0	12	22	13.1	7.6	0	25	9	4
8	17	9	15	12	18	21	17	4	2	15	4	15	0	4	31	12.3	8.4	0	31	9	1
9	21	7	12	7	4	1	5	17	6	0	10	6	7	3	19	8.3	6.3	0	21	4	1
10	22	13	12	11	17	19	0	12	4	3	9	6	9	2	21	10.7	6.9	0	22	8	2
11	15	5	10	3	28	15	1	13	3	18	3	2	0	11	16	8.2	6.2	0	28	7	1
12	17	3	12	5	9	14	0	18	3	11	3	7	0	2	9	7.5	5.9	0	18	5	0
13	4	0	7	2	0	15	0	11	1	4	7	4	0	0	3	3.9	4.5	0	15	2	0
14	14	3	6	0	11	9	0	11	2	4	3	2	0	1	0	4.4	4.7	0	14	3	0
15	18	2	5	0	2	12	8	11	1	3	4	0	0	0	3	3.9	4.0	0	18	2	0
16	13	10	2	0	6	2	9	0	0	1	0	4	0	0	12	3.9	4.8	0	13	2	0
17	0	0	4	1	6	0	17	0	1	1	2	0	0	3	12	3.1	5.0	0	17	2	0
18	6	1	0	0	0	0	2	4	4	3	0	0	0	0	2	1.1	1.5	0	6	0	0
19	6	0	5	0	0	1	6	9	1	0	1	0	0	0	0	1.9	3.0	0	9	0	0
20	9	0	0	0	10	0	0	6	0	0	0	0	0	0	3	1.9	3.5	0	10	0	0
21	0	0	0	2	0	2	0	0	0	0	0	0	0	0	2	0.4	0.8	0	2	0	0
22	0	0	0	0	0	9	2	1	0	0	1	0	0	0	3	1.1	2.4	0	9	0	0
23	0	0	2	0	1	0	1	0	0	0	0	0	0	0	0	0.3	0.6	0	2	0	0
24	0	0	1	0	1	0	1	0	0	0	0	0	0	0	4	0.5	1.1	0	4	0	0

In conclusion, based on annual averages, NSD max has always occurred at SSN min for SC10–SC24, inferring a very strong inverse linear correlation of the form $y = 24.536 - 0.068x$ and having $r = -0.925$ and $se = 1.844$ units of SSN. Hence, a large NSD max during SSN min indicates a smaller SSN min, while a small NSD max indicates a larger SSN min. Comparisons of NSD relative to Em and EM suggest that SC24's NSD behavior is quite similar to that experienced in SC12 and SC14, both in terms of size of NSD and timing. Hence, this seems to suggest that SC24 will be a long-period SC, having a minimum to minimum period of about 12 years. The FSD for SC25 occurred in July 2014, just 3 months following SC24's EM, an interval shorter than was observed for SC12 (13 months) and SC14 (8 months). Through December 2016, some 27 spotless days have been reported (an additional 10 have been reported in January 2017). The NSD occurring during the decline of SC24 (which are associated with the approaching SC25's minimum) will continue to increase over time. At present, it appears that SC25's SSN min remains more than 36 months away, since, as yet, there has been no occurrence of a monthly NSD >10 days per month.

LITERATURE CITED

Clette, F. and L. Lefèvre 2012. Are the Sunspots Really Vanishing? Anomalies in Solar Cycle 23 and Implications for Long-Term Models and Proxies, *Journal of Space Weather and Space Climate* 2, 9 pp.

Everitt, B. S. 1977. *The Analysis of Contingency Tables*, John Wiley & Sons, Inc., New York, 128 pp.

Gibbons, J. D. 1993. *Nonparametric Measures of Association*, 91(7), Sage, London, 97 pp.

Hady, A. A. 2013. Deep Solar Minimum and Global Climate Changes, *Journal of Advanced Research* 4(3), pp. 209–214.

Harvey, K. L. and O. R. White 1999. What is Solar Minimum? *Journal of Geophysical Research* 104 (A9), pp. 19,759–19,764.

Langley, R. 1971. *Practical Statistics Simply Explained*, 2nd ed., Dover, New York, pp. 322–330.

McCracken, K. G. and J. Beer 2014. Comparison of the Extended Solar Minimum of 2006–2009 with the Spoerer, Maunder, and Dalton Grand Minima in Solar Activity in the Past, *Journal of Geophysical Research: Space Physics* 119, pp. 2,379–2,387.

Mordvinov, A. V. and A. P. Kramynin 2010. Long-Term Changes in Solar Activity, Occurrence of Grand Minima, and Their Future Tendencies, *Solar Physics* 264, pp. 269–278.

Mőrner, N.-A. 2015. The Approaching New Grand Solar Minimum and Little Ice Age Climate Conditions, *Natural Science* 7, pp. 510–518.

Nielsen, M. L. and H. Kjeldsen 2011. Is Cycle 24 the Beginning of a Dalton-Like Minimum? *Solar Physics* 270, pp. 385–392.

Russell, C. T.; J. G. Luhmann; and L. K. Jian 2010. How Unprecedented a Solar Minimum was It? *Reviews of Geophysics* 48(RG2004), 16 pp.

Schwabe, H. 1844. Sonnenbeobachtungen im Jahre 1843, *Astronomy Nachrichten* 21(495), pp. 233–236.

Wilson, R. M. 1995. On the Use of 'First Spotless Day' as a Predictor for Sunspot Minimum, *Solar Physics* 158, pp. 197–204.

Wilson, R. M. 2015. Sunspot Cycle Characteristics Based on the Newly Revised Sunspot Number, *Journal of the Alabama Academy of Science* 86(3/4), pp. 203–221.

Wilson, R. M. and D. H. Hathaway 2005. On the Relation Between Spotless Days and the Sunspot Cycle, NASA/TP—2005–213608, NASA Marshall Space Flight Center, Huntsville, Alabama, 33 pp.

Wilson, R. M. and D. H. Hathaway 2006. On the Relationship Between Spotless Days and the Sunspot Cycle: A Supplement, NASA/TP—2006–214601, NASA Marshall Space Flight Center, Huntsville, Alabama, 64 pp.

Zięba, S. and Z. Nieckarz 2012. Sunspot Time Series – Relations Inferred From the Location of the Longest Spotless Segments, *Solar Physics* 278, pp. 457–469.

Zięba, S. and Z. Nieckarz 2014. Sunspot Time Series: Passive and Active Intervals, *Solar Physics* 289, pp. 2,705–2,726.

ILEAL INTERPOSITION SURGERY DID NOT PREVENT THE ONSET OF TYPE 2 DIABETES IN RATS

Ping Zhao[1,2] and April D. Strader[1]
[1]Department of Physiology, Southern Illinois University School of Medicine, Carbondale, Illinois 62901; [2]Department of Biology, University of North Alabama, Florence, AL 35632
Corresponding: Ping Zhao (pzhao1@una.edu)

ABSTRACT

Background: Bariatric surgeries are effective in resolving type-2 diabetes independent of body weight loss. We have used ileal interposition (IT) surgery, a special type of bariatric surgeries, to study the role of the lower intestine in metabolic improvement. The surgery effectively improved glucose tolerance after the rats were treated by low-dose streptozotocin (STZ). However, it is not known whether the surgery could have a similar effect if performed before STZ treatment. Methods: Fourteen male Long–Evans rats received either sham or IT surgery first and then were treated with STZ (35 mg/kg) eleven weeks after the surgeries. Body weight, food intake, body composition and glucose tolerance were measured before and after the surgery. Results: IT surgery improved glucose tolerance before STZ treatment. However, IT surgery did not delay the onset of diabetes as glucose tolerance was not improved four weeks after STZ treatment. No significant difference was found in either body weight or body composition during the experiment. Conclusion: IT surgery can improve glucose tolerance in euglycemic rats without STZ treatment, but IT surgery cannot prevent the onset of diabetes caused by low-dose streptozotocin (STZ).

INTRODUCTION

Surgical procedures referred to as Roux-en-Y in the USA and biliopancreatic diversion in Europe are effective in resolving type-2 diabetes (Sjostrom et al. 2004; Buchwald et al. 2004). Such surgeries produced restriction, malabsorption and increased stimulation of the distal (lower) small intestine (i.e., mainly ileum). The main effect of both restriction and malabsorption is to inhibit food intake and reduce body weight. Early and increased nutrient diversion to the ileum activates endocrine changes because the lower intestine has several unique characteristics. First, the ileum is a major site of producing gut peptides, such as glucagon like peptide-1 (GLP-1) and Peptide YY (PYY) from the enterocytes called "L" cells (Stanley et al. 2004). Second, the peptides, secreted from L cells in the ileum, slow gastrointestinal motility and gastric emptying, a phenomenon known as "ileal brake" (Spiller et al. 1984; Read et al. 1984). Third, 95% of bile acids are taken up at the ileum, and bile acids transporters are exclusively expressed in the ileum (Stelzner et al. 2000; Dawson et al. 2009). Also, bile acids have been shown to improve glucose tolerance both in vitro and in vivo (Thomas et al. 2009; Katsuma et al. 2005; Watanabe et al. 2006; Gerhard et al. 2013). These unique features of the ileum led us to propose the "hind-gut" hypothesis that an increased nutrient delivery to the lower small intestine, mainly ileum, results in the secretion of hormones or factors that act as mediators in diabetic improvement. To isolate the effects of lower intestinal stimulation in the absence of restriction and malabsorption, we utilized a novel surgical model called ileal interposition (or IT surgery).

IT surgery involves the relocation of a short portion of the lower intestine (10 cm in rats), primarily ileum, to a more proximal region at the beginning of the jejunum (Atkinson et al.

1982). The surgery is one type of metabolic/bariatric surgery, but it usually does not cause significant loss of body weight in rats (Cummings et al. 2010; Strader et al. 2009). Previous studies on human subjects with low BMI (below 30) showed improved glucose homeostasis and regression of dyslipidemia when IT surgery was combined with sleeve gastrectomy (De Paula et al. 2006; De Paula et al. 2010; De Paula et al. 2011). IT surgery also improved glucose tolerance and decreased insulin resistance in Long-Evans rats fed with either high-fat diet and STZ (Strader et al. 2005) or chow and STZ (Strader et al. 2009).

Although the remission of diabetes after IT surgery has been documented, there are only a few studies examining the effect of surgery on the prevention of the onset of diabetes. IT surgery can delay diabetes onset in UCD-T2DM (the University of California at Davis type-2 diabetes mellitus) rats (Cummings et al. 2010). Bariatric surgery, as compared with usual care, reduces the long-term incidence of type 2 diabetes by 78% in obese human subjects (Carlsson et al. 2012). However, no one has performed bariatric surgeries on healthy, non-diabetic rats or people to see if the surgeries could prevent the onset of diabetes. Therefore, we performed IT surgery on healthy, non-diabetic rats before the onset or induction of diabetes by STZ to determine if the procedure could delay or prevent the onset of diabetes.

METHODS

Timeline of Experiment

Fourteen male Long-Evans rats (about three months old, Harlan, Indianapolis, IN, USA) were provided with water and chow ad libitum during the experiment. The surgeries (as described below) were done at week 0. An EchoMRI was done (as described below) twice for each rat, one week before and six weeks after the surgeries. At eleven weeks after the surgeries, all rats were injected with streptozotocin (STZ), which is a nitrosourea analog and selectively induces pancreatic beta cell death by alkylation of DNA (Delaney et al. 1995; Elsner et al. 2000). A dose of 35mg/kg STZ intraperitoneally, which specifically destroys 80% of pancreatic beta cells, was used to create type 2 diabetes (Junod et al. 1969; Srinivasan et al. 2005). Oral Glucose Tolerance Test (OGTT) was done twice (as described below), nine weeks and fifteen weeks after the surgeries. OGTT coincided with two weeks before and four weeks after STZ treatment (Fig. 1). The rats were then sacrificed seventeen weeks after the surgeries. For each rat, body weight, food intake and glucose concentration were measured every day after STZ treatment.

Ileal Interposition Surgery

Rats were treated with either sham (n = 6) or ileal interposition (n = 8) surgery as described by Strader (Strader et al. 2009). Rats were anesthetized with isoflurane anesthesia (2%) during the procedure. Briefly, a midline abdominal incision was made and the caecum was externalized. Intestinal transections were made at 5 and 15 cm proximal to the ileocecal valve to isolate a 10-cm segment of ileum. A single anastomosis was made using 7-0 silk suture (Ethicon, Cincinnati, OH) at the site of the segment removal. The segment was laid aside and kept moist with warmed 0.9% saline while the remaining intestines were externalized to locate the Ligament of Treitz. The jejunum was transected 5 cm distal to the ligament of Treitz and the segment was interposed using anastomosis in an iso-peristaltic direction. The intestines were bathed in 0.9% saline and re-inserted into the abdominal cavity. Sham-operated rats were treated with three transections in the same locations as the ileal interposition group, which were immediately re-joined by anastomosis.

Oral Glucose Tolerance Test

The rats were not fed overnight for 16 hrs and then given an oral gavage of glucose (20% D-glucose; 1g/kg). After glucose ingestion, blood glucose in a blood sample from the rat tail was measured by handheld glucometers in duplicate (TheraSense Freestyle Glucometers) at 0, 15, 30, 45, 60 and 120 min.

EchoMRI

Body composition (fat and lean mass) was determined by nuclear magnetic resonance (EchoMRI-900 3-in-1, Echo Medical Systems, Houston, TX). Live conscious rats were inserted into an appropriate Plexiglas animal tube and placed into the EchoMRI machine.

Statistics

All statistics were performed with Prism Statistical Software, and significance was set as * $p < 0.05$. Body weight, food intake and blood glucose concentrations were analyzed by two-way ANOVA with repeated measures. Body composition (fat and lean mass) from EchoMRI was analyzed by *t*-test.

RESULTS

1. Effect of ileal interposition on body weight

Body weights for sham and IT surgery groups were not significantly different during the experiment (two-way ANOVA, $F = 0.42$, $DFn = 7$, $DFd = 84$, $P > 0.05$; Fig. 2). As we expected, before STZ treatment (at 11th week after surgery), both groups of rats kept increasing their body weights. After STZ treatment, both groups of rats had a trend of decreasing body weights. The statistical powers for ANOVA during the weeks were 0.06, 0.07, 0.13, 0.09, 0.11, 0.11, 0.07 and 0.07 at -1, 6, 9, 11, 12, 13, 14 and 15 weeks, respectively.

2. Effect of ileal interposition on body composition

Fat mass for sham and IT surgery groups was not significantly different either before the surgeries (*t*-test, $t = 1.81$, $DFn = 5$, $DFd = 7$, $P > 0.05$; Table 1) or after the surgeries (*t*-test, $t = 1.54$, $DFn = 5$, $DFd = 7$, $P > 0.05$; Table 1). Lean mass for sham and IT surgery groups was also not significantly different either before the surgeries (*t*-test, $t = 4.17$, $DFn = 5$, $DFd = 7$, $P > 0.05$; Table 1) or after the surgeries (*t*-test, $t = 1.50$, $DFn = 5$, $DFd = 7$, $P > 0.05$; Table 1).

3. **Effect of STZ treatment on food intake**

There was no significant difference in food intake between Sham and IT groups within thirteen days after STZ treatment (two-way ANOVA, $F = 0.02$, $DFn = 1$, $DFd = 120$; Fig. 3). The statistical powers during the weeks were 0.06, 0.13, 0.05, 0.23, 0.11, 0.06, 0.46, 0.05, 0.18, 0.07 and 0.1 at 3, 4, 5, 6, 7, 8, 9, 10, 11, 12 and 13 days after STZ, respectively. As we expected, the food intake of both Sham and IT groups increased from 17g/day to 40g/day after the STZ treatment (Fig. 3).

4. Effect of ileal interposition on glucose

The IT surgery group showed significantly improved glucose tolerance at the 60 min point during OGTT test (two-way ANOVA, $F = 2.39$, $DFn = 1$, $DFd = 60$, $P < 0.05$); however, no

significant difference was found at other time points (two-way ANOVA, F = 2.39, DFn = 1, DFd = 60, P > 0.05; Fig. 4a). However, no improved glucose tolerance was detected between Sham and IT after STZ treatment, which was also 15 weeks after the surgery (two-way ANOVA, F = 1.49, DFn = 1, DFd = 60, P > 0.05; Fig. 4b). The statistical powers for ANOVA were 0.285, 0.336, 0.11, 0.07, 0.05 and 0.07 at 0, 15, 30, 45, 60 and 120 minutes at 15th week after surgery, respectively.

DISCUSSION

"Ileal brake" has been proposed previously (Pironi et al. 1993; Spiller et al. 1984) and is associated with increased secretion of peptide hormones, including GLP-1 and PYY from L-cells located in the ileum. Increased secretion of these hormones may be responsible for the improved glucose tolerance (Strader 2006). The IT surgery has been shown to delay the onset of type-2 diabetes in University of California at Davis Type-2 Diabetes Mellitus (UCD-T2DM) rats. This delay of onset may be related to increased nutrient-stimulated secretion of GLP-1 (7–36) and PYY and improvements of insulin sensitivity, β-cell function and lipid metabolism (Cummings et al. 2010).

We examined whether ileal interposition (IT) surgery can prevent the development of diabetes in healthy, non-diabetic rats. As expected, IT surgery improved glucose tolerance before STZ treatment (Fig. 4a). However, IT surgery did not delay the onset of diabetes as glucose tolerance was not improved four weeks after STZ treatment (Fig. 4b). Our lab previously documented that IT surgery improves glucose tolerance in the same strain of rats (Long-Evans) fed with the same food (chow) (Strader et al. 2009). The only difference between the previous study and this study is which occurs first: STZ or IT surgery. It seems that IT surgery improves glucose tolerance in rats with STZ-induced diabetes, but not in healthy rats. Thus, our results suggest that IT surgery, a special type of bariatric surgery, on a healthy, non-diabetic person may not offer any protective effect from the onset of diabetes.

The mechanism for the lack of a protective effect of IT surgery on healthy rats is unknown. It has been shown that the "jejunized" ileum and ileum adaptation protects against obesity-related comorbidities following IT surgery (Kohli et al. 2010). The lack of a protective effect of IT surgery on the onset of diabetes might be related to adaptation of the interposed ileum. Because healthy Long-Evans rats do not have any glucose tolerance problem, the interposed ileum might be adapted in the nearby healthy jejunum. Therefore, the interposed ileum, if IT surgery occurs before STZ treatment, may not secrete any protective peptide hormones such as GLP-1 and PYY. By contrast, if IT surgery occurs after STZ treatment, the interposed ileum is close to the diabetic jejunum, which keeps activating the interposed ileum, "the brake", to secrete long-term protective hormones. Further studies could be PCR and western blot on the segments of the intestine to examine the gene adaptation and protein secretion levels. The limitations of the study are the small sample sizes of the experiment and the low statistical powers for the tests, and thus we emphasize that the negative results should be interpreted with caution.

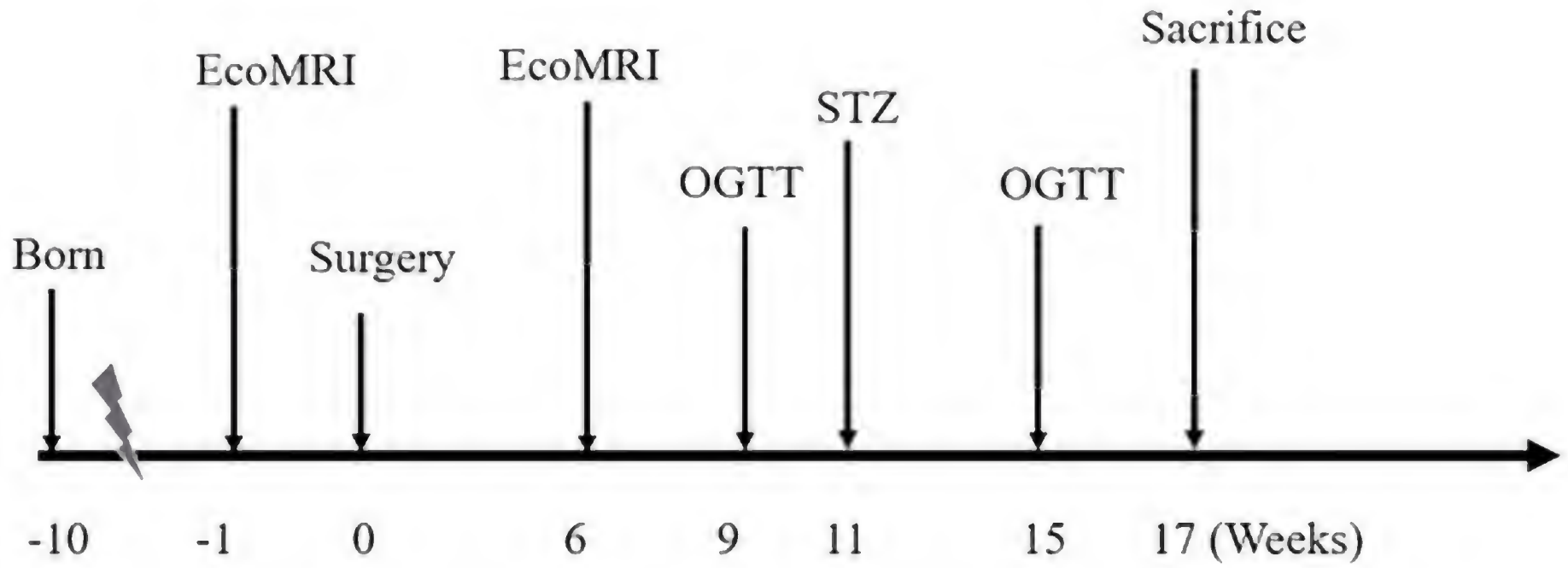

Figure 1: Timeline of experiment (OGTT = Oral Glucose Tolerance Test, STZ = streptozotocin)

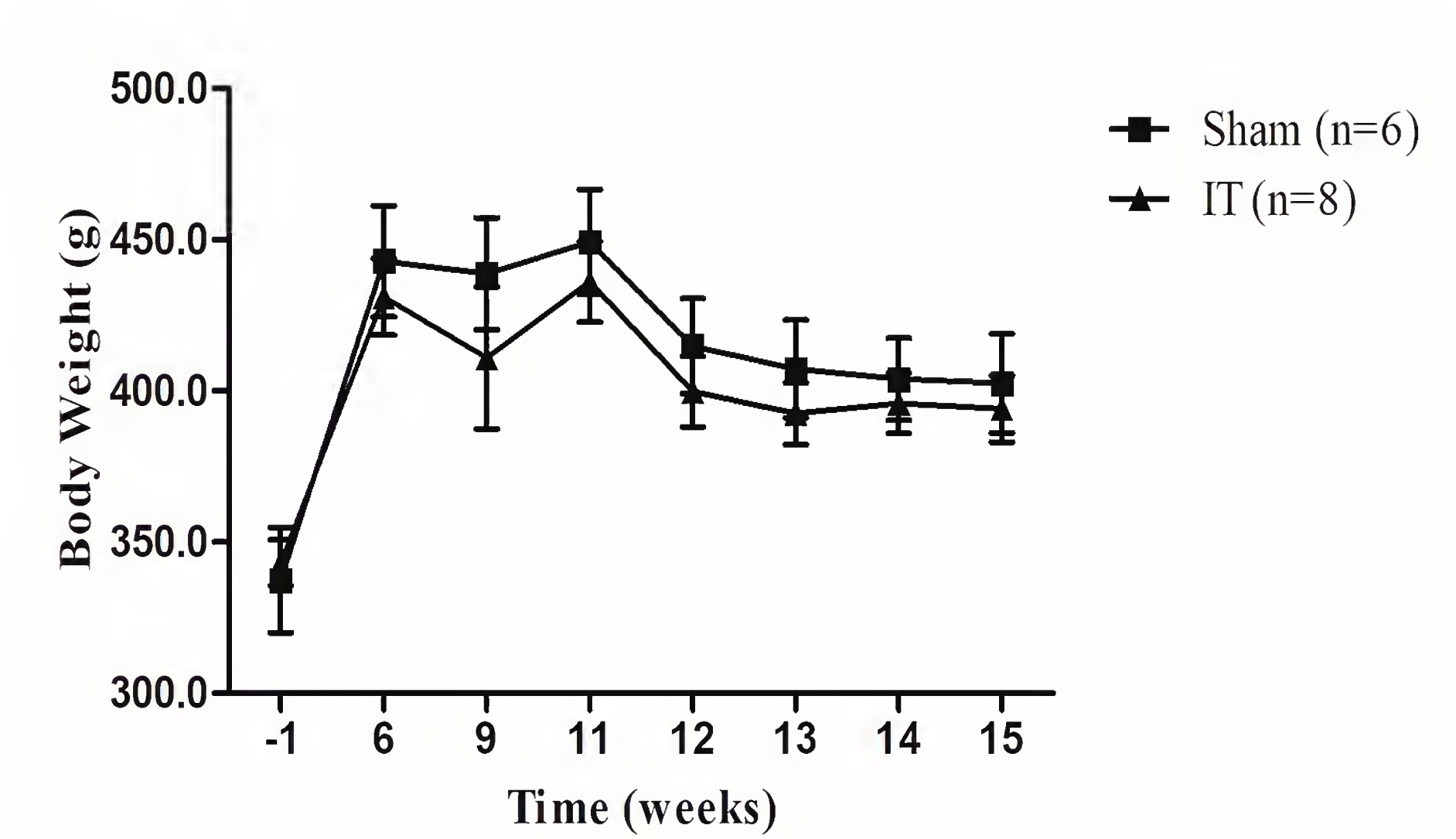

Figure 2: Body weight of Sham and IT rats before and after surgeries.

At 0^{th} week, rats received either Sham or IT surgery, as described in methods. Body weights for sham and IT surgery groups were not significantly different during the experiment (two-way ANOVA, $F = 0.42$, $DFn = 7$, $DFd = 84$, $P > 0.05$). The statistical powers during the weeks were 0.06, 0.07, 0.13, 0.09, 0.11, 0.11, 0.07 and 0.07 at -1, 6, 9, 11, 12, 13, 14 and 15 weeks, respectively. Error bar represents ± standard error of the mean.

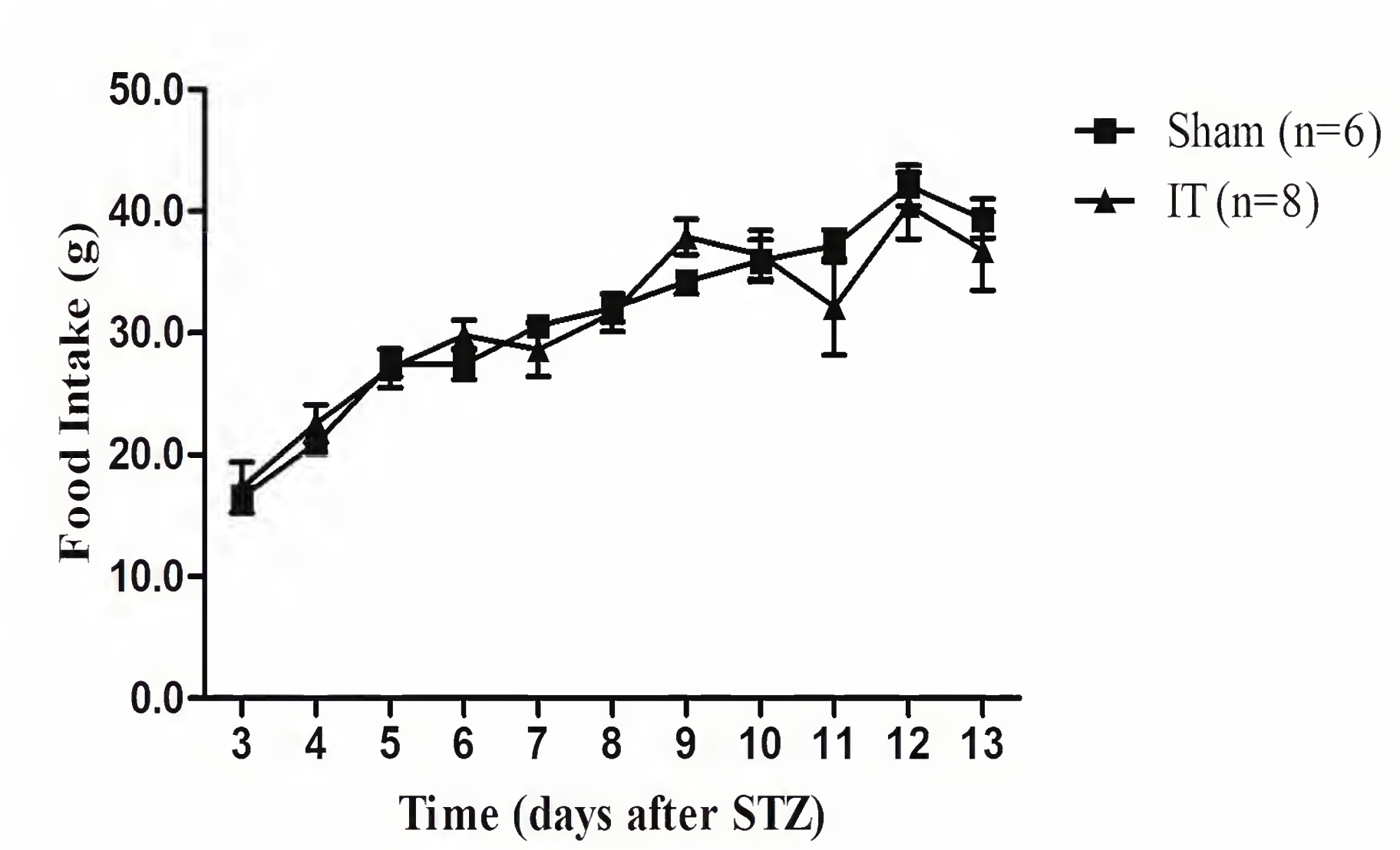

Figure 3: Food intake post STZ treatment (at 11th after surgery)

Food intake was measured daily after STZ treatment in rats for about fifteen days. Food intake amounts for sham and IT surgery groups were not significantly different during the experiment (two-way ANOVA, $F = 0.02$, $DFn = 1$, $DFd = 120$, $P > 0.05$). The statistical powers during the weeks were 0.06, 0.13, 0.05, 0.23, 0.11, 0.06, 0.46, 0.05, 0.18, 0.07 and 0.1 at 3, 4, 5, 6, 7, 8, 9, 10, 11, 12 and 13 days after STZ, respectively. Error bar represents ± standard error of the mean.

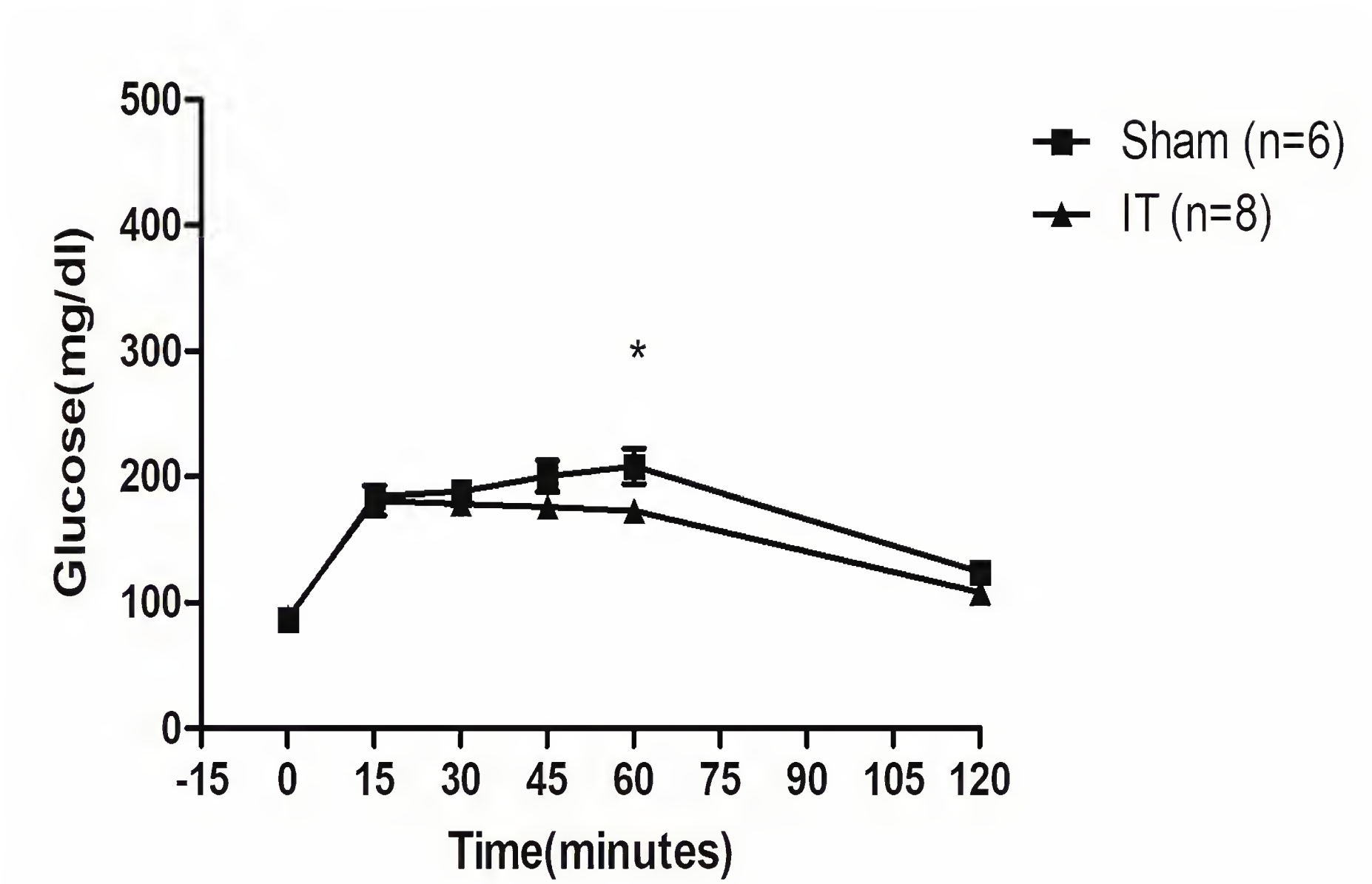

Figure 4a: Blood glucose levels two weeks before STZ treatment (at 9th week after surgery)

At 9th weeks following surgery, an oral glucose tolerance test was performed using 1g/kg oral glucose gavage. Glucose in tail blood was measured by handheld glucometers in duplicate at 0, 15, 30, 45, 60 and 120 min. The IT surgery group showed significantly improved glucose tolerance at 60 min, but not at other times (two-way ANOVA, $F = 2.39$, $DFn = 1$, $DFd = 60$, $P > 0.05$). Error bar represents ± standard error of the mean.

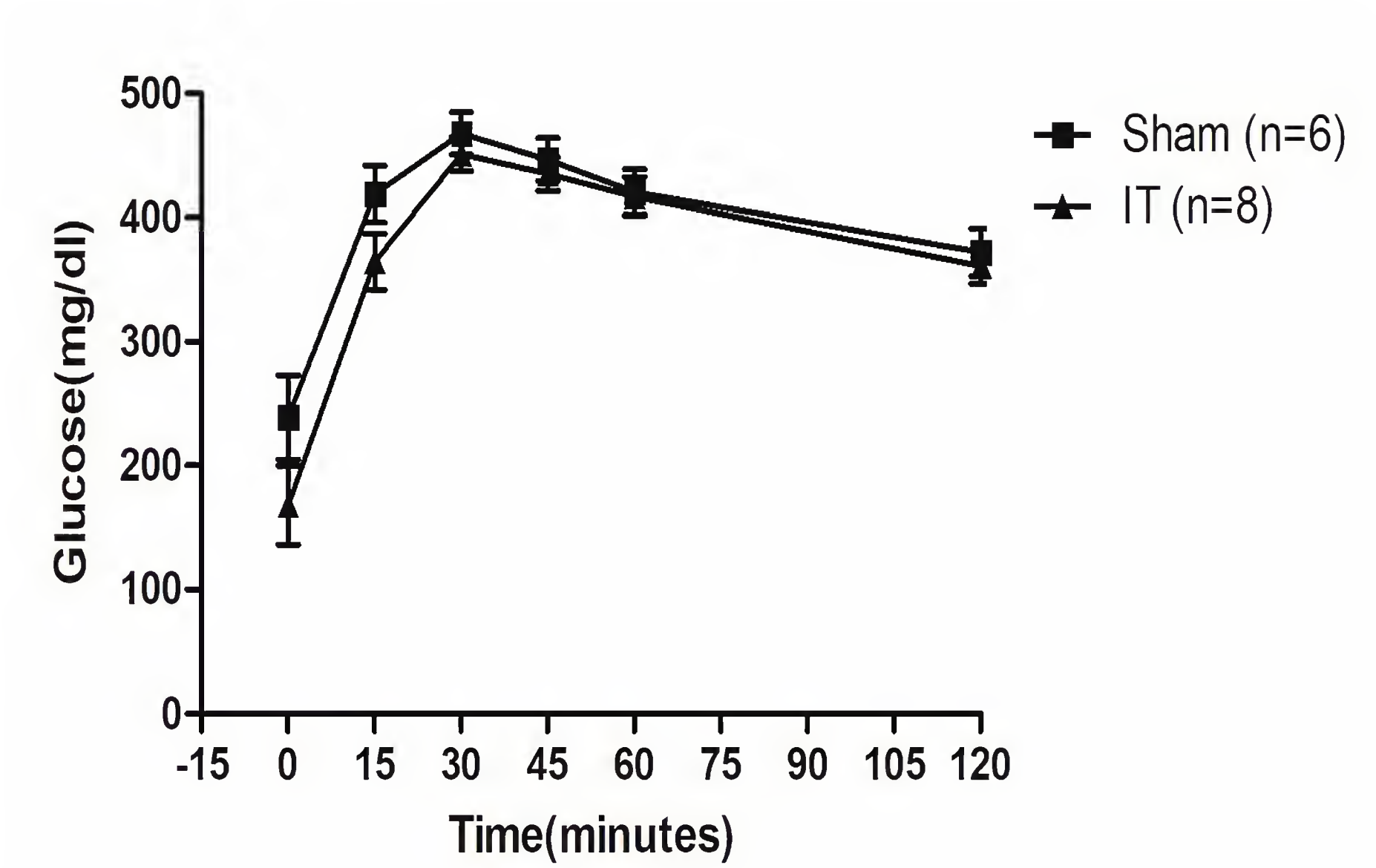

Figure 4b: Blood glucose levels four weeks after STZ treatment (at 15th week after surgery)

At 15th week following surgery an oral glucose tolerance test was performed using 1g/kg oral glucose gavage. Glucose levels for sham and IT surgery groups were not significantly different at 0, 15, 30, 45, 60 or 120 min (two-way ANOVA, $F = 1.49$, $DFn = 1$, $DFd = 60$, $P > 0.05$). The statistical powers were 0.285, 0.336, 0.11, 0.07, 0.05 and 0.07 at 0, 15, 30, 45, 60 and 120 minutes, respectively. Error bar represents ± standard error of the mean.

Table 1: Fat and lean mass (g)

		Sham (Mean ± SD)	IT (Mean ± SD)	P value	*t* value	Statistical power
Fat mass	Before surgery	26.91 ± 3.81	28.55 ± 2.83	0.37	1.81	0.21
	After surgery	50.6 ± 10.53	55.32 ± 13.08	0.48	1.54	0.09
Lean mass	Before surgery	258.8 ± 37.21	264.1 ± 18.22	0.73	4.17	0.17
	After surgery	309.43 ± 30.15	300.75 ± 24.65	0.56	1.50	0.14

ACKNOWLEDGEMENT

The present study was supported by funds to Dr. Strader from NIDDK – Challenge grant 1RC1DK086999-01. Also, funds from University of North Alabama College of Arts & Science grant for P. Zhao were used to complete the study.

LITERATURE CITED

Atkinson RL, Whipple JH, Atkinson SH, Stewart CC (1982) Role of the small bowel in regulating food intake in rats. American Journal of Physiology-Regulatory, Integrative and Comparative Physiology 242 (5):R429-R433

Buchwald H, Avidor Y, Braunwald E, Jensen MD, Pories W, Fahrbach K, Schoelles K (2004) Bariatric surgery. JAMA: the journal of the American Medical Association 292 (14):1724-1737

Carlsson LM, Peltonen M, Ahlin S, Anveden Å, Bouchard C, Carlsson B, Jacobson P, Lönroth H, Maglio C, Näslund I (2012) Bariatric surgery and prevention of type 2 diabetes in Swedish obese subjects. New England Journal of Medicine 367 (8):695-704

Cummings BP, Strader AD, Stanhope KL, Graham JL, Lee J, Raybould HE, Baskin DG, Havel PJ (2010) Ileal interposition surgery improves glucose and lipid metabolism and delays diabetes onset in the UCD-T2DM rat. Gastroenterology 138 (7):2437-2446. e2431

Dawson PA, Lan T, Rao A (2009) Bile acid transporters. Journal of lipid research 50 (12):2340-2357

De Paula AL, Macedo AL, Prudente AS, Queiroz L, Schraibman V, Pinus J (2006) Laparoscopic sleeve gastrectomy with ileal interposition ("neuroendocrine brake")—pilot study of a new operation. Surgery for Obesity and Related Diseases 2 (4):464-467

De Paula AL, Stival AR, Halpern A, DePaula CC, Mari A, Muscelli E, Vencio S, Ferrannini E (2011) Improvement in insulin sensitivity and B-cell function following ileal interposition with sleeve gastrectomy in type 2 diabetic patients: potential mechanisms. Journal of Gastrointestinal Surgery 15 (8):1344-1353

De Paula AL, Stival AR, Macedo A, Ribamar J, Mancini M, Halpern A, Vencio S (2010) Prospective randomized controlled trial comparing 2 versions of laparoscopic ileal interposition associated with sleeve gastrectomy for patients with type 2 diabetes with BMI 21–34 kg/m< sup> 2</sup>. Surgery for Obesity and Related Diseases 6 (3):296-304

Delaney CA, Dunger A, Di Matteo M, Cunningham JM, Green MH, Green IC (1995) Comparison of inhibition of glucose-stimulated insulin secretion in rat islets of Langerhans by streptozotocin and methyl and ethyl nitrosoureas and methanesulphonates: lack of correlation with nitric oxide-releasing or O6-alkylating ability. Biochemical pharmacology 50 (12):2015-2020

Elsner M, Guldbakke B, Tiedge M, Munday R, Lenzen S (2000) Relative importance of transport and alkylation for pancreatic beta-cell toxicity of streptozotocin. Diabetologia 43 (12):1528-1533

Gerhard GS, Styer AM, Wood GC, Roesch SL, Petrick AT, Gabrielsen J, Strodel WE, Still CD, Argyropoulos G (2013) A role for fibroblast growth factor 19 and bile acids in diabetes remission after Roux-en-Y gastric bypass. Diabetes care 36 (7):1859-1864

Junod A, Lambert AE, Stauffacher W, Renold AE (1969) Diabetogenic action of streptozotocin: relationship of dose to metabolic response. Journal of Clinical Investigation 48 (11):2129

Katsuma S, Hirasawa A, Tsujimoto G (2005) Bile acids promote glucagon-like peptide-1 secretion through TGR5 in a murine enteroendocrine cell line STC-1. Biochemical and biophysical research communications 329 (1):386-390. doi:10.1016/j.bbrc.2005.01.139

Kohli R, Kirby M, Setchell KD, Jha P, Klustaitis K, Woollett LA, Pfluger PT, Balistreri WF, Tso P, Jandacek RJ (2010) Intestinal adaptation after ileal interposition surgery increases bile

acid recycling and protects against obesity-related comorbidities. American Journal of Physiology-Gastrointestinal and Liver Physiology 299 (3):G652-G660

Pironi L, Stanghellini V, Miglioli M, Corinaldesi R, De Giorgio R, Ruggeri E, Tosetti C, Poggioli G, Morselli Labate A, Monetti N (1993) Fat-induced ileal brake in humans: a dose-dependent phenomenon correlated to the plasma levels of peptide YY. Gastroenterology 105 (3):733

Read N, McFarlane A, Kinsman R, Bates T, Blackhall N, Farrar G, Hall J, Moss G, Morris A, O'Neill B (1984) Effect of infusion of nutrient solutions into the ileum on gastrointestinal transit and plasma levels of neurotensin and enteroglucagon. Gastroenterology 86 (2):274-280

Sjostrom L, Lindroos AK, Peltonen M, Torgerson J, Bouchard C, Carlsson B, Dahlgren S, Larsson B, Narbro K, Sjostrom CD, Sullivan M, Wedel H (2004) Lifestyle, diabetes, and cardiovascular risk factors 10 years after bariatric surgery. N Engl J Med 351 (26):2683-2693. doi:351/26/2683 [pii]
10.1056/NEJMoa035622

Spiller R, Trotman I, Higgins B, Ghatei M, Grimble G, Lee Y, Bloom S, Misiewicz J, Silk D (1984) The ileal brake--inhibition of jejunal motility after ileal fat perfusion in man. Gut 25 (4):365-374

Srinivasan K, Viswanad B, Asrat L, Kaul C, Ramarao P (2005) Combination of high-fat diet-fed and low-dose streptozotocin-treated rat: a model for type 2 diabetes and pharmacological screening. Pharmacological research 52 (4):313-320

Stanley S, Wynne K, Bloom S (2004) Gastrointestinal satiety signals III. Glucagon-like peptide 1, oxyntomodulin, peptide YY, and pancreatic polypeptide. Am J Physiol Gastrointest Liver Physiol 286 (5):G693-697. doi:10.1152/ajpgi.00536.2003
286/5/G693 [pii]

Stelzner M, Hoagland V, Somasundaram S (2000) Distribution of bile acid absorption and bile acid transporter gene message in the hamster ileum. Pflügers Archiv 440 (1):157-162

Strader AD (2006) Ileal transposition provides insight into the effectiveness of gastric bypass surgery. Physiology & behavior 88 (3):277-282

Strader AD, Clausen TR, Goodin SZ, Wendt D (2009) Ileal interposition improves glucose tolerance in low dose streptozotocin-treated diabetic and euglycemic rats. Obesity Surgery 19 (1):96-104

Strader AD, Vahl TP, Jandacek RJ, Woods SC, D'Alessio DA, Seeley RJ (2005) Weight loss through ileal transposition is accompanied by increased ileal hormone secretion and synthesis in rats. American Journal of Physiology-Endocrinology And Metabolism 288 (2):E447-E453

Thomas C, Gioiello A, Noriega L, Strehle A, Oury J, Rizzo G, Macchiarulo A, Yamamoto H, Mataki C, Pruzanski M (2009) TGR5-mediated bile acid sensing controls glucose homeostasis. Cell metabolism 10 (3):167-177

Watanabe M, Houten SM, Mataki C, Christoffolete MA, Kim BW, Sato H, Messaddeq N, Harney JW, Ezaki O, Kodama T (2006) Bile acids induce energy expenditure by promoting intracellular thyroid hormone activation. Nature 439 (7075):484-489

Bench-top, Indirect-detection Experiments for ^{13}C-NMR Acquisition: Utilizing low-field NMR at a Primarily Undergraduate Institution

Collin Plourde, Alexandra MacLean, Taylor Clark, Paul A. Wiget. Chemistry and Biochemistry Department, Samford University, Birmingham, AL 35229. Corresponding: Paul Wiget (pwiget@samford.edu)

INTRODUCTION

In order to publish an article containing the synthesis of new molecules in a peer-reviewed research journal, accurate and reproducible NMR data must be obtained.[1] For many Primarily Undergraduate Institutions (PUIs), obtaining or allocating infrastructure and resources for the acquisition and maintenance of a high-field NMR is impractical.[2] Partnerships with local PhD-granting universities is the solution of choice for those research-oriented synthetic chemists working at PUIs. The challenge with these partnerships is often the time-cost of commuting to and from the location, the training of students, and the scheduling challenge associated with the walk-in nature of many instruments and monetary cost. In order to successfully utilize these partnerships, the principle investigator (PI) must often take time away from the high teaching load associated with PUIs. Any time spent at the distant NMR site without the students also subtracts from the valuable and essential mentoring time allotted to undergraduate researchers. Scheduling group field trips to the facility often complicate and lengthen the process further. Other obligations must also be rescheduled, reduced or eliminated altogether in order to arrive at the instrument in the early morning prior to graduate student use, or use the instrument on the weekend. These times are not ideal as troubleshooting is left up to the PI, with little help from the spectroscopist or instrumentation manager. These time-based challenges draw out the length of projects and often deny undergraduate students opportunities to perform synthesis-based research and the subsequent characterization adequate for undergraduate chemistry curriculum. Here we report the use of the MagriTek Spinsolve, a new, bench top, low-field NMR spectrometer, as it pertains to in-house, relatively low-concentration, ^{13}C-NMR acquisition of three different compounds, in conjunction with teaching advanced NMR techniques to undergraduate researchers for complex structure elucidation.

For many compounds that do not present a sufficiently resolved ^{1}H-NMR spectra due to low signal dispersion at low field instruments signal, a ^{13}C-NMR must be acquired for product verification. Due to the low natural abundance and hence concentration of ^{13}C nuclei (c) (see **Eq. 1**) in samples and low magetogyric ratio (γ) of the ^{13}C isotope (~4 times lower than ^{1}H), the direct detection of ^{13}C resonances is ~ 6000 time *less* sensitive than that of ^{1}H, and thus it's much more difficult to obtain a useful spectrum in a feasible amount of time.[3] As seen in Equation 1, and most well taught in undergraduate texts, the signal-to-noise ratio (S/N) is directly proportional to the cube root of the magnet strength, and square root of the number of scans (NS).

$$\frac{S}{N} = cT_2\gamma_{exc}\left(\frac{\sqrt[3]{B_0\gamma_{det}}\sqrt{ns}}{T}\right) \quad \textbf{Eq. 1}$$

The typical means of overcoming the poor S/N in ^{13}C acquisition is to increase the concentration of the sample (increase c), run the experiment for a longer time (increase ns), take the sample to a high-field instrument (increase B_0), or a combination of all these variables. However, if each variable is looked at individually, increasing the sample concentration is the simplest way to raise S/N, however this is not always possible when

dealing with costly chemicals or those with poor solubility, doubling *ns* only increases S/N by ~1.41 and doubling B_0 increases S/N by 1.25. Therefore, as the γ is a constant, the quickest way to increase S/N is by optimizing T_2 in the pulse sequence to match T_2 in the system, but this would require additional experiments and thus more time. However valuable, ultimately none of these factors affect the degree of dispersion.

Another option exists for the NMR-focused researcher: indirect detection (ID). In an indirect detection experiment, both the ^{13}C and ^{1}H nuclei are excited, but only the ^{1}H is detected. The observed free induction decay (FID) acquired allows observations of the neighboring ^{13}C nuclei. Thus, ^{13}C NMR data can be obtained through the ^{1}H nucleus. Consequently, the increase in S/N is greatly improved by detecting the more abundant ^{1}H nuclei, with the greater γ. This process is the basis for HSQC, HMQC, and HMBC NMR experiments. The direct detection HETCOR experiment also correlates the ^{13}C and ^{1}H nuclei, but is 30 times less sensitive due to limits on directly detecting the ^{13}C nucleus instead of the ^{1}H nucleus.[3] Therefore, until the recent availability of the MagriTek Spinsolve 2-channel NMR with ID protocols, no other option existed to increase S/N or overcome dispersion forces, and therefore obtain ^{13}C-NMR data of dilute samples at a PUI lacking a high-field instrument.

Indirect detection experiments work on the premise that the ^{13}C and ^{1}H are spin-coupled. It is the result of this coupling that is detected. One-bond coupling constants ($^{1}J_{CH}$) are ~145 Hz, and the two ($^{2}J_{CH}$) and three ($^{3}J_{CH}$) bond couplings are in the range of ~5-15Hz (See **Figure 1**). Karplus and others discovered $^{3}J_{CH}$ is dependent on cos(θ) and cos^2(θ), both of which are largest at 0°, and 180°, and smallest at 90°, and 270°.[4,5]

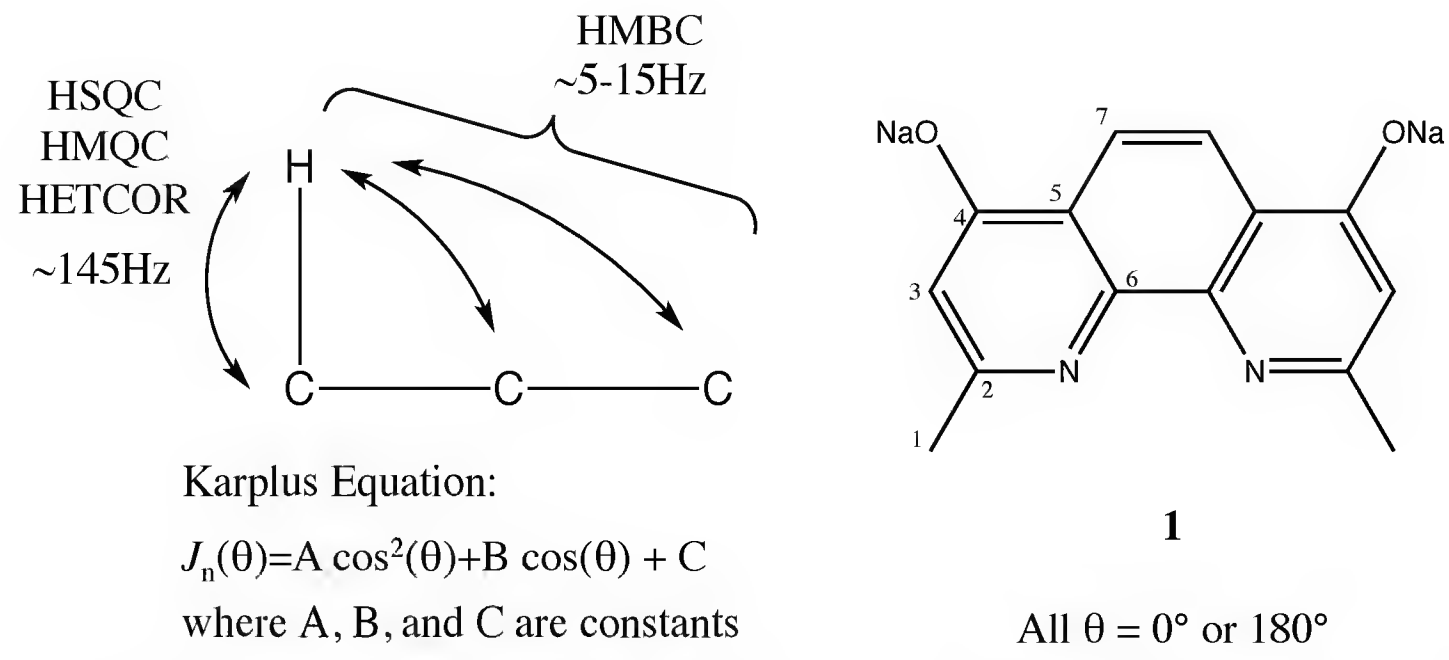

Karplus Equation:

$J_n(\theta)=A\cos^2(\theta)+B\cos(\theta)+C$

where A, B, and C are constants

1

All θ = 0° or 180°

Figure 1 1D coupling constants for different experiments (left), a compound that should be highly sensitive to 1D experiments (right).

Therefore, planar compounds would have the highest sensitivity in ID NMR experiments as all θ would be 0° or 180°. As the range of the coupling constants is an order of magnitude larger, the ID experiments run to detect the ~145 Hz are called the HSQC or HMQC. The ID experiment for the smaller, 5-15 Hz coupling is the HMBC. Consequently, in HSQC and HMQC experiments, $^{2}J_{CH}$ and $^{3}J_{CH}$ are not typically observed, and in the HMBC experiment the single bond coupling ($^{1}J_{CH}$) is not typically observed. Thus, adequate reference for such experiments should contain both single-bond and multiple-bond coupling, such as acetonitrile or ethanol, allowing both spectra to be referenced to the same scale. However, such a reference is unnecessary if, in a single spin-system solvent such as benzene, the analyte

contains an easily identifiable $^{2}J_{CH}$ or $^{3}J_{CH}$ coupling such as in sodium 2,9-dimethyl-1,10-phenanthroline-4,7-bis(olate) (**1**).

METHODS AND RESULTS

In our work we aimed to synthesize the known compound sodium 2,9-dimethyl-1,10-phenanthroline-4,7-bis(olate) (**1**).[6] This molecule has only 3 distinct proton signals, but has 7 distinct carbon signals. **Figure 2** shows a comparison of the 45Hz and 300MHz, direct-detection, ^{13}C-broadband decoupled NMR of **1** (20mg), 0.147M in D_2O, CH_3CH_2OH (20:1). Only the ethanol reference is visible, as it is ~5.5 times more concentrated than the sample, after 16283 scans (a). When the number of scans is increased to 29304 scans, signals for **1** begin to appear, though are not will resolved (b). It is clear that at this low concentration, the higher-field instrument must be used to obtain a viable spectrum (c).

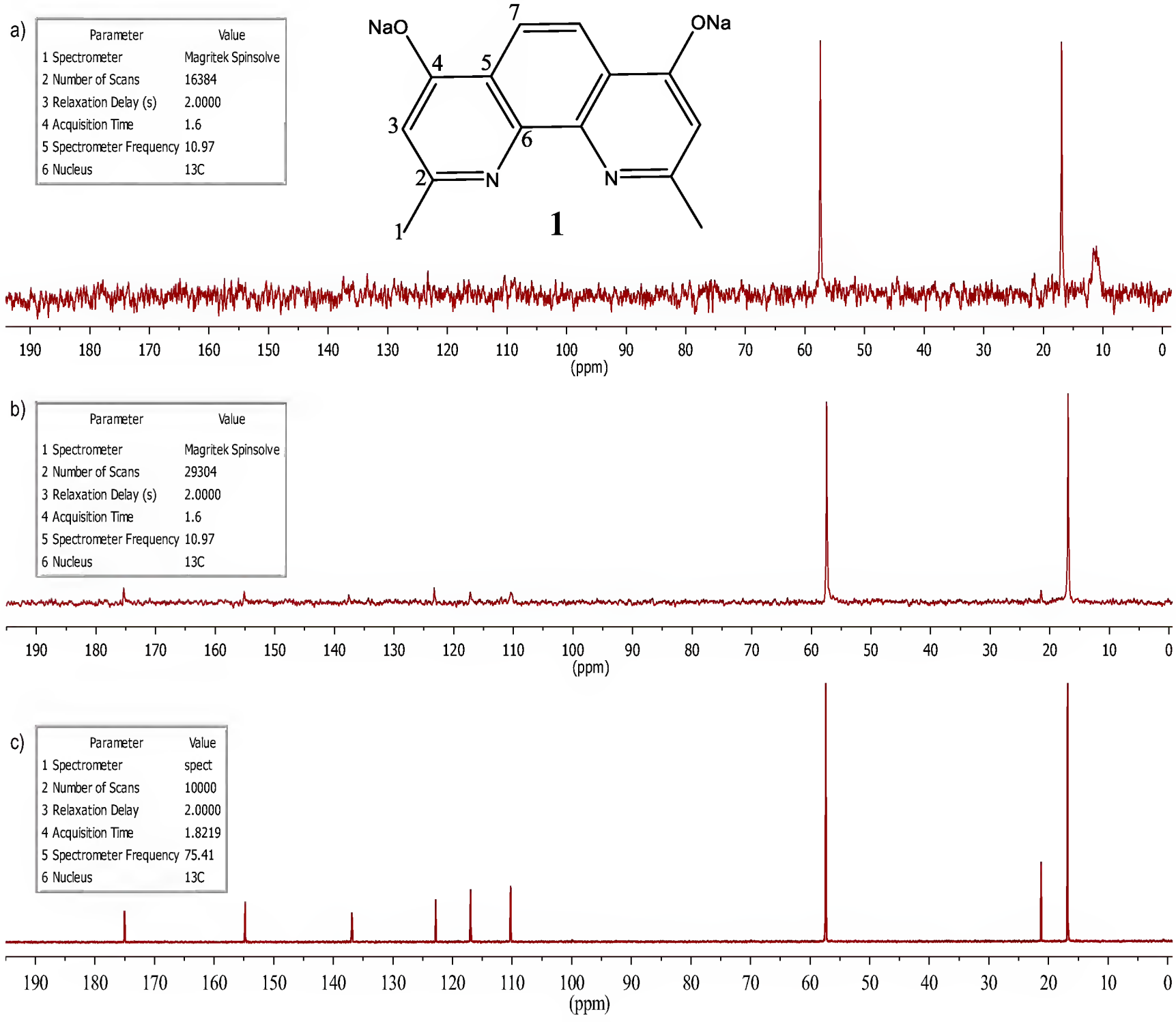

Figure 2 Comparison of broadband decoupled ^{13}C-NMR. A) 16384 scans on Bench-top NMR, B) 29304 scans on Bench-top NMR, c) 10000 scans on high-field (75MHz for ^{13}C) NMR.

When the HSQC and HMBC indirect protocols are used in sequence, referenced, and stacked (**Figure 3**), the ^{13}C data can be easily extracted with a high degree of confidence in two

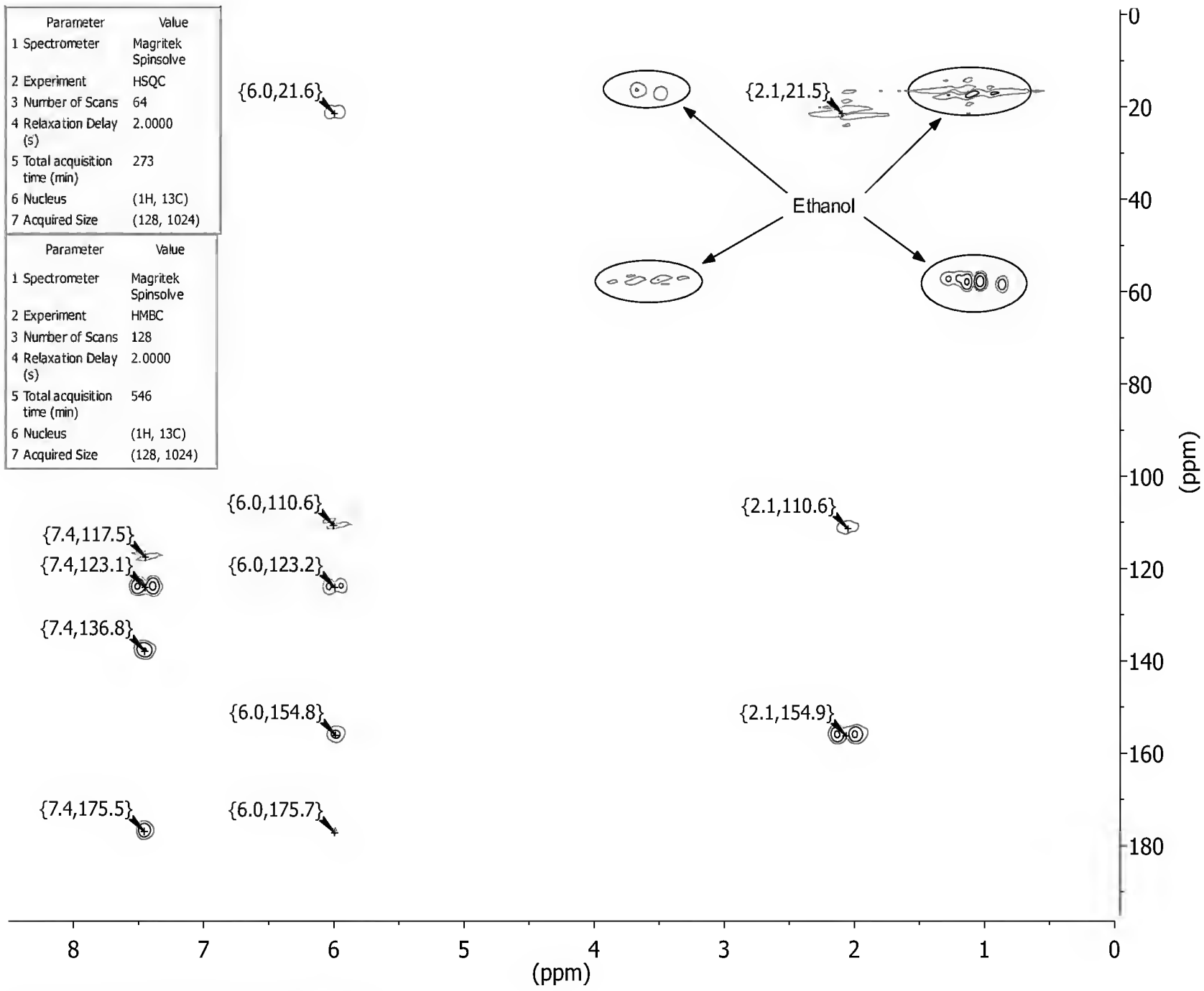

Figure 3 Stacked HSQC and HMBC of 1

sequential experiments totaling ~14hrs of instrument time. Additionally, as typical of such experiments, the carbons can now be assigned easily (**Table 1**), something not explicitly done in the literature.

When this technique is applied to another rigid system, where the dihedral angle are locked, but the system is non-planar, complications arise. We synthesized (1*R*,2*R*,5*S*,6*S*)-2,5-dimethyl-11-oxatricyclo[4.3.1.$1^{2,5}$]undec-3-en-10-one (**2**) via 3+4 cycloaddition reaction.[7,8,9] This tricyclic molecule has some interesting dihedral angle characteristics. The proton on C_1 is gauche to C_3 yet nearly perpendicular to C_4. We prepared a 30mg sample of this species in benzene-d_6 and performed the same consecutive HSQC+HMBC experiments. As expected, H_1 only shows correlation with C_3, not C_4 (**Figure 4**). However, in this instance, C_6 cannot be located at all (**Table 2**).

Table 1 Extracted ^{13}C chemical shifts for 1

Position	δ (ppm)	
	^{1}H	^{13}C
1	2.1	21.5
2	-	154.85
3	6	110.6
4	-	175.5
5	-	123.15
6	-	136.85
7	7.4	117.5

We performed numerous experiments changing the relaxation delay and the NS in the hopes of locating C6 to no avail. The absence of the C6 signal can be rationalized in two ways

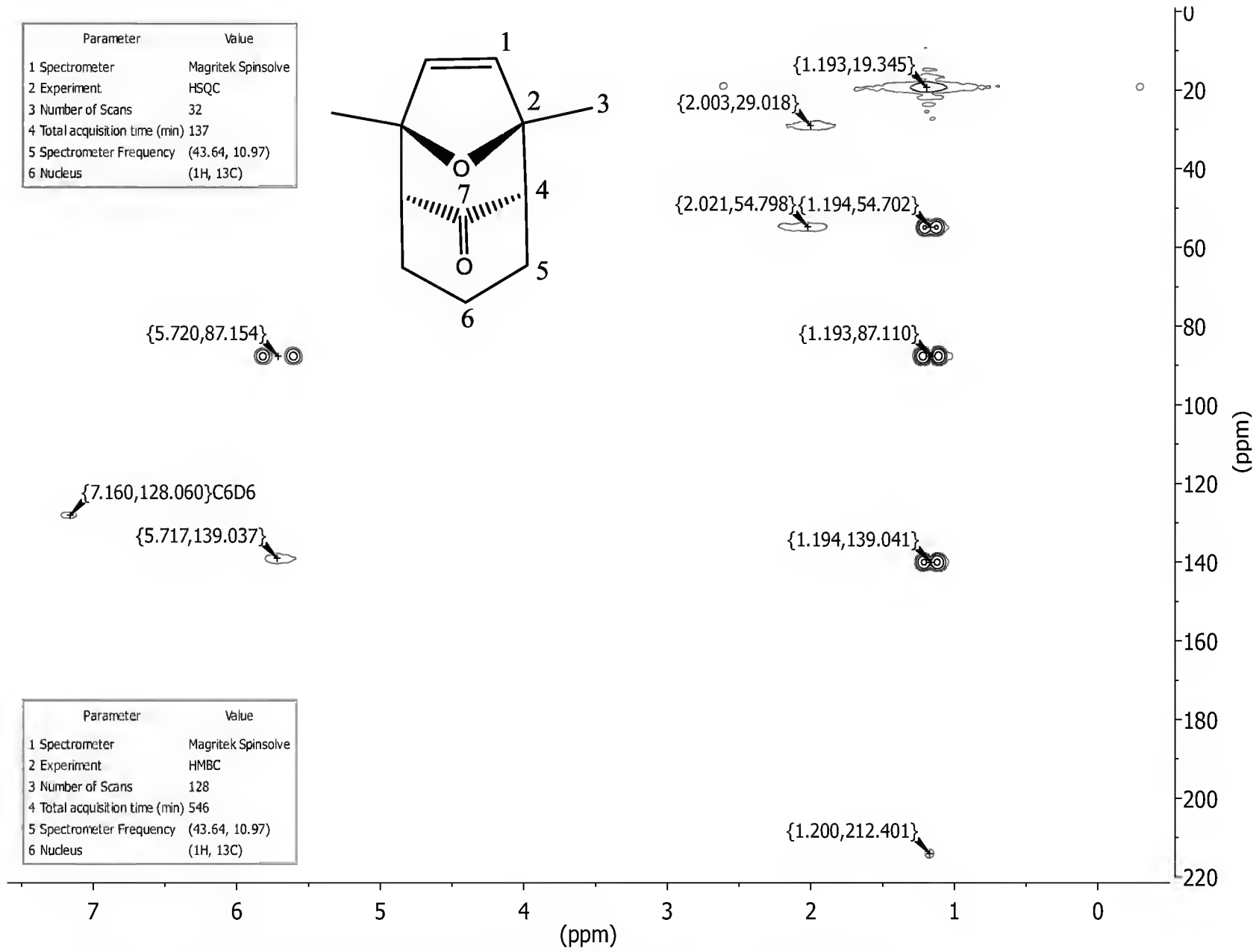

Figure 3 Stacked HSQC and HMBC of 2. Structure of 2 (inset)

1) the resonances for both ^{1}H and ^{13}C at positions 3 and 6 are overlapping in both 2D spectra, or 2) the coupling constants for C_6 are too small to transfer magnetization (whether due to field-strength issues or, perhaps due to the quality of the pulse sequence). After contacting MagriTek for a potential solution, we were invited to use a pre-release phase-sensitive HSQC-ME experiment. It never occurred to us that the pulse sequence could be the culprit for the lack of signal at C6. Nowhere in Eq.1 is there a pulse sequence-specific term. Though skeptical, we pressed forward and obtained the spectrum in **Figure 5**. This phase-sensitive spectra indicates CH and CH3 signals as positive (in red) and CH2 signals as negative (in blue). There is data correlating to the 20.76 ppm ^{13}C resonance, but it is not in any clear pattern, and looks a bit like noise. However, using the 1D projection tool in MestreNova we were able to extract what is essentially an Attached Proton Test (APT) spectrum suggesting a new CH2 was present in the region expected for C_6. We performed a ^{1}H-broadband decoupled ^{13}C-NMR of **2**, and subsequent DEPT (**Figure 6**) after accumulating enough material (185mg). **Figure 5** shows the C_6 resonance of **2** at 20.8 ppm is remarkable close to the methyl group resonance at C_3. These spectra are in excellent agreement with the extracted data, and show conclusively that the pulse sequence was the primary issue.

Table 2 Extracted ^{13}C chemical shifts for 2

Position	δ (ppm)	
	^{1}H	^{13}C
1	5.72	139.0
2	-	87.1
3	1.19	19.6
4	2.02	54.7
5	2.03	29
6	?	?
7	-	212.4

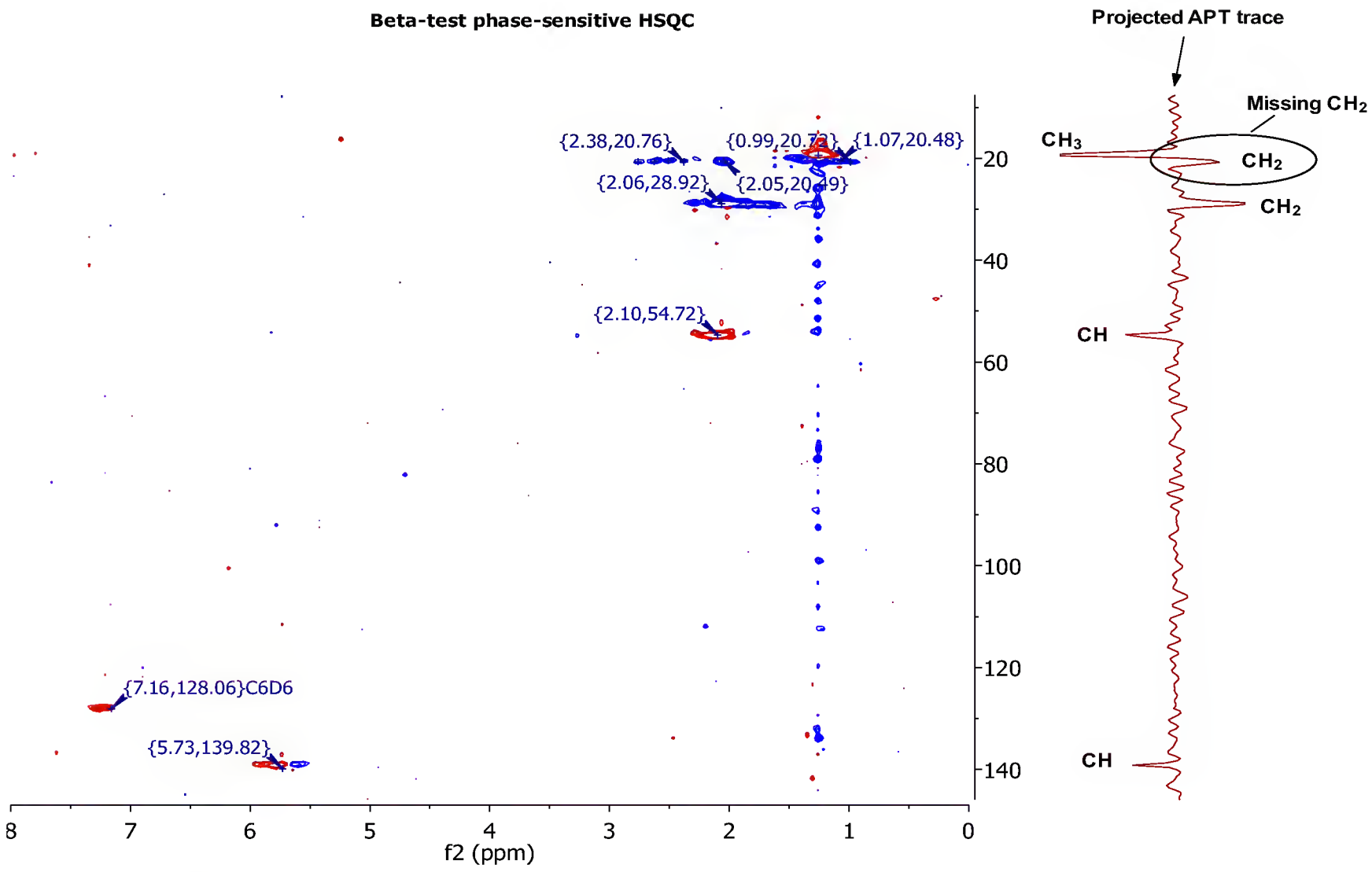

Figure 4 HSQC-ME (beta test courtesy of MagriTek) of 2.

We found another useful application of this technology during our attempts at

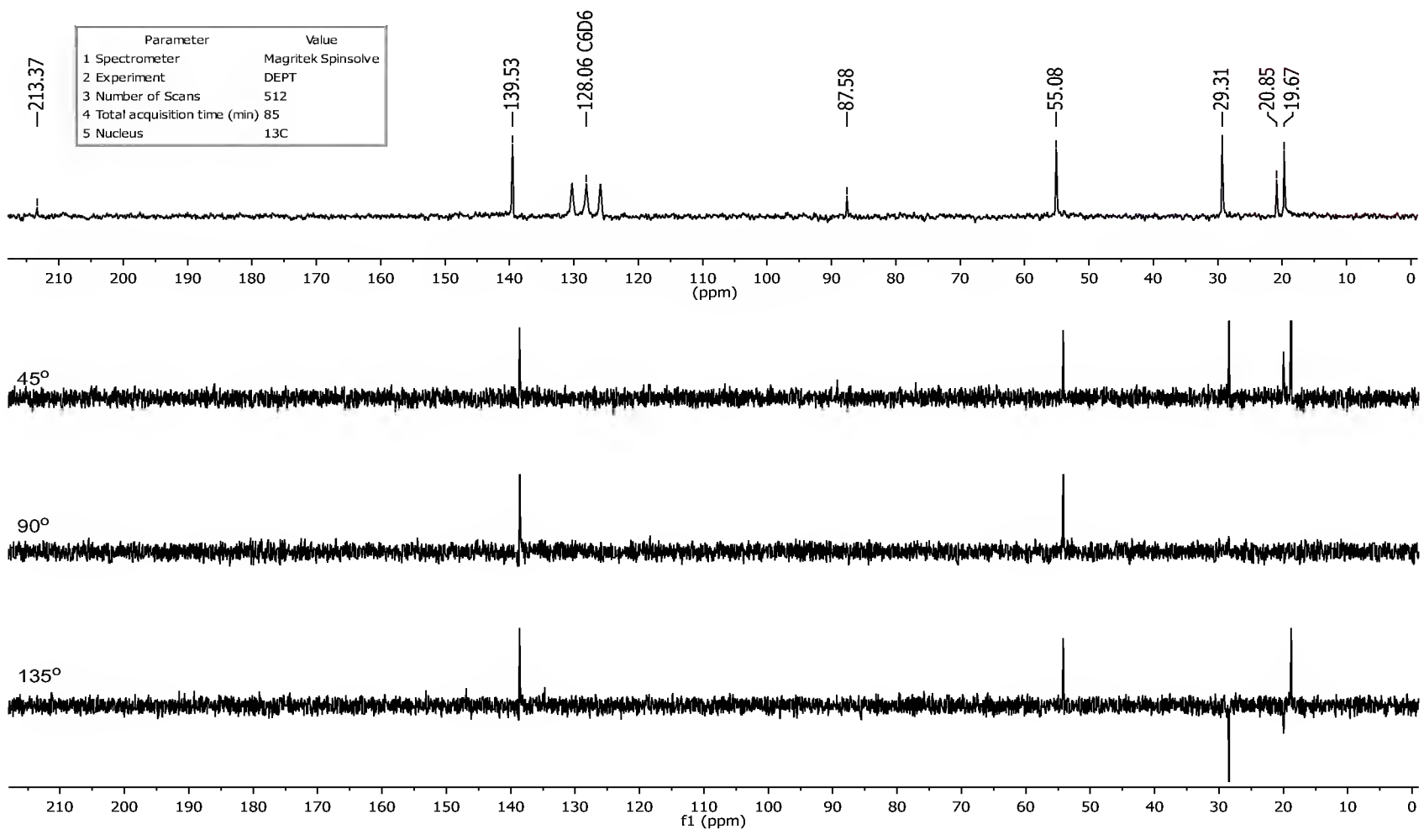

Figure 6 DEPT of pure 2

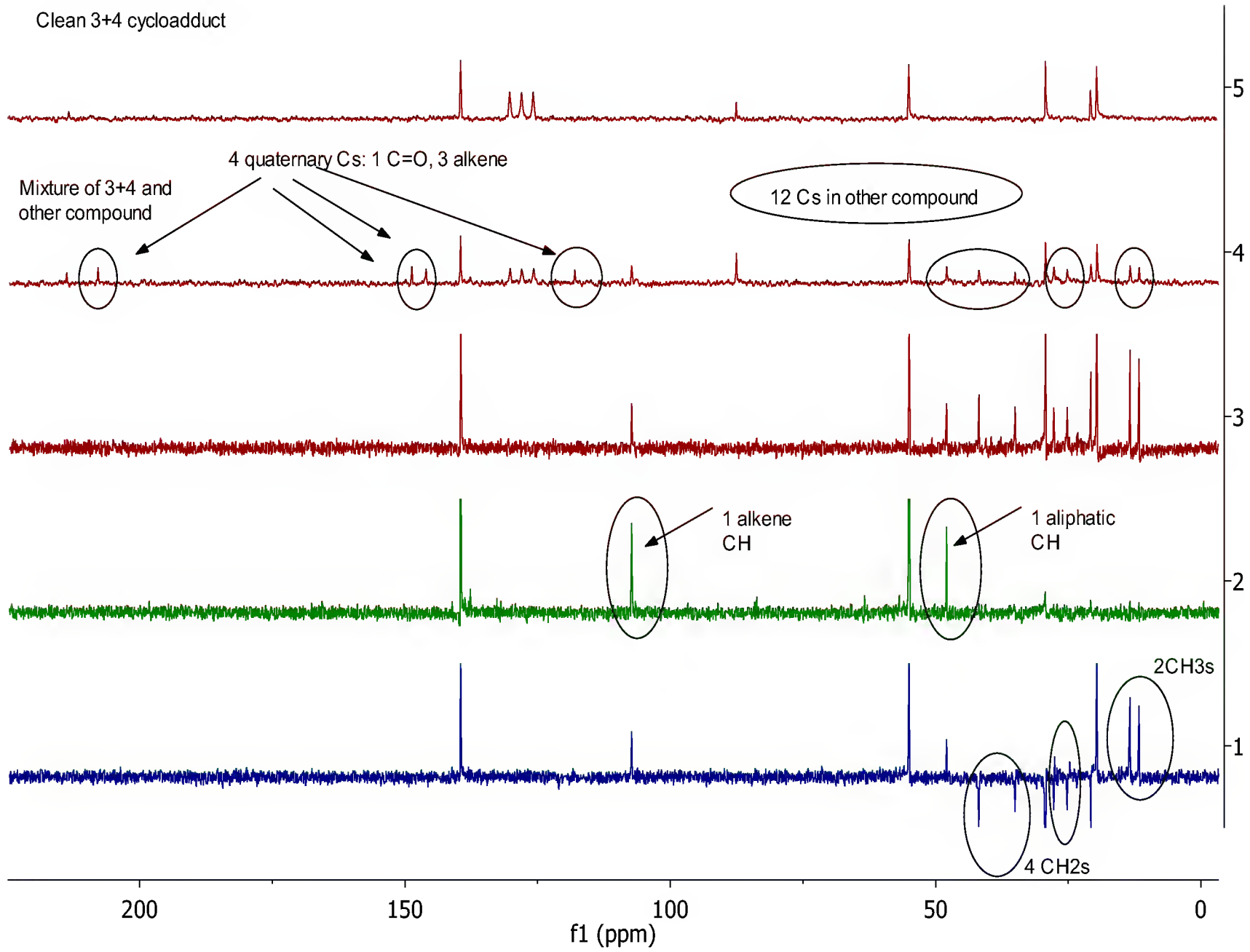

Figure 7. Pure 1 ^{13}C of (5), mixture of 2 and 2' ^{13}C (4), mixture of 2 and 2' DEPT 45° (3), 90° (2), 135° (1)

synthesizing this compound. We were able to use DEPT in order to determine the possible identity of impurities we were finding in our early attempts at this reaction. In similar reactions it was noted that the final tricyclic compound could decompose into a ring-open form.[7,8] We believed this to be the reason for the extra 12 peaks visible in our carbon NMR (**Figure 7**), but were unable to make this assertion using normal C-NMR scans. Through our proposed mechanism, (**Scheme 1**) we postulated a possible impurity, **2'**. We were then able to use DEPT (**Figure 7**) to rule out other possibilities and determine with reasonable certainty the identity of the impurity. This gave us valuable information about what might be causing our product to decompose.

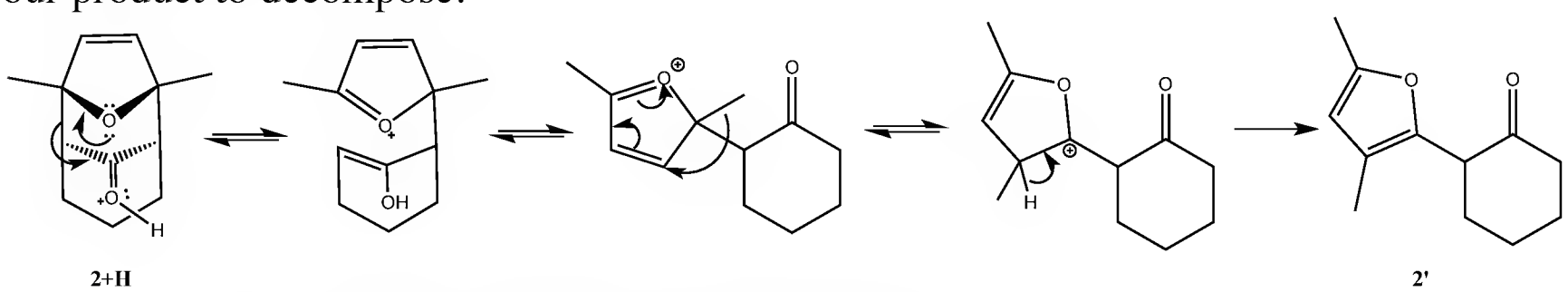

2+H 2'

Scheme 1 Proposed mechanism for the generation of 2'

Last, we analyzed the more flexible system in alkyne thioester **3** (**Figure 8** inset). This molecule showed indistinguishable resonances for C3 and C4, regardless of the experiment employed. The tandem 2D and stacking protocol used previously allowed for the assignment of all other carbons, but convoluted these two protonated resonances. Though we were confident we had synthesized the molecule *via* ^{1}H-NMR and GCMS analysis we still

wanted to see that we had all six of the proton-bearing carbon resonances. We were unable to obtain an adequate ^{13}C NMR even when a large concentration was employed. This suggested that C3 and C4 were isochronous in our spectrometer. When searching the literature for a means to change the chemical shift of resonances, and thereby deconvolute two signals, Lanthanide Shift Reagents (LSRs) were at the forefront. As we were not interested in any separation of stereoisomers, we settled on the cheapest, achiral LSR, Erbium(III) tris(2,2,6,6-tetramethyl-3,5-heptanedionate), $Er(TMHD)_3$. We found that in our spectrometer $Er(TMHD)_3$ had no 2D spectrum alone plausibly due to the typical line broadening associated with LSRs, and the low concentration present.[10] This line broadening also made the ^{1}H even more difficult to interpret (though improved ^{1}H signal dispersion wasn't the goal). Additionally, the HMBC had no data. However, when the HSQC was performed in the presence of $Er(TMHD)_3$, the proton-bearing resonances deconvoluted and all six carbon signals were visible (**Figure 8**).

CONCLUSION

We have shown that a benchtop NMR with 2D capabilities is adequate to determine ^{13}C framework of complex molecular structures, in particular when a tandem 2D and stacking approach is employed. When this approach fails, lanthanide shift reagents can be applied as a workaround. This method saved us countless hours traveling to and from an off-site high-field NMR. We discovered that the pulse sequence of the 2D protocol was just as important as the other system-specific factors. The improved dispersion and resolution of the HSQC-ME experiment allowed for viewing a ^{13}C resonance previously undetectable on our instrument, and allowed for assigning the resonances as C, CH, CH2 due to its phase-sensitivity. The CH3 resonances were then assigned by comparing the HSQC-ME scans to a standard ^{13}C

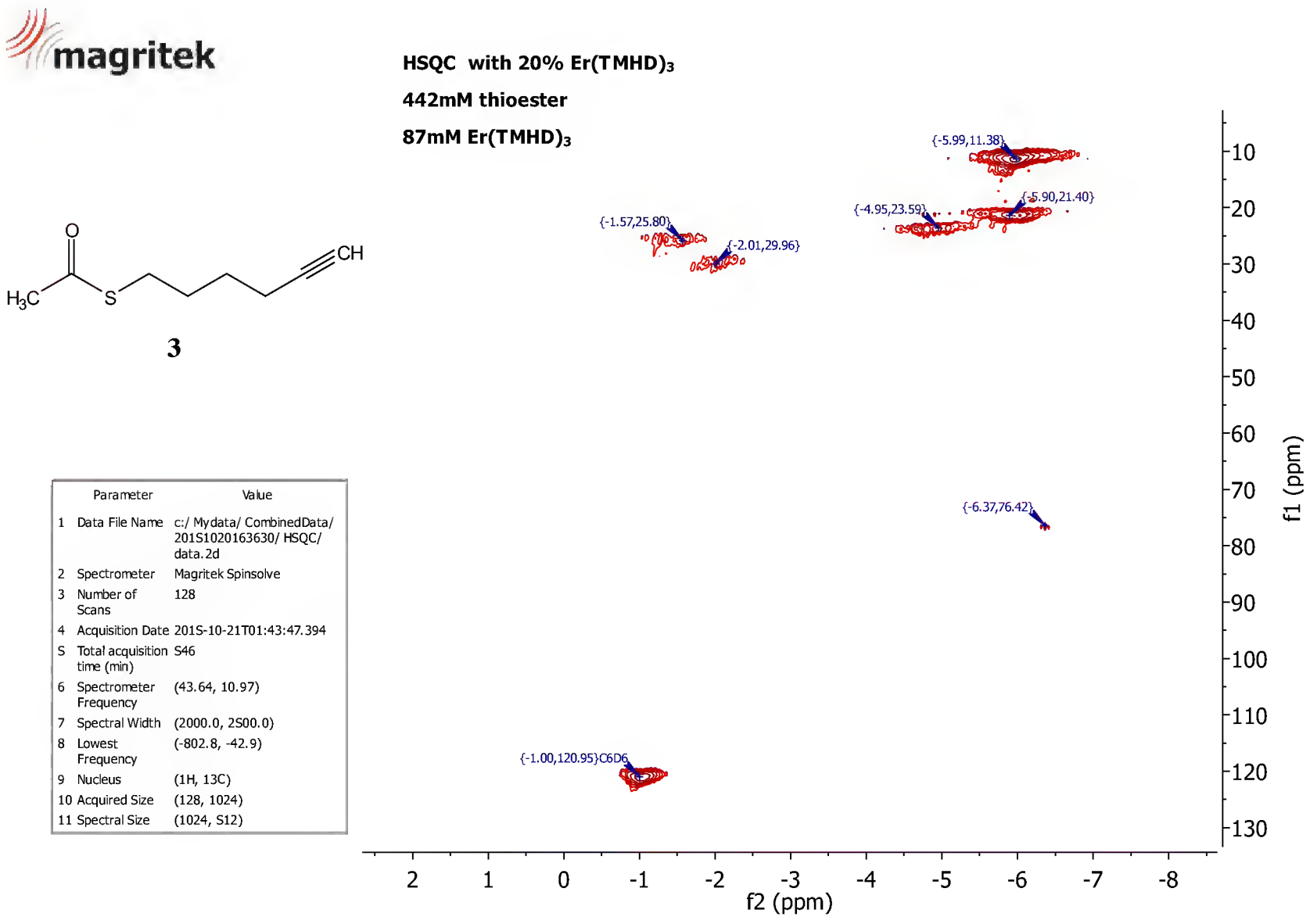

Figure 8 HSQC of 3 with 20% $Er(TMHD)_3$

experiment. The use of DEPT experiments also proved useful in elucidating the identities of compounds when presented with a mixture of products. All direct-detection methods, and their concentration or dispersion shortcomings were overcome using the methods described. There are two major experiments we would like to see these bench-top NMR companies include in the future. The first is called a PSYCHE[11] experiment that decouples the entire ^{1}H spectra while still allowing for accurate integration. This amazing experiment would elevate proton utility on low-field instruments by bypassing dispersion-based signal isochrony. Researchers would be able to simply count the resonances and evaluate their integration to gauge whether a reaction succeeded or failed. The second experiment is called Pure Shift HSQC NMR.[12] This experiment decouples the ^{1}H resonances in the 2D so that all resonances are presented as singlets, thereby increasing the strength of the signal that is correlated to any given ^{13}C. This experiment could have been useful when analyzing compound **2.** This experiment would have allowed for a much more robust and expeditious route toward ^{13}C NMR extraction from a dilute sample. As compound **3** showed that signal isochrony is still an issue, we encourage these companies to continue to strive for more powerful bench top magnets to decrease signal dispersion.

ACKNOWLEDGEMENTS

We are especially appreciative of the assistance of the following people at MagriTek: Paul Bowyer for providing the HSQC-ME and for his willingness to provide helpful conversations and processing assistance whenever necessary, Robert Espina for his technical support of the Spinsolve system, and Randal Hall for his support and friendship for the past two years. We would like to thank Mike Jablonski of the University of Alabama at Birmingham for the acquisition of the high-field nmr data. We are grateful to the faculty and department of Chemistry and Biochemistry at Samford University for their continual moral and monetary support. The acquisition of the Spinsolve system was made possible by David Chapman, former Dean of the College of Arts and Sciences at Samford University, to whom this work is dedicated.

CITATIONS

[1] Guidelines for Authors, *The Journal of Organic Chemistry*, Jan 2016, pp 13.

[2] Clewett, C. F. M.; Flynn, N. *E. J. Chem. Educ.* **2015**, 92 (3), 589–592.

[3] Silverstein, R. M.; Webster, F. X.; Kiemle, D. J. *Spectrometric identification of organic compounds*, 7th ed.; John Wiley & Sons: Hoboken, NJ, 2005.

[4] Frank A. A. M. De Leeuw; Haasnoot, C. A. G.; Altona, C. *J. Am. Chem. Soc.* **1984**, 106 (8), 2299–2306.

[5] Jaworski, A.; Ekiel, I.; Shugar, D. *J. Am. Chem. Soc* **1978**, 100 (14), 4357–4361.

[6] Xiang Liu, Xiaoyong Li, Yu Chen, Yimin Hu, and Yoshito Kishi
J. Am. Chem. Soc. **2012**, 134 (14), 6136-6139

[7] Vinter, J. G.; Hoffmann, H. M. R. *J. Am. Chem. Soc.* **1974**, *96* (17), 5466–5478.

[8] Oh, J.; Ziani-Cherif, C.; Choi, J.-R.; Cha, J. K. *Org. Synth.* **2003**, 212–212.

[9] Berry, E.; Gomes, G. D. P.; Maclean, A.; Martin, J. R.; Wiget, P. A. *J. Org. Chem.* **2016**, 81 (13), 5740–5744.

[10] Cockerill, A. F.; Davies, G. L. O.; Harden, R. C.; Rackham, D. M. *Chem. Rev.* **1973**, 73 (6), 553–588.

[11] Foroozandeh, M.; Adams, R.W.; Meharry, N.J.; Jeannerat D.; Nilsson, M.; Morris A.G. *Angew. Chem. Int. Ed.* **2014,** *53*, 6990 –6992 .

[12] Paudel L.; Adams, R.W.; Kirμly, P.; Aguilar, J.A.; Foroozandeh, M.; Cliff, M.J.; Nilsson, M.; Sμndor, P.; Waltho J.P.; and Morris G.A. *Angew. Chem. Int. Ed.* **2013**, *52*, 11616 –11619.

Differential expression of the stress-associated proteins FKBP51 and FKBP52 in human and New World primate cells.

Caroline M. Thomas[1], John F. Repass[2], Jonathan G. Scammell[3], Patti W. Adams[4], Tina R. Hubler[1,5]
[1]University of North Alabama, Department of Biology, Florence AL
[2]ARQ Genetics, Bastrop TX
[3]University of South Alabama, Department of Comparative Medicine, Mobile AL
[4]South University, School of Pharmacy, Savannah GA
[5]Correspondence: (256)765-4761, Fax (256)765-4430, trhubler@una.edu

Key words: FKBP51, FKBP52, gene regulation, comparative genomics

ABSTRACT

The proteins FKBP51 and FKBP52 are involved in regulation of the stress response due to their effects on the glucocorticoid receptor (GR) that binds cortisol. FKBP51 and FKBP52 may occupy the same site in the GR complex. When FKBP52 is included in the complex, cortisol responsiveness is enhanced. In contrast, the inclusion of FKBP51 inhibits cortisol responsiveness. Therefore, the relative expression of these proteins partly determines cellular responsiveness to cortisol. To begin to understand how these proteins are regulated, we have studied their gene expression in two cell lines, EBV-transformed squirrel monkey lymphoblasts (SML) and human lymphoblasts (HL), that exhibit different levels of the two proteins. The relative levels of FKBP51 and FKBP52 and their respective messenger RNAs were measured in SMLs and HLs. FKBP51 was 3.7-times higher in SMLs than in HLs, whereas FKBP52 in SMLs was 40% of that in HL. FKBP51 mRNA was 3.2-times higher in SML and FKBP52 mRNA was 53% of that in HL. Our results show that the changes in mRNA and protein levels correspond, suggesting that mechanisms controlling mRNA levels are important for determining the overall proteins levels in the two cell lines. Understanding regulation of the levels of FKBP51 and FKBP52 may be important for glucocorticoid signaling dysfunction.

INTRODUCTION

FKBP51 and FKBP52 are proteins associated with the glucocorticoid receptor (GR), a member of a family of steroid hormone receptors that proceed through an assembly pathway to form a mature receptor heterocomplex. This process involves a number of chaperone proteins, including Hsp90. The mature GR complex, that binds glucocorticoids with high affinity, contains the complex-stabilizing protein p23, Hsp90 and the FK506-binding protein FKBP52 (Nair et al. 1997; Riggs et al. 2003; Davies et al. 2005). However, FKBP52 is not the only protein that can incorporate into the GR complex. There are several proteins that occupy the same site in the GR complex through their association with Hsp90. These are FK506-binding FKBP51, cyclosporin A-binding cyclophilin 40, and the protein phosphatase 5 (PP5). A model has emerged for GR responsiveness in which incorporation of FKBP52 or FKBP51 into the GR heterocomplex has opposing effects on GR signaling. When FKBP52 is present in the GR heterocomplex, the GR exhibits high activity, whereas the presence of FKBP51 in the heterocomplex confers low GR activity (Cheung and Smith 2000; Denny et al.

2000; Davies et al. 2005; Wochnik et al. 2005). Therefore, the *relative* expression of FKBP51 and FKBP52 would be expected to impact overall GR responsiveness.

To gain insight into the mechanisms controlling the levels of FKBP51 and FKBP52, cell lines that differentially express FKBP51 and FKBP52 were used for comparative studies. The cell lines chosen as models of differential expression of FKBP51 and FKBP52 were Epstein-Barr virus (EBV)-transformed human and squirrel monkey lymphoblasts (Reynolds et al. 1999). Squirrel monkeys are South American New World primates that exhibit reduced GR responsiveness and high levels of the GR-activating hormone cortisol relative to humans. New World primate glucocorticoid resistance has been associated with high levels of FKBP51 and low levels of FKBP52 (Scammell et al. 2001). The EBV-transformed squirrel monkey lymphoblasts (SML) were shown to exhibit low glucocorticoid hormone binding affinity relative to the EBV-transformed human lymphoblasts (HL). Furthermore, analysis of the glucocorticoid receptor (GR)-associated proteins, FKBP51 and FKBP52, by Western blot demonstrated that SML underexpress FKBP52 and overexpress FKBP51 relative to HL (Reynolds et al. 1999). Thus, the SML cell line is an in vitro model that recapitulates glucocorticoid resistance in New World primates. As a result of differences in the levels of FKBP51 and FKBP52, SML and HL also serve as useful models in which to study differential expression of FKBP51 and FKBP52.

To begin to understand how the FKBP51 and FKBP52 genes (*FKBP5* and *FKBP4,* respectively) are expressed, protein and mRNA levels in SML and HL were determined. Protein levels were evaluated by Western blot to confirm differential expression of FKBP51 and FKBP52 in the two cell lines. Next, steady state mRNA levels were determined by qPCR. The results show that differences in mRNA levels were consistent with the observed differences in protein levels in the two cell lines. These data provide a foundation on which researchers may continue to explore the regulation of FKBP51 and FKBP52 gene expression.

MATERIALS AND METHODS

Materials

Culture medium, penicillin-G, streptomycin and defined fetal bovine serum (FBS) were obtained from MidSci (St. Louis, MO). Nitrocellulose, precast 7.5% polyacrylamide gels, anti-mouse IgG secondary antibody and the Clarity Western ECL Substrate immunodetection kit were from Bio-Rad Laboratories (Hercules, CA). Generation of monoclonal antibodies to FKBP51 and FKBP52 was described earlier (Nair et al. 1997). Monoclonal antibody to beta actin was purchased from Santa Cruz Biotechnology, Inc. (Dallas TX). RIPA buffer and protease inhibitor were from Cell Signaling Technology, Inc. (Danvers, MA).

Cell culture

Squirrel monkey and human lymphoblasts were described previously (Reynolds et al. 1999). Squirrel monkey lymphoblasts may be obtained from American Type Cell Collection (Rockville, MD), ATCC number CRL-2311. Both cell lines were grown in suspension cultures in RPMI 1640 supplemented with 10% FBS, 50 U/mL penicillin G and 0.05 mg/mL streptomycin, at 37° C in a humidified atmosphere of 5% CO_2-95% air.

Comparison of Protein Levels: Western Blot

Whole cell extracts were prepared in RIPA buffer containing protease inhibitors, then dissolved in 2X concentrated sample buffer. Total protein (10 μg) was separated by sodium dodecyl sulfate-polyacrylamide gel electrophoresis (SDS-PAGE) and transferred to nitrocellulose. The blots were incubated in PBS (pH 7.4), containing 0.1% Tween-20 and 5% nonfat milk (blocking buffer), for 1 h at room temperature. Incubation with primary antibodies was carried out at 4^0 C in blocking buffer overnight. After washing, blots were incubated with secondary antibody for 1 h at room temperature and developed using the Clarity Western ECL Substrate (Bio-Rad Laboratories) Western Blotting Immunodetection System. Western blots were quantified by densitometry and normalized against beta actin, the loading control. Results were expressed as protein levels relative to HL.

Comparison of mRNA levels: qPCR

Cell collection, RNA Extraction and cDNA Synthesis

Cells were collected by centrifugation at 500 g for 5 min, washed with PBS and placed immediately on dry ice for shipment to ARQ Genetics (Bastrop, TX). Total RNA was extracted using the Qiagen RNeasy Mini Kit (Qiagen Sciences, Germantown, MD) according to the manufacturer's instructions with optional DNase treatment. Subsequently, 1 μg total RNA was used as template to synthesize cDNA with the High Capacity cDNA Reverse Transcription Kit (Applied Biosystems, Foster City, CA).

Primer Design

Primers for all SYBR assays were designed using Primer 3 (Ye et al. 2012) and alignment tools available at http://www.ncbi.nlm.nih.gov/tools/primer-blast/index.cgi). Squirrel monkey and human FKBP51 and FKBP52 mRNA sequences were compared using data from GenBank at the National Center for Biotechnology Information, NCBI, (FKBP51 mRNA accession numbers NM_001145775.2, NM_001145777.1, NM_0011457776.1, NM_004117.3 and NM_001280014.1; FKBP52 mRNA accession numbers NM_002014.3 and XM_010330055.1). Regions of identical sequences were selected for analysis and primers were designed to target multiple regions of each transcript. Four regions of FKBP51 mRNA were targeted using the primers FKBP51.1-FKBP51.4 in Table 1. Two regions were suitable for targeting the FKBP52 mRNA in squirrel monkey and human using the primers FKBP52.1-FKBP52.2 in Table 1. Melting curve analysis was performed to ensure single-product amplification for all primer pairs. Sequences for all primers are listed in Table 1.

Real Time PCR Analysis

Real time PCR was performed on the ABI 7900HT Fast Real Time PCR System (Applied Biosystems) using assays specific for each gene of interest. For SYBR assays, each reaction well contained 5 μL of Power SYBR Green PCR Master Mix (Applied Biosystems), cDNA equivalent to 20 ng of total RNA and 400 nM each of forward and reverse amplification primers in a reaction volume of 10 μL. Cycling conditions were as follows: 95° C for 10 minutes for polymerase activation, followed by 40 cycles of 95° C for 15 seconds and 60° C for 1 minute. Data analysis was performed using Sequence Detection System software from Applied Biosystems, version 2.4. The experimental Ct (cycle threshold) was calibrated against an endogenous control, 18s RNA or beta actin RNA. Relative gene expression levels were calculated by the ddCt method (Pfaffl 2001).

Data Analysis

For Western blot analysis, protein levels were quantified by densitometry and normalized to beta-actin as a loading control. Each experiment was repeated at least two times. Statistical analysis was performed on normalized data using a t-test with $p < 0.05$ considered as statistically different. Data was then represented as the average fold change relative to HL protein levels.

For real time PCR, relative levels of SML and HL amplicons were calculated by the ddCt method (Pfaffl 2001) for each mRNA region targeted by the primers in Table 1. Each experiment was performed at least two times. Data from all FKBP51 or FKBP52 primer pairs in a single analysis were statistically analyzed using a t-test with $p < 0.05$ considered as statistically different. The data was represented as the average fold change relative to HL mRNA levels.

RESULTS

Comparison of Protein Levels: Western Blot

Western Blot was performed on SML and HL to confirm differential expression of FKBP51 and FKBP52 in the cell lines used for our experiments (Figures 1a and 1b). For comparison of protein levels, data were graphically represented as protein levels relative to HL protein levels. Our results show that SML express 3.7-times greater FKBP51 protein relative to HL (3.7 ± 0.75, Figure 1c). As reported previously, squirrel monkey FKBP51 exhibits greater electrophoretic mobility than human FKBP51 (Reynolds et al. 1999; Scammell et al. 2001). In contrast to FKBP51 protein, the levels of FKBP52 were 40% of that in HL (0.4 ± 0.02, Figure 1d). These data confirm differential expression of FKBP51 and FKBP52 in SML and HL cell lines, as previously reported in the literature (Reynolds et al. 1999).

Comparison of mRNA Levels: qPCR

qPCR was used to determine the relative amount of FKBP51 and FKBP52 mRNA in each cell line. Because the cells were from distinct species, the primers for qPCR were designed to target exon sequences that are conserved in squirrel monkeys and humans. For comparison of mRNA levels, data were graphically represented as mRNA levels relative to HL mRNA levels. The comparison of mRNA levels for each cell line showed FKBP51 mRNA was 3.2-times higher in SML than in HL (3.2 ± 0.19, Figure 2a). FKBP52 mRNA in SML was 53% of HL (0.5 ± 0.08, Figure 2b). These results are consistent with the relative differences in FKBP51 and FKBP52 protein observed in SML and HL. Furthermore, the results suggest that differences in mRNA levels may contribute to the differences in relative FKBP51 and FKBP52 protein levels in these cells.

DISCUSSION

A number of mechanisms may contribute to the regulation of gene expression. These include promoter activity, nuclear processing and transport of mRNA, mRNA stability, translational regulation, protein stability and epigenetic mechanisms such as gene silencing. As a result, changes in protein may be a reflection of changes occurring by any or all of these mechanisms. To date, the underlying mechanisms by which cellular FKBP51 and FKBP52 protein levels are regulated are not well understood. Our results show that, in SML and HL cell lines, the relative levels of FKBP51 and FKBP52 mRNA and protein are consistent. These data provide evidence that regulation of FKBP51 and FKBP52 protein levels occur, in part, at the level of mRNA.

There are at least three mechanisms that may explain the observed differences in squirrel monkey and human FKBP51 and FKBP52 mRNA levels: (1) interspecies differences in enhancer or promoter regions of the FKBP51 and FKBP52 genes, *FKBP5* and *FKBP4* respectively, (2) differences in microRNA activity in cells, and (3) single nucleotide polymorphisms. We previously isolated and sequenced a 2000 bp segment immediately upstream of squirrel monkey *FKBP5* (Accession number JX503530). Comparison of this segment with the corresponding region of the human transcript variant 1 promoter reveals the presence of two Alu elements in the human *FKBP5* promoter sequence that are absent in the squirrel monkey promoter sequence (unpublished data). Similarly, the human *FKBP4* 5'-flanking region contains multiple Alu-like sequences that are absent in the squirrel monkey sequence. The presence of Alu insertions may affect the activity of regulatory sequences (Schmitz 2012). Therefore, such insertions may impact the relative levels of mRNA present in cells from different species.

MicroRNAs (miRs) miR-511, miR-100, miR-15a and miR-29c have been identified as regulators of FKBP51 (Bhushan and Kandpal 2011; Li et al. 2013; Volk et al. 2016; Zheng et al. 2016) or FKBP52 levels (Joshi et al. 2016). A comparison of the 3' untranslated region sequences (3' UTRs) in human and squirrel monkey *FKBP5* revealed that sequences potentially targeted by miR-511, miR-100 and miR-15a (AAAAGA, UACGGGU and UGCUGCU, respectively) were identical in human and squirrel monkey DNA. In addition, the target sequence for miR-29c, GGUGCUA, was identical in human and squirrel monkey *FKBP4*. A comparison of miR-511, miR-100, miR15a and miR-29c sequences in human and squirrel monkey DNA revealed no differences in the regions that align with the target sequences (above) in *FKBP4* and *FKBP5* 3' UTRs. These data suggest that these miRs may interact with and regulate *both* human and squirrel monkey FKBP51 and FKBP52 mRNAs.

A number of single nucleotide polymorphisms (SNPs) have been identified in human *FKBP5*. *FKBP5* SNPs have been associated with altered stress responses (Ising et al. 2008; Bortsov et al. 2013), altered susceptibility to mental disorders (Binder et al. 2004; Koenen et al. 2005; Klengel et al. 2013), and development of or recovery from substance abuse disorders (Levran et al. 2014). Such influences are hypothesized to relate to the effect of FKBP51 on cortisol responsiveness. Currently, how these SNPs affect *FKBP5* expression levels is not fully understood.

The present study has shown that FKBP51 and FKBP52 protein levels are consistent with mRNA expression levels in two cell types that exhibit differential expression of the two proteins. These data contribute to our understanding of the regulation of these important

antagonistic glucocorticoid signaling proteins by suggesting that mechanisms controlling mRNA levels are significant contributors to overall protein levels. As a consequence of differential expression of FKBP51 and FKBP52 in New World primates and humans, cell lines derived from squirrel monkeys and humans may provide a useful model for the discovery of important regulatory mechanisms of FKBP51 and FKBP52 gene expression.

ACKNOWLEDGEMENTS

Funding for this research project was made available by The University of North Alabama's Quality Enhancement Plan Undergraduate Research Grant and the Department of Biology. Caroline Thomas was awarded 1st Place for her oral presentation on this work at the 93rd Annual Alabama Academy of Science Meeting, Feb. 17-19, 2016, University of North Alabama, Florence AL (Thomas and Hubler 2016).

LITERATURE CITED

Bhushan, L. and R. P. Kandpal. 2011. EphB6 receptor modulates micro RNA profile of breast carcinoma cells. *PLoS One*. 6: e22484.

Binder, E. B., D. Salyakina, P. Lichtner, G. M. Wochnik, M. Ising, B. Putz, S. Papiol, S. Seaman, S. Lucae, M. A. Kohli, T. Nickel, H. E. Kunzel, B. Fuchs, M. Majer, A. Pfennig, N. Kern, J. Brunner, S. Modell, T. Baghai, T. Deiml, P. Zill, B. Bondy, R. Rupprecht, T. Messer, O. Kohnlein, H. Dabitz, T. Bruckl, N. Muller, H. Pfister, R. Lieb, J. C. Mueller, E. Lohmussaar, T. M. Strom, T. Bettecken, T. Meitinger, M. Uhr, T. Rein, F. Holsboer and B. Muller-Myhsok. 2004. Polymorphisms in FKBP5 are associated with increased recurrence of depressive episodes and rapid response to antidepressant treatment. *Nature Genetics*. 36: 1319-1325.

Bortsov, A. V., J. E. Smith, L. Diatchenko, A. C. Soward, J. C. Ulirsch, C. Rossi, R. A. Swor, W. E. Hauda, D. A. Peak, J. S. Jones, D. Holbrook, N. K. Rathlev, K. A. Foley, D. C. Lee, R. Collette, R. M. Domeier, P. L. Hendry and S. A. McLean. 2013. Polymorphisms in the glucocorticoid receptor co-chaperone FKBP5 predict persistent musculoskeletal pain after traumatic stress exposure. *Pain*. 154: 1419-1426.

Cheung, J. and D. F. Smith. 2000. Molecular chaperone interactions with steroid receptors: an update. *Molecular Endocrinology*. 14: 939-946.

Davies, T. H., Y. M. Ning and E. R. Sanchez. 2005. Differential control of glucocorticoid receptor hormone-binding function by tetratricopeptide repeat (TPR) proteins and the immunosuppressive ligand FK506. *Biochemistry*. 44: 2030-2038.

Denny, W. B., D. L. Valentine, P. D. Reynolds, D. F. Smith and J. G. Scammell. 2000. Squirrel monkey immunophilin FKBP51 is a potent inhibitor of glucocorticoid receptor binding. *Endocrinology*. 141: 4107-4113.

Ising, M., A. M. Depping, A. Siebertz, S. Lucae, P. G. Unschuld, S. Kloiber, S. Horstmann, M. Uhr, B. Muller-Myhsok and F. Holsboer. 2008. Polymorphisms in the FKBP5 gene region modulate recovery from psychosocial stress in healthy controls. *European Journal of Neuroscience*. 28: 389-398.

Joshi, N. R., E. H. Miyadahira, Y. Afshar, J. W. Jeong, S. L. Young, B. A. Lessey, P. C. Serafini and A. T. Fazleabas. 2017. Progesterone resistance in endometriosis is modulated by the altered expression of microRNA-29c and FKBP4. *Journal of Clinical Endocrinology and Metabolism*. 102:141-149.

Klengel, T., D. Mehta, C. Anacker, M. Rex-Haffner, J. C. Pruessner, C. M. Pariante, T. W. Pace, K. B. Mercer, H. S. Mayberg, B. Bradley, C. B. Nemeroff, F. Holsboer, C. M. Heim, K. J. Ressler, T. Rein and E. B. Binder. 2013. Allele-specific FKBP5 DNA demethylation mediates gene-childhood trauma interactions. *Nature Neuroscience*. 16: 33-41.

Koenen, K. C., G. Saxe, S. Purcell, J. W. Smoller, D. Bartholomew, A. Miller, E. Hall, J. Kaplow, M. Bosquet, S. Moulton and C. Baldwin. 2005. Polymorphisms in FKBP5 are associated with peritraumatic dissociation in medically injured children. *Molecular Psychiatry*. 10: 1058-1059.

Levran, O., E. Peles, M. Randesi, Y. Li, J. Rotrosen, J. Ott, M. Adelson and M. J. Kreek. 2014. Stress-related genes and heroin addiction: a role for a functional FKBP5 haplotype. *Psychoneuroendocrinology*. 45: 67-76.

Li, X. J., X. Q. Luo, B. W. Han, F. T. Duan, P. P. Wei and Y. Q. Chen. 2013. MicroRNA-100/99a, deregulated in acute lymphoblastic leukaemia, suppress proliferation and promote apoptosis by regulating the FKBP51 and IGF1R/mTOR signalling pathways. *British Journal of Cancer*. 109: 2189-2198.

Nair, S. C., R. A. Rimerman, E. J. Toran, S. Chen, V. Prapapanich, R. N. Butts and D. F. Smith. 1997. Molecular cloning of human FKBP51 and comparisons of immunophilin interactions with Hsp90 and progesterone receptor. *Molecular and Cellular Biology*. 17: 594-603.

Pfaffl, M. W. 2001. A new mathematical model for relative quantification in real-time RT-PCR. *Nucleic Acids Research*. 29: e45.

Reynolds, P. D., Y. Ruan, D. F. Smith and J. G. Scammell. 1999. Glucocorticoid resistance in the squirrel monkey is associated with overexpression of the immunophilin FKBP51. *Journal of Clinical and Endocrinololgy Metabolism*. 84: 663-669.

Riggs, D. L., P. J. Roberts, S. C. Chirillo, J. Cheung-Flynn, V. Prapapanich, T. Ratajczak, R. Gaber, D. Picard and D. F. Smith. 2003. The Hsp90-binding peptidylprolyl isomerase FKBP52 potentiates glucocorticoid signaling in vivo. *EMBO Journal*. 22: 1158-1167.

Scammell, J. G., W. B. Denny, D. L. Valentine and D. F. Smith. 2001. Overexpression of the FK506-binding immunophilin FKBP51 is the common cause of glucocorticoid

resistance in three New World primates. *General and Comparative Endocrinolology.* 124: 152-165.

Schmitz, J. 2012. SINEs as driving forces in genome evolution. *Genome Dynamics*. 7: 92-107.

Thomas, C. and T. Hubler. 2016. Stressed? How FKBP proteins can help. Paper presentation at the 93rd Annual Alabama Academy of Science Meeting, Feb. 17-19, 2016, University of North Alabama, Florence AL.

Volk, N., J. C. Pape, M. Engel, A. S. Zannas, N. Cattane, A. Cattaneo, E. B. Binder and A. Chen. 2016. Amygdalar MicroRNA-15a Is Essential for Coping with Chronic Stress. *Cell Reports*. 17: 1882-1891.

Wochnik, G. M., J. Ruegg, G. A. Abel, U. Schmidt, F. Holsboer and T. Rein. 2005. FK506-binding proteins 51 and 52 differentially regulate dynein interaction and nuclear translocation of the glucocorticoid receptor in mammalian cells. *Journal of Biological Chemistry*. 280: 4609-4616.

Ye, J., G. Coulouris, I. Zaretskaya, I. Cutcutache, S. Rozen and T. L. Madden. 2012. Primer-BLAST: a tool to design target-specific primers for polymerase chain reaction. *BMC Bioinformatics*. 13: 134.

Zheng, D., J. J. Sabbagh, L. J. Blair, A. L. Darling, X. Wen and C. A. Dickey. 2016. MicroRNA-511 binds to FKBP5 mRNA, which encodes a chaperone protein, and regulates neuronal differentiation. *Journal of Biological Chemistry.* 291: 17897-17906

TABLES

Table 1. Primer sequences used for qPCR of FKBP51 and FKBP52 mRNA.

Primer Name	Exon	Forward or Reverse	Sequence
FKBP51.1F	6	F	5'ATGGGACATTGGGGTGGCTA3'
FKBP51.1R	6	R	5'TGCATATTCTGGTTTGCACAGT3'
FKBP51.2F	5	F	5'CATCAAGGCATGGGACATTGG3'
FKBP51.2R	5	R	5'GCATATTCTGGTTTGCACAGT3'
FKBP15.3F	8	F	5'AGATGTGGCATTCACTGTGGG3'
FKBP51.3R	8	R	5'CTCCAGAGCTTTGTCAATTCCA3'
FKBP51.4F	8	F	5'GAGATGTGGCATTCACTGTGG3'
FKBP51.4R	8	R	5'TCTCCAGAGCTTTGTCAATTCC3'
FKBP52.1F	6	F	5'GGTTGCACTGGAAGGGTACT3'
FKBP52.1R	6	R	5'TGGCCCTCTCCAGACCATAA3'
FKBP52.2F	3	F	5'CAGTCTGGATCGCAAGGACA3'
FKBP52.2R	4	R	5'TATGGCAATGTCCCAAGCCT3'

FIGURE LEGENDS

Figure 1. FKBP51 and FKBP52 proteins are expressed differently in SML and HL. Whole cell extracts were separated by SDS-PAGE and analyzed by Western Blot for FKBP51 (1a) or FKBP52 (1b) and beta actin as a loading control. Protein levels were quantified by densitometry and represented graphically as fold change relative to HL protein levels (Figures 1c and 1d). Bar represents standard error, n=2. *, protein levels considered statistically different.

Figure 2. The relative levels of FKBP51 and FKBP52 mRNA differ in SML and HL. Total RNA was extracted and used as template for qPCR. Primers shown in Table 1 were designed to target specific exons that contain conserved sequences in humans and squirrel monkeys. Relative levels of mRNA were calculated by the ddCt method for FKBP51 (2a) or FKBP52 (2b) and represented graphically as fold change relative to HL mRNA levels. Bar represents standard error, n=2 for FKBP5 and n=3 for FKBP4. *, mRNA levels considered statistically different.

FIGURES

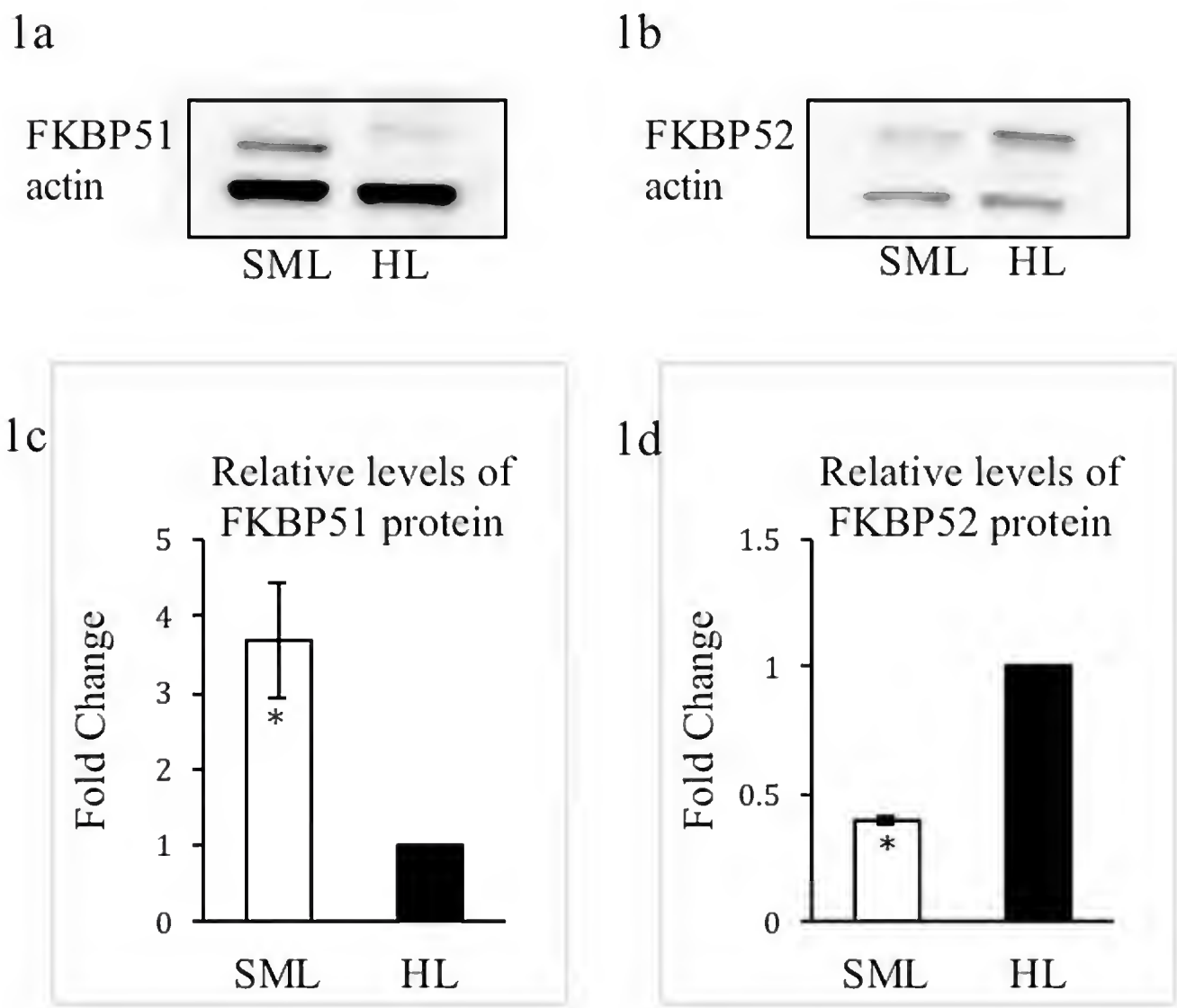

2a

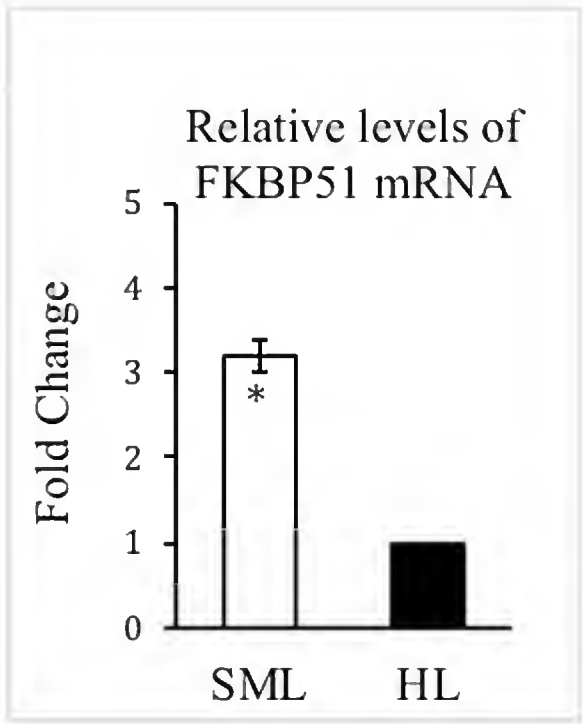
Relative levels of
FKBP51 mRNA
Fold Change
5
4
3
2
1
0
*
SML
HL

2b

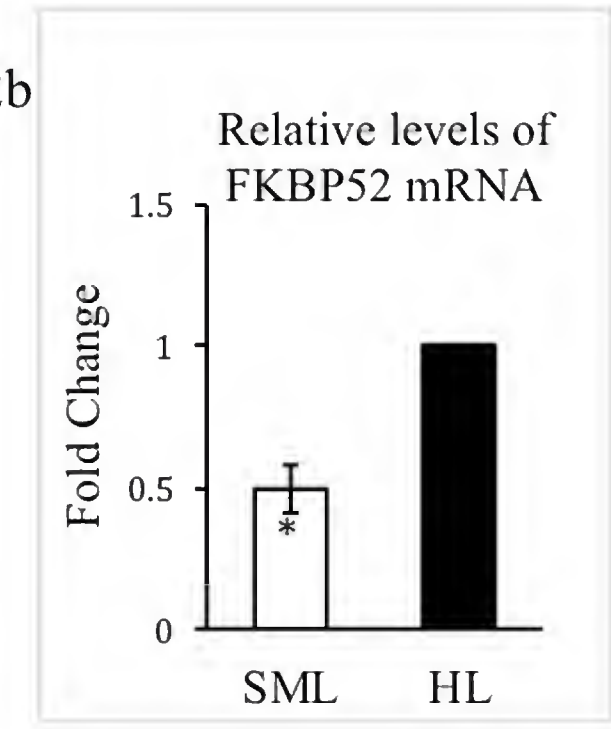
Relative levels of
FKBP52 mRNA
Fold Change
1.5
1
0.5
0
*
SML
HL

Minutes of the Fall Executive Committee Meeting, October 14, 2017

Room 1222, Bldg 1, College of Health Sciences
Samford University

Meeting was called to order at 8:40 a.m. by Ketia Shumaker and the minutes from the spring 2017 Executive Committee Meeting were approved. [Minutes on the Academy Website]

Attendees:

Ellen Buckner
Matthew Edwards
Cameron Gren
Drew Hataway
Ron Hunsinger
Larry Krannich
Akshaya Kumar
Ken Marion
Prakash Sharma
Ketia Shumaker
Brian Toone

Ken Marion moved to approve minutes. Drew Hataway seconded. Minutes were approved.

Action Items Updated
Fall 2017 Executive Committee Meeting

Action Item	Person Responsible	Due Date
Reconsider the role of the Development Committee	Larry Krannich and John McCall	Spring 2018
Identify a mechanism to assess the success of the journal in the next one to two years. This Ad-Hoc Steering Committee is to develop a mission statement and objectives for the journal. Will address Associate editors, online JAAS publication, and Journal Indexing.	Drew Hataway, Ellen Buckner, Cameron Gren, Jack Shelley-Tremblay, Jim Bradley, Akshaya Kumar, Adriane Ludwick	Tabled pending assessment of outcomes from the JAAS changes being implemented
Creation of an AAS mini-grant program to fund small initiatives for STEM outreach	STEM section	Spring 2017
Creation of a silent auction for the 2018 meeting. Held in the afternoon through Sci-Mix. Items to be picked-up after the banquet	Ketia Shumaker and Bettina Riley	Work underway and plan to hold at 2018 Annual Meeting.
Consider the recommendations of the long range planning committee. Move	Larry Krannich	Long Range Planning

the charge, duties, and responsibilities of the membership committee to the development committee and have the first vice president chair that committee.		moved and Approved

1. Ken Marion noted that the Board of Trustees does not give a report at the Fall Executive Meeting, but has a report at the Spring 2018 meeting.
2. Ketia Shumaker asked for an update on the ASIM budget cut and was informed by Ellen Buckner that when Kay Ivey took over as Governor, she recognized the value of ASIM and did not cut the ASIM budget. Ellen Buckner requested that the Academy's statement regarding ASIM Funding be published in the JAAS.
3. Drew Hataway stated that he will be working on nominations to be presented at the spring 2018 Executive Committee meeting for discussion and approval.
4. Brian Toone, Journal Editor, discussed the situation regarding JAAS hard copy distribution. Brian moved and Ken Marion seconded the motion: *The membership dues application will include an opt-in link for indicating a preference for receiving a hard copy of the JAAS and all current, multiple year, and lifetime members be contacted about the opt-in preference link.* The motion was approved unanimously. There was also discussion about a provision to provide authors with 25 reprints with their article publication. Because the Journal will be published in electronic form with free access, mention was made that authors can easily print out their own reprints. The Journal upon payment of a voluntary $100 publication fee will provide 25 Xerox copy reprints, which include a cover noting these as JAAS reprints.
   The editor encouraged section chairs to solicit papers from annual meeting presenters. After some discussion, a motion was made by Brian Toone and seconded by Ken Marion: *Beginning in 2018, the JAAS will publish the Gorgas/AJAS competition papers in a Student Competition online only issue.*
   The motion was approved unanimously.
5. The written report of Jane Nall, Alabama Science Olympiad (ASO) State Director, noted she wished to retire from this position, which she has held since 1996. The Executive Committee formed an ASO Search Committee [Drew Hataway, Brian Toone, and Jane Nall] to select, as soon as possible, a candidate for this position. If the selection occurs prior to the Spring meeting, the nomination will be distributed to the Steering Committee for approval. This would assure the candidate could work with the current director for the 2018 Olympiad.
6. The Biological Sciences Section will be discussing how best to manage the section's programming for this large section. A subdivision arrangement is being considered and this will be discussed at their spring 2018 business meeting. Because the Chair and Vice-Chair positions for Section VIII (Environmental and Earth Science) are vacant and Section VIII programming has been distributed among Sections I & II for the past two years, there was discussion about dissolution of Section VIII. The Academy President and 2nd Vice President will search for a Chair and Vice-Chair and encourage section growth. Because the State has a new policy concerning travel reimbursement, i.e. full reimbursement for in-state conferences when the State employee is a member of the organization, she recommended that this policy be stated in correspondence that advertises the meeting. The website master will include a portal for obtaining an official membership card with dues payment. There are plans to have an author book signing event at the annual meeting and Beth Motherwell from Alabama Press will be contacted about organizing this event. The Call for Papers was approved, but will not be distributed until a Section VIII chair is designated.
7. Matthew Edwards discussed the Long-Range Planning Committee action items relating to pairing

down the number of function committees and moved approval of the two changes:

a. The Committee on Membership be combined with the Committee on Development with the current members of these two committees serving until their terms expire and the 1st Vice President serve as the Chair.
b. The Committee on Science and Public Policy be combined with the Public Relations Committee to give a new committee: Committee on Science, Public Policy, and Public Relations. The current members of these two committees will serve until their terms expire.

The Executive Committee approved both. Because these become By-Law changes, these will be rewritten as By-Law changes, distributed to the membership prior to the spring 2018 meeting, and voted on at the spring business meeting.

The additional recommendation of the Long-Range Planning Committee regarding the senior and junior academy auditing committees complies with the By-Laws. These changes will be automatically made.

There was discussion concerning formation of a Distinguished Service Award and the distinctiveness of this award relative to the other Academy awards. This was referred back to the Long-Range Planning Committee with a recommendation to work with the Gardner and FAS Award committee to develop this as a distinctive award.

8. The Executive Committee discussed and moved that the Editorial Board of the Journal solicit Section Chairs and one member from AJAS to serve as ad hoc members of the Editorial Board. This was unanimously approved.
9. Place and Date of Meeting Committee noted that meeting locations are designated through 2021 with 2022 and 2023 available. Ellen Buckner said that pending approval from Samford University, the College of Health Science would like to host the 2023, 100th AAS anniversary meeting.
10. Ellen Buckner suggested and the Committee approved a resolution be written commending Governor Kay Ivey for supporting ASIM.
11. The Nomination Committee will present a slate of nominees for officers and committees at the spring 2018 Executive Committee meeting.
12. Ron Hunsinger stated that the William H Mason Scholarship information was up-to-date on the website. Application information will be sent shortly to the School of Education Deans in Alabama. There is now a vacancy on the committee.
13. Under New Business, Ellen Buckner extended an invitation to the Executive Committee to hold the spring 2018 meeting at her home on Wednesday, March 14, 2018 with dinner beginning at 6:15 pm. The Committee graciously accepted.
14. There being no further business, the meeting was adjourned at 11:35 a.m.

Action Items From
Fall 2017 Executive Committee Meeting

Action Item	Person Responsible	Due Date
Modify 2018 Meeting Registration form and implement on Academy website	Larry Krannich and Jack Shelley-Tremblay	November 2017
Include a portal on the Academy website for members to obtain an	Jack Shelley-Tremblay	November 2017

official membership card		
Create a few @alabamaacademyofscience.org email addresses	Jack Shelley-Tremblay & Brian Toone	November 2017
Include an opt-in portal on the Academy website for members to indicate their preference to receive a hard copy of the JAAS	Jack Shelley-Tremblay	November 2017
Designate a Section VIII Chair and Vice-Chair	Ketia Shumaker and Drew Hataway	November 2017
ASO Search Committee identifies and recommends a candidate for ASO State Director	Drew Hataway, Brian Toone, & Jane Nall	December 2017
Write By-Law Changes regarding the combination of the Development and Membership Committees and formation of the Committee on Science, Public Policy and Public Relations. Distribute to membership in Winter 2018.	Larry Krannich	January 2018
Write a resolution commending Governor Kay Ivey for supporting ASIM	Brian Burnes	March 2018
Creation of an AAS mini-grant program to fund small initiatives for STEM outreach	STEM section	Spring 2018
Reconsider the role of the Development Committee	Larry Krannich and John McCall	Spring 2018
Creation of a silent auction for the 2018 meeting. Held in the afternoon through Sci-Mix. Items to be picked-up after the banquet	Ketia Shumaker and Bettina Riley	2018 Annual Meeting
Slate of Nominees for Officers and Committees	Drew Hataway	2018 Annual Meeting

Alabama Academy of Science Journal

Scope of the Journal:

The Alabama Academy of Science publishes significant, innovative research of interest to a wide audience of scientists in all areas. Papers should have a broad appeal, and particularly welcome will be studies that break new ground or advance our scientific understanding.

Information for the Authors:

- Manuscript layout should follow the specific guidelines of the journal.
- The authors are encouraged to contact the editor (E-mail: brtoone@samford.edu) prior to paper submission to obtain the guidelines for the author.
- At least one author must be a member of the *Alabama Academy of Science* (except for Special Papers).
- The author(s) should provide the names and addresses of at least two potential reviewers.
- Assemble the manuscript in the following order: Title Page, Abstract Page, Text, Brief acknowledgments (if needed), Literature Cited, Figure Legends, Tables, Figures.

Review Procedure and Policy:

Manuscripts will be reviewed by experts in the research area. Manuscripts receiving favorable reviews will be tentatively accepted. Copies of the reviewers' comments (and reviewer-annotated files of the manuscript, if any) will be returned to the correspondent author for any necessary revisions. The final revision and electronic copy are then submitted to the *Alabama Academy of Science Journal* Editor. The author is required to pay $100 for partial coverage of printing costs of the article.